L'Université canadienne
Canada's university

FACULTÉ DES ÉTUDES SUPÉRIEURES ET POSTOCTORALES

u Ottawa

L'Université canadienne
Canada's university

FACULTY OF GRADUATE AND POSDOCTORAL STUDIES

Xiuzhu Yang
AUTEUR DE LA THÈSE / AUTHOR OF THESIS

M.Sc. (Systems Science)
GRADE / DEGREE

Systems Science
FACULTÉ, ÉCOLE, DÉPARTEMENT / FACULTY, SCHOOL, DEPARTMENT

Noisy Transistor Models for Microwave Circuit CAD

TITRE DE LA THÈSE / TITLE OF THESIS

Mustapha C. E. Yagoub
DIRECTEUR (DIRECTRICE) DE LA THÈSE / THESIS SUPERVISOR

CO-DIRECTEUR (CO-DIRECTRICE) DE LA THÈSE / THESIS CO-SUPERVISOR

EXAMINATEURS (EXAMINATRICES) DE LA THÈSE / THESIS EXAMINERS

A. El Saddik

E. Gad

Gary W. Slater
LE DOYEN DE LA FACULTÉ DES ÉTUDES SUPÉRIEURES ET POSTDOCTORALES /
DEAN OF THE FACULTY OF GRADUATE AND POSTDOCORAL STUDIES

Noisy Transistor Models for Microwave Circuit CAD

Thesis

by

Xiuzhu Yang

Master of Science

Systems Science Program

Faculty of Graduate and Postdoctoral Studies

University of Ottawa

© 2005 Xiuzhu Yang, Ottawa, Canada

University of Ottawa

March 2005

Ottawa, Canada

Library and Archives Canada

Published Heritage Branch

395 Wellington Street
Ottawa ON K1A 0N4
Canada

Bibliothèque et Archives Canada

Direction du Patrimoine de l'édition

395, rue Wellington
Ottawa ON K1A 0N4
Canada

Your file Votre référence
ISBN: 0-494-11463-0
Our file Notre référence
ISBN: 0-494-11463-0

NOTICE:
The author has granted a non-exclusive license allowing Library and Archives Canada to reproduce, publish, archive, preserve, conserve, communicate to the public by telecommunication or on the Internet, loan, distribute and sell theses worldwide, for commercial or non-commercial purposes, in microform, paper, electronic and/or any other formats.

The author retains copyright ownership and moral rights in this thesis. Neither the thesis nor substantial extracts from it may be printed or otherwise reproduced without the author's permission.

AVIS:
L'auteur a accordé une licence non exclusive permettant à la Bibliothèque et Archives Canada de reproduire, publier, archiver, sauvegarder, conserver, transmettre au public par télécommunication ou par l'Internet, prêter, distribuer et vendre des thèses partout dans le monde, à des fins commerciales ou autres, sur support microforme, papier, électronique et/ou autres formats.

L'auteur conserve la propriété du droit d'auteur et des droits moraux qui protège cette thèse. Ni la thèse ni des extraits substantiels de celle-ci ne doivent être imprimés ou autrement reproduits sans son autorisation.

In compliance with the Canadian Privacy Act some supporting forms may have been removed from this thesis.

While these forms may be included in the document page count, their removal does not represent any loss of content from the thesis.

Conformément à la loi canadienne sur la protection de la vie privée, quelques formulaires secondaires ont été enlevés de cette thèse.

Bien que ces formulaires aient inclus dans la pagination, il n'y aura aucun contenu manquant.

Abstract

Because of their high performance, *Metal-Semiconductor Field Effect Transistors* (MESFETs) and *High-Electron-Mobility Transistors* (HEMTs) are widely used in microwave and millimeter wave communication systems, particularly in low noise applications. Therefore, accurate noise models are essential to ensure robust simulation and optimization during the design process. The sophistication of modern communication systems urged the need of *monolithic microwave integrated circuits* (MMICs), which contain several MESFETs or HEMTs on the same chip. As the chip density increases, the request for accurate MESFET or HEMT noise models becomes more pronounced.

In this study, a new method has been developed to extract a 15-element small signal model of MESFET and HEMT devices. This method uses three sets of S-parameter measurements at different bias conditions. The technique consists of two major steps; in the first step, part of the bias-independent extrinsic parameters is evaluated in preparation to the second step. In the second step, all other parameters should be extracted at the bias point of interest using an optimization method. This method has been tested on S-parameters of a hypothetical device model with ideal and noisy data, compared with other optimization-based techniques, and shows reliable results and a unique solution for all parameter values.

Another method has been proposed to extract the noise parameters of a packaged device at any frequency. This technique has also been tested on S-parameters of a hypothetical device model with ideal and noisy data, and compared with other noise parameter extraction techniques. The study shows consistent results and demonstrates its accuracy, simplicity and efficiency as a noise parameter extraction method of microwave/millimeter-wave transistors.

Acknowledgment

I would like to thank my committee for taking time out of their busy schedules to evaluate this thesis. My sincerest thanks go to Dr. Mustapha C.E. Yagoub for his support, guidance and invaluable advices. I would also like to thank Dr. Farah Mohammadi for her help, support and comments. Special thanks go to Dr. Tet-Hin Yeap and Mrs. Monique Walker for their help.

My deep gratitude is due to my wife and my parents for their continuous love, encouragement, and support during my life.

Finally, I would like to thank my friends, and colleagues who presented me any advice or assistance during my work.

TABLE OF CONTENTS

Chapter 1. Introduction ... 1

1.1 State of art ... 1
1.2 Why developing Noise Models for MESFET and HEMT Devices ... 2
1.3 Technical Contributions ... 4
1.4 Thesis Organization ... 5

Chapter 2. MESFET and HEMT Physics and Modeling ... 7

2.1 Physical Structure ... 7
2.2 Principles of the MESFET and HEMT Operation: ... 9
2.3 MESFET and HEMT Small-Signal Models ... 12
2.3.1 Parasitic Inductances ... 15
2.3.2 Parasitic Resistances ... 15
2.3.3 Pad Capacitances ... 15
2.3.4 Intrinsic Capacitances ... 16
2.3.5 Charging Resistance ... 18
2.3.6 Transconductance ... 19
2.3.7 Transconductance Delay ... 19
2.3.8 Output Conductance: ... 20
2.4 Literature Review ... 20

Chapter 3. Noise Models ... 24

3.1 Noise in linear Two-ports ... 26
3.1.1 Noise Description in Two-Port Networks ... 27
3.1.2 Representation of Noise Parameters ... 31
3.1.3 Noise Figure of Cascaded Networks ... 33
3.2 Noise Models ... 33
3.2.1 Gupta noise model ... 33

3.2.2 Fukui Noise Model 35
3.2.3 Cappy Noise Model 37
3.2.4 Pucel Noise Model 38
3.2.5 POSPIESZALSKI Noise Model 40

Chapter 4 Extraction Method and Results 46

4.1 Extraction of Small-Signal Model at Normal Bias Conditions: 46
4.1.1 Determination of the Intrinsic Y-Parameters 47
4.1.2 Extracting Intrinsic Elements from Intrinsic Y-Parameters 50
4.2 New Method for Determining the FET Small-Signal Equivalent Circuit Elements 51
4.2.1 Determination of the Pad Capacitances 52
4.2.2 Determination of the parasitic inductances and ΔR_{ds} 53
4.2.3 The Procedure of the New Method for the extraction of the FET Small-Signal Equivalent-Circuit Elements 57
4.2.4 The Iterative Scheme for Extracting FET Small-Signal Model Parameters at Normal Bias Condition 58
4.3 Method of Extracting Noise Parameters 60
4.3.1 New Method for Extracting the FET Two Noise Temperatures 61
4.3.2 The Procedure for Extraction of FET Noise Parameters 62
4.3.3 The Iterative Scheme for Extraction of FET Noise Parameters 66
4.4 Results and Analyses 67
4.4.1 S-Parameter Data 68
4.4.2 Results of Extracting Small-Signal Equivalent Circuit on "Ideal Data" 74
4.4.3 Results of Extracting Small-Signal Equivalent Circuit on "Noisy Data" 78
4.4.4 Comparison with other methods 82
4.4.5 Results of Extraction of FET Noise Parameters 86
4.4.6 Influence of gate width on device noise performance 94

Chapter 5. Conclusion 97

Appendix A. Intrinsic Small-Signal Model 99

A.1 Derivation of Intrinsic Y-Parameters 99
A.2 Derivation of Intrinsic Parameters 100

Appendix B. Nonlinear Optimization 104

B.1 Gauss-Newton Method 107
B.2 Levenberg-Marquardt Method 109
B.3 The First Derivative Calculation 110
B.4 Properties of the New Optimization Method 111

REFERENCES 113

LIST OF FIGURES

Figure 2.1. Cross-section of a GaAs MESFET device. 7
Figure 2.2. Actual GaAs MESFET layouts: (a) interdigitated-gate, (b) π-gate. 8
Figure 2.3. Cross section of a HEMT structure 9
Figure 2.4 GaAs MESFET operation under different Vds biasing with Vgs ≤ 0: (a) Linear region (Vds is very low), (b) Vds at the onset of saturation, (c) Vds is big.. 10
Figure 2.5: I-V Characteristic curves for a MESFET or HEMT device for different values of Vgs; ideal current is drawn in solid curve while dashed curve indicates the real current. 12
Figure 2.6: Standard MESFET-HEMT equivalent circuit 13
Figure 2.7: The physical origin of the equivalent circuit for (a) MESFET (b) HEMT ... 13
Figure 2.8: Depletion region shapes for different applied bias voltage: (a) gate-source voltage is equal to gate-drain voltage, (b) gate-drain reverse bias is greater than gate-source reverse bias. 17
Figure 3.1 The maximum transfer of noise power generated in a resistor requires a matched load. 25
Figure 3.2 An unmatched load reflects noise power... 25
Figure 3.3: Noisy linear two-ports: (a) general form (b) admittance form (c) impedance form (d) ABCD form. 28
Figure 3.4: noisy linear two-ports in S-parameters form.. 30
Figure 3.5: A Circuitry is connected at the input of a device 31
Figure 3.6 An equivalent circuit of a FET amplifier consisting of a generator, input circuit, an active device and a receiver (load)... 34
Figure 3.7: Equivalent model of a FET to predict noise performance based on the Fukui method.. 36
Figure 3.8: The Pucel noise model based on a simplified FET model with noise sources represented by voltage and current sources 39
Figure 3.9: Equivalent circuit of FET (HEMT, MODFET) chip. Noise properties of an intrinsic chip are represented by equivalent temperatures: T_g *of* R_{gs}, and T_d *of* g_{ds}. Noise contribution of ohmic resistances r_s, r_g, *and* r_d are determined by physical temperature T_a of a chip. 41
Figure 3.10: Noise equivalent circuit of an intrinsic chip 41

Figure 4.1 16-element small-signal FET model. 47
Figure 4.2 Extraction of intrinsic Y-parameters from measured S-parameters. 48
Figure 4.3. Small-signal equivalent circuit of a FET with zero drain bias voltage and gate voltage lower than the pinchoff voltage 52
Figure 4.4 Sketch of the distributed RC network under Vds=0 and Vgs fairly above pinchoff voltage. 53
Figure 4.5. Flow chart of the algorithm for extracting the FET small-signal model parameters 59
Figure 4.6: The flow chart of the iterative scheme for extraction of FET noise parameters 67
Figure 4.7 "Ideal Data" and "Noisy Data" of S-parameters for the hypothetical model.. 74
Figure 4.8 S-parameters of the hypothetical device versus calculated model using the "Ideal Data" 78
Figure 4.9 S-parameters of the hypothetical device versus calculated model using the "Noisy Data" 81
Figure 4.10 Equivalent circuit of FHR01F HEMT at $T_a = 297$ K, $V_{ds} = 2V$, $I_{ds} = 10mA$. Values of resistance, capacitance, and inductance are given in Ω, pF, and nH ... 87
Figure 4.11 Noise parameters of FHR01FH (chip) HEMT at $T_a = 297\,K$, $V_{ds} = 2V$ $I_{ds} = 10mA$. (a) Minimum noise temperature ($T_{\min}$) vs. frequency. (b) Optimum source resistance (R_{opt}) vs. frequency. (c) Optimum source reactance (X_{opt}) vs. frequency. (d) Equivalent noise conductance (g_n) vs. frequency. 92
Figure 4.12 Comparisons of measured and predicted noise parameters versus frequency for two MESFET's of different dimensions biased at $I_{ds} = 0.6 I_{dss}$ and $I_{ds} = 0.45 I_{dss}$ with $V_{ds} = 5V$ 95
Figure A.1 Intrinsic model for MESFET or HEMT devices. 99
Figure B.1: Flow Chart for Gauss-Newton optimization method 108

LIST OF TABLES

Table 4.1 Correlation matrices and electrical matrices of various representations 63
Table 4.2: Transformation Matrices T 64
Table 4.3 Equivalent circuit element values for a hypothetical device. 68
Table 4.4 IDEAL S-PARAMETERS of EF018A 69
Table 4.5 NOISY S-PARAMETERS of EF018A 70
Table 4.6 The extracted equivalent circuit element values for a hypothetical device based on "Ideal Data". 75
Table 4.7 The extracted equivalent circuit element values for a hypothetical device using new method based on "Noisy Data". 79
Table 4.8 The extracted equivalent circuit element values for a hypothetical device using Ooi's method based on "Ideal Data" with initial value: Lg=0, Ld=0, Ls=0, Rd=0, Rs=0. 83
Table 4.9 The extracted equivalent circuit element values for a hypothetical device using Ooi's method based on "Ideal Data" with initial value: Lg = 2.2e-010; Ld = 2.2e-010; Ls = 6.2e-011; Rd = 0.98; Rs = 0.22 83
Table 4.10 The extracted equivalent circuit element values for a hypothetical device using Shirakawa's method based on "Ideal Data" with initial value: Lg=0, Ld=0, Ls=0, Rg=0,Rd=0, Rs=0. 84
Table 4.11 the extracted equivalent circuit element values for a hypothetical device using Shirakawa's method based on "Ideal Data" with initial value: Lg =2.22e-010; Ld =2.2e-010; Ls =6.29e-011; Rd =0.98; Rs =0.22; Rg =0.49 84
Table 4.12 The extracted equivalent circuit element values for a hypothetical device using Ooi's method based on "Noisy Data" with initial value: Lg=0, Ld=0, Ls=0, Rd=0, Rs=0. 85
Table 4.13 the extracted equivalent circuit element values for a hypothetical device using Shirakawa's method based on "Noisy Data" with initial value: Lg =0; Ld =0; Ls =0; Rd =0; Rs =0; Rg =0 85
Table 4.14 the comparison of the new proposed method with the Ooi's and Shirakawa's method for extraction of small-signal equivalent circuit 86
Table 4.15 Equivalent circuit of FHR01F HEMT at $T_a = 297$ K, $V_{ds} = 2V$, $I_{ds} = 10mA$. 87
Table 4.16 Noise parameters of FHR01FH as a packaged FET at $f = 8.5\ GHz$, $V_{ds} = 2V$ 87

Table 4.17 De-embedding the noise parameters of FHR01FH at different stages ($f = 8.5\ GHz$, $V_{ds} = 2V$) 88
Table 4.18 Computation of T_g, T_d, and noise parameters of modeled FHR01FH intrinsic chip ($f = 8.5\ GHz$, $V_{ds} = 2V$) 88

List of Glossary or Symbols

k: Boltzmann's constant ($1.374\times10^{-23} J/K$)
T: Temperature in Kelvin
B: Bandwidth in Hertz
V: Voltage in V
I: Current in A
R: Resistance in Ω
L: Inductance in H
C: Capacitor in F
G: Gain
g: Conductance in S
τ: Time delay in second
F: Noise figure in dB
f: Frequency in Hz
P: Power in Watt
Γ: Reflection coefficient
Z: Impedance in Ω
R: Resistor in Ω
X: Reactance in Ω
Y: Admittance in S
G: Conductance in S
B: Susceptance in S
S: Scattering parameter with no unit
M: The noise measure with no unit

Acronyms

CAD:	Computer Aided Design
FET:	Field Effect Transistor
GaAs:	Gallium Arsenide
HEMT:	High-Electron-Mobility Transistor
IF:	Intermediate Frequency
IMD:	Intermodulation Distortion
LNA:	Low-Noise Amplifiers
LO:	Local Oscillator
MESFET:	Metal-Semiconductor Field Effect Transistor
MMIC:	Monolithic Microwave Integrated Circuits
PIN:	P-type, Intrinsic layer, and N-type regions
RF:	Radio Frequency
RMS:	Root Mean Square

Chapter 1. Introduction

The 21st century will be the information age characterized by ever-increasing need for communication. There are several constraints on the nature of the communicating terminal, (i) it must be wireless and portable, (ii) cost-effective production in large numbers must be possible, and (iii) the communication device must be suitable for broadband operation. At the same time, the need for concurrent and multi-disciplinary design with simultaneous consideration of thermal, electrical, and reliability criteria becomes increasingly important. This trend leads to massive and highly repetitive computational tasks during simulation, optimization and statistical design. As the electrical equivalent component models used in conventional commercial software are not accurate enough, continued research in certain new areas of the subject has been fueled by the demand of efficient models for circuit simulators, including higher order thermal effects, where there are both technological challenges and economic opportunity.

1.1 State of art

The drive in the electronics industry for manufacturability-driven design and time-to-market demands powerful and efficient computer-aided design (CAD) techniques. Furthermore, the need for statistical analysis and yield optimization, taking into account process variations and manufacturing tolerances in the components, requires that the component models be accurate and fast so that the design solutions can be achieved feasibly and reliably.

With the expansion of wireless and satellite systems, the tendency is to generate more power and reduce the system size. The combination of these desires will increase the circuit temperature and at the same time will give less opportunity to the system to dissipate the heat. This results in a more sensitive dependence of the system on temperature, and therefore on noise.

Since noise is one major limiting factor for the performance of modern communication system, there is a demand for transistor models that can accurately predict noise. In order to describe the RF noise performance of a FET (MESFET or HEMT), one has to determine the parameters of the noise model in addition to the small-signal equivalent-circuit elements.

So, the small-signal model is the corner stone of the noise model. If an accurate noise model is required, an accurate small-signal model should be devised first. In order to extract a noise model, small-signal model parameters should be extracted at different bias points through out the region of interest. Those parameters should fit bias dependent equations to represent the dependence of the device on the bias point.

It is worthy to note that the modeling techniques presented in this dissertation can be applied to both HEMTs and MESFETs. The fact is that although the two devices are physically and structurally different, they have the same equivalent circuit model with different parameter values. HEMT devices operate over larger frequency ranges than those of MESFET devices; and thus the model parameter values reflect this distinction.

1.2 Why developing Noise Models for MESFET and HEMT Devices

MESFET has been found many applications in the microwave and millimeter-wave for the past three decades and so has HEMT for the past two decades. Having accurate noise models for MESFET and HEMT devices would facilitate the use of circuit design and analysis tool to allow better use and evaluation of these devices. Most of the currently available models in computer-aided design (CAD) packages are circuit models. The circuit models are expected to stay for some time because of their computational efficiency and availability in the commercial CAD packages. New models can also be developed into CAD tools easily, or the built-in models can be upgraded with a little effort.

It is obvious that the accuracy of the model determines the accuracy of the design analysis. An accurate model is essential for quick design and fabrication process development. The inaccuracy in the model results in many trials before you get a working design or a successful process. Moreover, modern communication systems require more sophisticated monolithic microwave integrated circuits (MMICs) with smaller and smaller sizes. The miniaturization of MMICs and increasing the chip density emphasized the need of accurate noise models to minimize the number of design and fabrication cycles.

The more accurate the small-signal model is, the more accurate the noise model is. The small-signal model provides a useful tool for the device performance analysis: gain, noise...etc. It also provides valuable insight into the operation of the device in a circuit.

As a step towards a large-signal thermal model, a small-signal thermal noise model is essential.

When we talk about the modeling of MESFETs or HEMTs, we also have to talk about their uses and applications. In the following paragraphs, a brief overview of these various applications of MESFET and HEMT devices will be presented.

1) MESFETs and HEMTs as LNAs: MESFET and HEMT are widely used as small-signal low-noise amplifiers (LNAs) in various communication application and EW systems. These circuits are designed to operate as linear gain blocks, with specific requirements determined by their location within the system. The noise added by these amplifiers can be kept low, thus yielding improved signal-to-noise ratio performance. Amplifier applications range from a few hundreds of MHz to 40 GHz, and they are successful in various broadband, low noise and high frequency applications [1].

2) MESFETs and HEMTs as Power Amplifiers: Solid-state power amplifiers are typically used in communication systems to provide sufficient signal power to allow transmission from one site to another. The popularity of mobile and hand-held communication devices has pushed the development of compact and efficient power amplifiers. Additionally, the size, weight, and power constraints on satellite communication systems require such amplifiers at high frequencies. Power amplifiers are usually designed for maximum efficiency, in contrary to LNAs that are usually designed for maximum linearity and minimum noise. Output power and gain are also important parameters in the design of power amplifiers. Class A MESFET power amplifier can have output power as high as 17 W and theoretical maximum efficiency is 50%. While HEMT power amplifiers at 44 GHz have 250 mW of output power and 27% efficiency [1].

3) MESFETs and HEMTs as Oscillators: Oscillators are used in many communication systems, along with the mixers, to perform generation and frequency conversion of desired signals. MESFET- and HEMT- based oscillators have been popular because of their dc-to-RF conversion efficiencies. In addition, the three terminal devices allow greater design flexibility to meet specific performance requirements [1].

4) MESFETs and HEMTs as Mixers: A mixer is a three-port device that functions to convert an input RF signal in conjunction with a LO signal to an intermediate signal termed IF on which further precise signal processing is performed. Ideally, a mixer

performs this frequency conversion with perfect fidelity and thus generates no intermodulation distortion (IMD). Other desirable characteristics include high isolation between three ports and a low noise figure along with minimal loss or preferably gain while performing frequency conversion. [1]

More recently, MESFETs and HEMTs are being used as the nonlinear element in mixers; primarily for reasons of compatibility with MMIC processing and to achieve conversion gain. Frequency conversion of the RF signal to an IF results in a larger amplitude signal. This conversion gain, rather than loss, cancelled the requirement of a LNA preceding the mixer in some applications. This may also result in a net decrease in dc power, which is particularly important for portable and space-based equipments. [1]

5) MESFETs and HEMTs as Attenuators: A Variable attenuator is a two-port device that allows adjustment of the signal amplitude by application of an external voltage or current. The attenuation is proportional to the applied voltage or current. If it is directly proportional, the attenuator is termed linearized. The attenuator should perform this task with low harmonic distortion, minimal insertion loss, and low VSWR at its ports. Attenuators commonly employed in feedback networks, communication systems, and in temperature compensation networks to maintain constant signal amplitude.

More recently, MESFETs and HEMTs are being used to realize the variable resistive element in attenuator avoiding the disadvantages of PIN diodes. In this case, the FET is unbiased ($V_{ds} = 0$, $I_{ds} = 0$), and the drain-source resistance r_{ds} is varied with an applied gate potential. Unlike a PIN-based attenuator, FET-based attenuators are voltage controlled and require very little dc power [1].

As we have seen, Both MESFETs and HEMTs are employed in a wide range of applications. The availability of accurate small-signal and noise models is extremely important to evaluate the design of their circuits more accurately at lower cost. A small-signal and noise model is typically needed for designing of LNAs.

1.3 Technical Contributions

The main focus of this research has two aspects. First, we propose a new approach to extract an accurate small-signal model from Scattering-parameter measurements (S-parameters). Many extraction techniques are described in detail. Advantages and

disadvantages of each technique along with range of validity are discussed. A robust technique is concluded and used to extract an accurate small-signal model over any frequency range from S-parameter measurements whose accuracy is reasonable. Second, we propose a systematic approach for extracting the noise parameters of a packaged device at any frequency. Many noise models and noise parameter extraction techniques are discussed and disputed in detail. Consequently, a new and efficient noise parameter extraction technique concluded and used to predict the noise properties of the device.

1.4 Thesis Organization

Chapter 2 provides a brief discussion of the physical structure of MESFET and HEMT devices. The physical operation is also explained qualitatively along with some features of the I-V characteristic curves of MESFET and HEMT devices. This chapter also discusses small-signal models. In addition, the physical origin of each element is clarified. Each element of the small-signal model is discussed to explore its physical meaning along with the factors that affect its value. Existing works done in the modeling field will be also explored.

Chapter 3 provides summary discussions of noise and noise models for the MESFET and HEMT devices. Advantages and disadvantages of different noise models are discussed in detail.

In Chapter 4, various optimization-based extraction techniques for small-signal models are discussed in detail. Strengths and weaknesses of each technique are presented. Different small-signal models for different schemes are described. Models at different bias conditions and their implications are explained as well. Pinched-off device models are derived and discussed based on different proposed extraction schemes. A Cold-measurement model is presented; its simplicity is explored for the extraction of some parameters. Our new technique is explained showing its strengths versus other techniques.

In addition, we also discussed various extraction techniques for the device noise parameters and proposed our new technique. The new technique is explained and compared with other techniques in detail showing its strengths. Some least-squares nonlinear optimization techniques are mathematically described.

Chapter 4 also shows results of the different techniques and comparison between

different techniques.

In chapter 5, conclusions and possible future work are provided.

Chapter 2. MESFET and HEMT Physics and Modeling

Understanding the physical structure and operation of a semiconductor device is a crucial step in the device modeling process. A device model basically reflects how we understand the physics and physical operation of this device. The method of characterization of this device depends on its physics. This chapter will discuss some physical aspects of MESFET and HEMT devices. A small-signal model will be proposed and discussed in terms of physical reflections.

2.1 Physical Structure

A MESFET is a three-terminal device [2], [3]. Since it is a FET transistor, it has three electrodes: drain, source, and gate as shown in Figure 2.1 [1]. For microwave and millimeter wave frequencies, the MESFET devices are fabricated using mainly GaAs material. GaAs has attractive features at high frequencies since the carrier mobility is much larger than that of silicon. In addition, electron saturation velocity for GaAs is higher than that for silicon which results in increased operating frequency range.

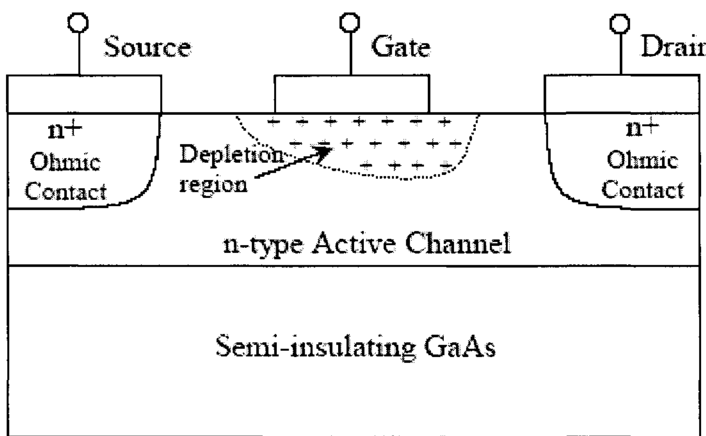

Figure 2.1. Cross-section of a GaAs MESFET device.

A thin layer of n-type GaAs is deposited on top of a semi-insulating GaAs substrate. The back face of the substrate is covered with a metal Au/Ge alloy [4], which is usually connected to the source terminal during measurements. Both drain and source are connected to the n-type layer through n+ ohmic contacts. The metal of the source and drain electrodes can be made of Au/Ge alloy, which is coated with Ti, Pt, and Au layers,

respectively. The gate is a thin layer of metal, usually aluminum coated with Au, deposited on top of the n-type layer between drain and source. The metal semiconductor junction of the gate represents a Schottky barrier junction. This junction is used to control the height of the active channel layer beneath the gate by applying a bias voltage to the gate. The area just beneath the gate is charge depleted as per the applied bias.

The most important dimensions of a MESFET device are the gate length "L" and width "W". Those LxW dimensions usually characterize the device. For example, a device can be referred as 0.3x300 μm^2 when the gate length is equal to 0.3 μm and the gate width is equal to 300 μm. A typical value of gate length ranges from 0.1 to 1 μm. The gate length determines the maximum frequency of operation. As the gate length decreases, the maximum frequency increases [2]. On the other hand, the gate width determines the performance of the device such as the maximum current capability.

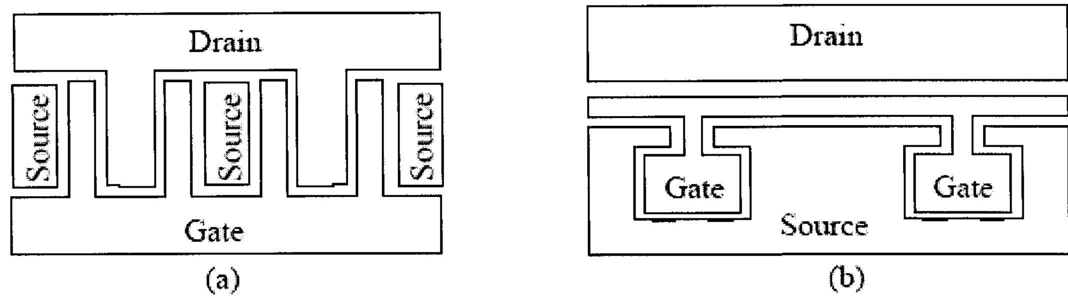

Figure 2.2. Actual GaAs MESFET layouts: (a) interdigitated-gate, (b) π-gate.

The actual layout of a MESFET device is more complex than that shown in Figure 2.1. Figure 2.2 [1] shows two different examples of actual layouts: interdigitated-gate and π-gate layout. Those layouts are usually used to increase the gate width while decreasing the parasitic gate resistance. The patterns shown in Figure 2.2 can be repeated to achieve the required gate width. This layout implies crossover areas between metalization traces, which should be filled with either silicon dioxide or air [4].

A HEMT (High-electron-mobility transistor) is a heterostructure field effect device. Figure 2.3 [5] presents a cross-sectional view of a conventional HEMT structure. It is also a three-terminal device and has three electrodes: drain, source, and gate. But it is more complex than the MESFET. However, because the structure takes advantage of the superior transport properties (high mobility and velocity) of electrons in a potential well of lightly doped semiconductor material, the HEMT has significant improvements in the

device noise figure and some improvements in high frequency performance [1].

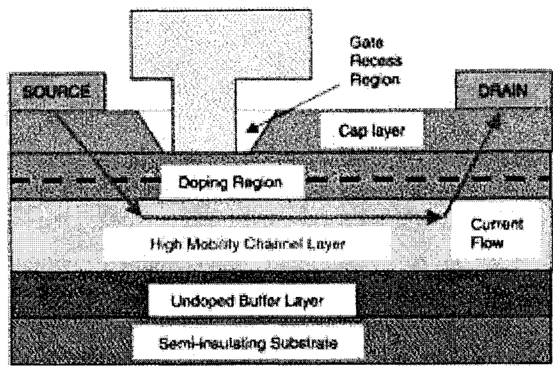

Figure 2.3. Cross section of a HEMT structure

2.2 Principles of the MESFET and HEMT Operation:

A MESFET or HEMT device is biased by applying two voltages: V_{gs} between gate and source and V_{ds} between drain and source [6]. These voltages control the channel current between the drain and source by varying the height of the gate-depletion region and the longitudinal electric field. The operation can be explained qualitatively without going into deep physical analysis. Three cases can be recognized for the I_{ds}-V_{ds} characteristic curve of the MESFET or HEMT, if V_{gs} is larger than the pinch-off voltage, low V_{ds} voltage where I_{ds} is linearly proportional to V_{ds}, high V_{ds} where the current is almost constant, and moderate V_{ds} where I_{ds} has nonlinear relationship of V_{ds}.

Imagine first that V_{gs}=0 V and V_{ds} is raised from zero to some low value as shown in Figure 2.4. (a) [6]. When V_{gs}=0V, the depletion region under the Schottky-barrier gate is relatively narrow, and as V_{ds} is raised, a longitudinal electric field and current are established in the channel. Because of V_{ds}, the voltage across the depletion region is greater at the drain end than at the source end, so the depletion region becomes wider at the drain end.

The narrowing of the channel and the increased V_{ds} increase the electric field near the drain, causing the electrons to move faster. Although the channel depth, and in turn channel's conductive cross section, is reduced, the net effect is increased current. When V_{ds} is low, the current is approximately proportional to V_{ds}. However, if the gate reverse bias is increased while the drain bias is held constant, the depletion region widens and the conductive channel becomes narrower, reducing the current. When V_{gs}=V_p, the pinch-off

voltage, the channel is fully depleted and the drain current is zero, regardless of the value of V_{ds}. Thus, both V_{gs} and V_{ds} can be used to control the drain current. When the MESFET or HEMT is operated under such bias voltages, where both V_{gs} and V_{ds} have a strong effect on the drain current, it is said to be in its linear or voltage controlled resistor region.

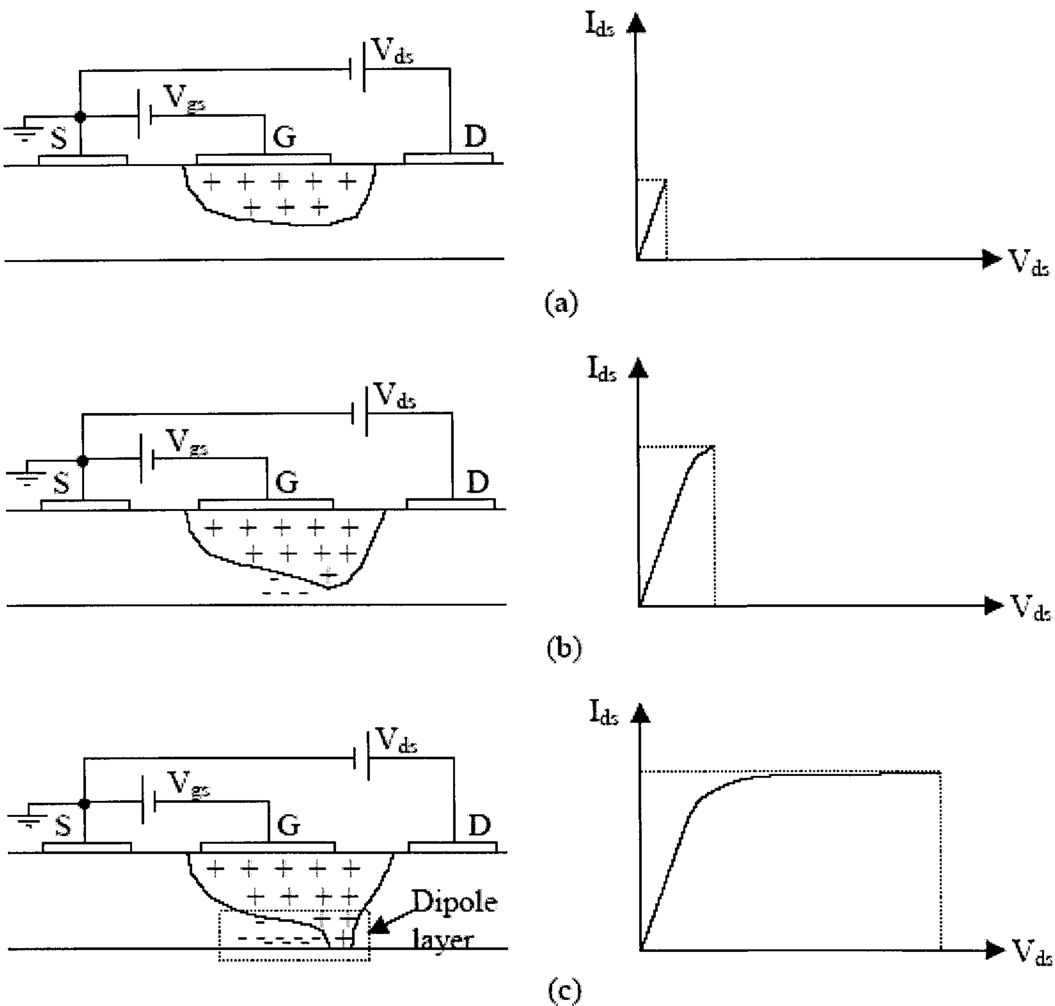

Figure 2.4 GaAs MESFET operation under different V_{ds} biasing with $V_{gs} \leq 0$: (a) Linear region (V_{ds} is very low), (b) V_{ds} at the onset of saturation, (c) V_{ds} is big.

If V_{ds} is raised further, as shown in Figure 2.4(b), while V_{gs} is larger than the pinch-off voltage, the channel current increases, the depletion region becomes deeper at the drain end, and the conductive channel becomes narrower. The current clearly must be constant throughout the channel. As a result, and as long as the conductive channel near the drain becomes narrower, the electrons must move faster. However, the electron velocity cannot increase indefinitely; the average velocity of the electrons in GaAs cannot exceed a

velocity called the saturated drift velocity, approximately 1.3×10^7 cm/s.

If V_{ds} is increased beyond the value that causes velocity saturation (usually only a few tenths of a volt), the electron concentration rather than velocity must increase in order to maintain current continuity. Accordingly, a region of electron accumulation forms near the end of the gate. Conversely, after the electrons transit the channel and move at saturated velocity into the wide area between the gate and drain, an electron depletion region is formed. The depletion region is positively charged because of the positive donor ions remaining in the crystal. As V_{ds} is increased further, as shown in Figure 2.4(c), progressively more of the voltage increase is dropped across this region to enforce the electrons to cross it and less is dropped across the unsaturated part of the channel. This region is called a dipole layer or charge domain. Eventually, a point is reached where further increase in V_{ds} is dropped entirely across the charge domain and does not substantially increase the drain current. At this point, the electrons move at saturated drift velocity over a large part of the channel length. When the MESFET or HEMT is operated in this manner, which is the normal mode of operation for small-signal devices, it is said to be in its saturated region.

Accurate models may include the effect of the charge domain in some way. Therefore, some models include a capacitor between the drain and the gate-source equivalent circuit to account for the charge domain.

The I-V characteristic curves of a MESFET or HEMT device are shown in Figure 2.5 [1] for an ideal and actual MESFET or HEMT. The curves are plotted for different values of V_{gs}. It is obvious that the real I-V curve exhibits finite positive slope in the saturation region. Many reasons may be responsible for this phenomenon. One of the most dominant reasons in a short gate device is the carrier injection into the semi-insulating substrate. This finite slope is the source of the finite output conductance in a MESFET or HEMT model.

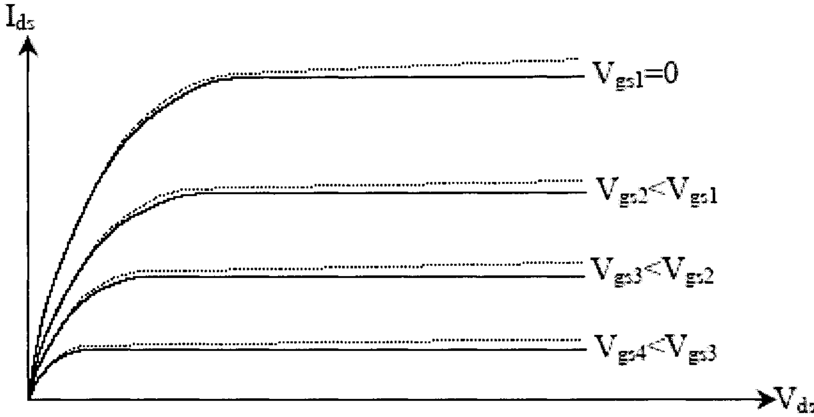

Figure 2.5: I-V Characteristic curves for a MESFET or HEMT device for different values of V_{gs}; ideal current is drawn in solid curve while dashed curve indicates the real current.

2.3 MESFET and HEMT Small-Signal Models

The small-signal model of MESFET and HEMT is extremely important for active microwave circuit operation. It provides a vital link between measured S-parameters and the electrical processes occurring within the device. Each of the elements in the equivalent circuit provides a lumped element approximation to some aspect of the device physics. A properly chosen topology, in addition to being physically meaningful, must provide an excellent match to measured S-parameters over a very wide frequency range. When element values are properly extracted, the model is valid above the frequency range of the measurements, providing the possibility of extrapolating device performance to frequencies beyond some equipment's measurement capabilities. In addition, equivalent circuit element values can be scaled with gate width, thereby enabling the designer to predict the S-parameters of different size devices from a given foundry. The ability to include device gate width scaling as part of the circuit design process is important in MMIC design applications.

A fairly standard MESFET-HEMT equivalent circuit topology is shown in Figure 2.6 [1]. Although other circuit topology involving additional elements have been described in many literatures, the topology of figure 2.6 has been shown to provide an excellent match to measured S-parameters. Another advantage for this topology is that the elements can be uniquely extracted. Figure 2.7 [1] [5] illustrates the physical origin of the equivalent circuit in this general model. A brief discussion follows of each equivalent circuit element and its role in modeling the device physics.

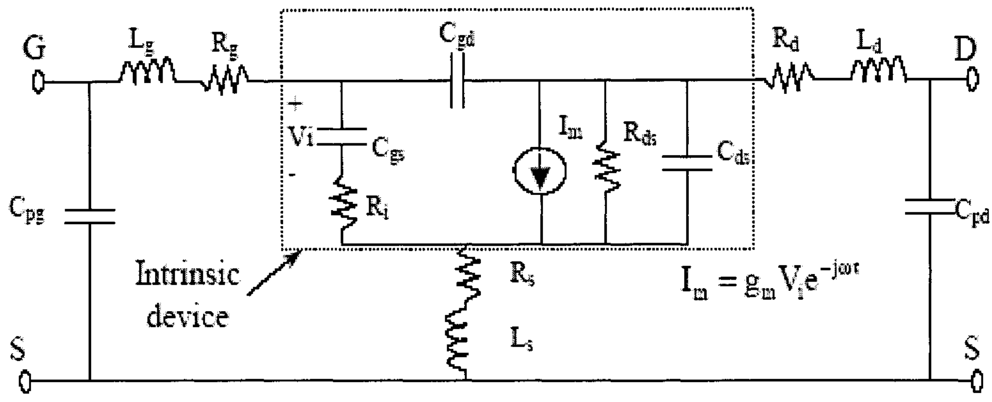

Figure 2.6: Standard MESFET-HEMT equivalent circuit

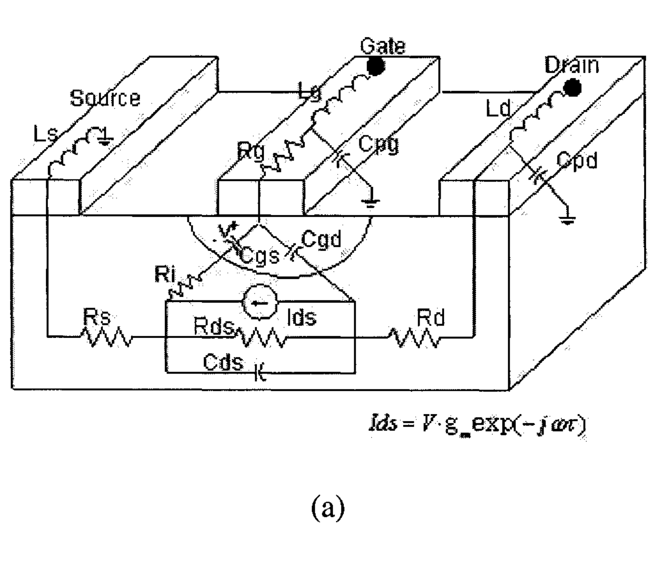

(a)

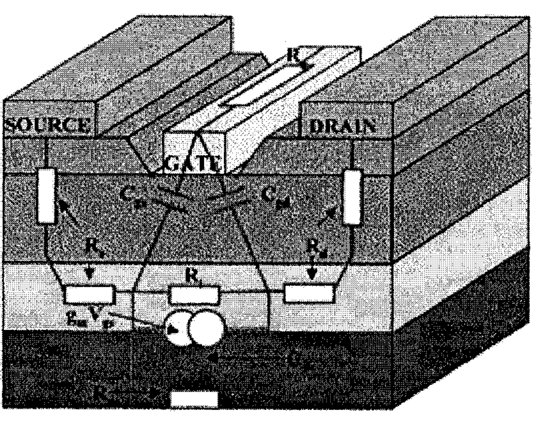

(b)

Figure 2.7: The physical origin of the equivalent circuit for (a) MESFET (b) HEMT

The physical meaning of each element is clearly interpreted. R_g is the ohmic resistance of the gate while R_s and R_d are the source and drain ohmic resistances, respectively. L_g is the inductance of the gate while L_d and L_s are the inductances of the source and the drain metallization, respectively. R_i is the resistance of the semiconductor region under the gate, between the source and the channel. C_{ds} is the drain-source capacitance, which is dominated by geometric capacitance and is often treated as a constant. C_{gs} and C_{gd} are the channel capacitances which in general are nonlinear. I_{ds} is the controlled drain-source current from which the transconductance g_m, transit time delay τ, and output resistance R_{ds} can be calculated. C_{pg} and C_{pd} are the pad capacitances of both gate and drain, respectively.

If voltages are expected to be great enough to forward–bias or reverse avalanche breakdown the gate junction, one can include diodes in parallel with C_{gs} and C_{gd}. Such diodes are of limited practical value, however, because operation with gate-channel avalanche breakdown or high values of rectified gate current usually destroys the device.

Some of the model elements are nonlinearly dependent on the internal voltages V_{gs} and V_{ds}. Others are linear, or can be approximated as linear elements. I_{ds}, C_{gs}, and C_{gd} are usually nonlinear elements for their strong dependence on V_{gs} and V_{ds}.

On the other hand, the circuit model can be divided into two parts: the extrinsic parameters and the intrinsic parameters. The intrinsic parameters characterize the active region under the gate and are functions of biasing conditions, whereas the extrinsic parameters depend, at least to a first approximation, only on the technological parameters. The intrinsic parameters include C_{gs}, R_i, C_{gd}, g_m, τ, R_{ds}, and C_{ds} whereas the extrinsic parameters include all other elements in the model C_{pg}, C_{pd}, R_g, R_d, R_s, L_g, L_d, and L_s. Some of the intrinsic elements can be assumed linear for their weak dependence on the internal voltages; those elements are R_i, τ, and C_{ds}. In contrast, some of the extrinsic elements may be nonlinear if their dependence on the internal voltages is significant. We will discuss the significance of each element of the small-signal model in the following subsections.

2.3.1 Parasitic Inductances

The parasitic inductances are the inductances of the extrinsic part of circuit model which include L_g , L_d and L_s . The parasitic inductance arises primarily from metal contact pads deposited on the device surface. Because these values are dependent on the surface features of the device, they are essentially equal for MESFETs and HEMTs. Typically, L_g and L_d are on the order of few pH. The source inductance is often smaller. In many cases, bonding inductances are on the order of few nH and dominate the device parasitics [1].

2.3.2 Parasitic Resistances

The parasitic resistances R_g, R_d, and R_s are also included in the extrinsic part of the circuit model. The resistance R_g and R_d are included to account for the contact resistance of ohmic contacts as well as any bulk resistance leading up to the active channel. The gate resistance R_g results from the metallization resistance of the gate Schottky contact. All three resistances are on the order of few ohms for a modern microwave device. Also, R_s and R_d tend to be slightly less in HEMTs than in MESFETs. Although measurements of R_s and R_d indicate a slight bias dependence in these values, they are held constant in the large-signal models commonly available in the commercial simulators nowadays. However, accurate models should take into consideration their bias dependence, especially if their values are significantly depends on the bias voltages. All parasitic resistance values can be estimated either from forward DC conduction measurements or directly from S-parameters using an optimization technique [1]. However, the latter technique is preferable for more accurate results because it calculates the resistance values from typical high frequency data at the bias point of concern.

2.3.3 Pad Capacitances

These capacitances are also included in the extrinsic part of the circuit model. The pad capacitances come from the stray capacitance between the metal pads. The pad capacitance consists of crossover capacitance of the metal lines and the capacitance

between the pad and the back face of the semi-insulating substrate, which is usually connected to the source terminal. However, the crossover capacitance is usually much smaller than the substrate capacitance [4]. Two pad capacitances are often included in the circuit model: C_{pg} gate pad capacitance and C_{pd} drain pad capacitance. C_{pg} is the capacitance between gate and source pads whereas C_{pd} is the capacitance between the drain and source pads. Although the pad capacitance between gate and drain pads can be included in the circuit model, it is usually neglected for its small value compared to other capacitance values in the model. C_{pg} and C_{pd} are typically on the order of a few tens of fF. Nevertheless, they may be omitted from many models in the literature if their values are insignificant or if their effect can be accounted for throughout other capacitive elements in the circuit. On the other side, pad capacitances may be placed in two different positions in the model, either on the most outer terminals of the model as seen in Figure 2.6 or between the corresponding parasitic inductances and resistances. Pad capacitance values depend on the utilized layout. Pad capacitances can be estimated either from special structures without the active device.

2.3.4 Intrinsic Capacitances

Intrinsic capacitances are indicated in the model by C_{gs}, C_{gd} and C_{ds}. C_{gs} and C_{gd} model the change in the depletion charge with respect to the gate-source and gate-drain voltages, respectively. Figure 2.9 [1] shows the depletion region beneath the gate for a symmetric structure where the gate is located directly in the middle of the gap between the source and the drain terminals. Figure 2.9 (a) represents the symmetric bias case in which $V_{gs} = V_{gd}$. Figure 2.9 (b) represents the case in which the gate-drain reverse bias is greater than the gate-source reverse bias. This case represents the normal MESFET bias conditions in most applications. Figure 2.9 is only used to clarify the physics of both C_{gs} and C_{gd}. However, the discussion is also valid for any geometrical structure and bias conditions.

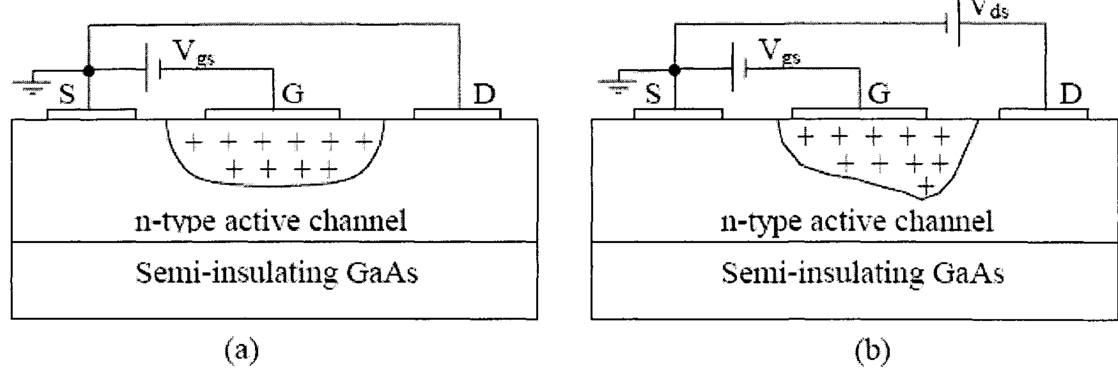

Figure 2.8: Depletion region shapes for different applied bias voltage: (a) gate-source voltage is equal to gate-drain voltage, (b) gate-drain reverse bias is greater than gate-source reverse bias.

The distribution of the depletion charge is symmetric with respect to the drain and source in Figure 2.8 (a). On the other hand, the depletion charge extends deeper at the drain end of the gate than at the source end of the gate, and it also extends closer to the drain than to the source. This charge redistribution in the depletion region with the bias voltage variation identifies the two depletion capacitances C_{gs} and C_{gd}. The charge of the depletion region is shared between C_{gs} and C_{gd}. Thus, they should be defined carefully as [1]:

$$C_{gs} = \left.\frac{dQ_g}{dV_{gs}}\right| V_{gd} = \text{constant} \tag{2.1a}$$

$$C_{gd} = \left.\frac{dQ_g}{dV_{gd}}\right| V_{gs} = \text{constant} \tag{2.1b}$$

Under normal operation conditions, V_{gs} and V_{ds} are the DC controlling bias voltages. For this reason, the gate to source capacitance is often defined as:

$$C_{gs} = \left.\frac{dQ_g}{dV_{gs}}\right| V_{ds} = \text{constant} \tag{2.2}$$

Equations (2.1a) and (2.2) are not equivalent, but slightly different quantities. The distinction is usually minor, but can be significant if calculations are based on a

physically based model in which the depletion charge is defined by a mathematical expression. When capacitance is determined by measurements or derived from empirical models, the capacitance definition given by equations (2.1a) and (2.2) are not applied. Instead, the capacitance values are defined in terms of an equivalent circuit, and so, the values are determined to accurately predict the device behavior [1]. Thus, it does not matter in our thesis which definition of C_{gs} should be taken because C_{gs} is calculated from S-parameter measurements. One might also have noticed that the voltages indicated in the capacitance definitions are the internal voltages, and not the external terminal voltages.

Under typical MESFET bias conditions, C_{gs} is larger than C_{gd} because it models the change in depletion charge resulting from fluctuations in the gate-source voltage while the gate-source reverse bias voltage is less than the gate-drain reverse bias voltage. It is well known from depletion capacitance analysis that the depletion capacitance decreases as the reverse junction voltage increases [1]. For this reason and under normal bias conditions, the gate-drain capacitance C_{gd} is considerably smaller in magnitude than C_{gs}; nevertheless, C_{gd} is critical for obtaining accurate S-parameter predictions.

The drain-source Capacitance C_{ds} is included in the equivalent circuit to account for geometric capacitance effects between the source and drain electrodes. It is usually not considered to be bias dependent for the purposes of device modeling. Values for C_{gs} are typically on the order of 1 pF/mm gate width under normal MESFET bias conditions. The values of C_{gd} and C_{ds} are about one tenth of the value of C_{gs}. Moreover, because of symmetry, C_{gs} and C_{gd} are approximately equal for V_{ds}=0 V [1].

2.3.5 Charging Resistance

Although the charging resistance R_i represents the intrinsic resistance under the gate between the source and the channel, it is included primarily to improve the match to S_{11}. For many devices, however, the presence of R_g is sufficient to match the real part of S_{11}. So, R_i is difficult to extract and is of questionable physical significance [1]. The difficult discrimination between R_i and R_g in the extraction process will be discussed in Chapter 4, also, some results will also be introduced.

2.3.6 Transconductance

The intrinsic gain mechanism of the FET is provided by the transconductance. The transconductance g_m is a measure of the incremental change in the output current I_{ds} for a given change in the internal input voltage V_{gs}. The internal input voltage is the voltage across the gate source junction. In other words, the device transconductance is defined as the slope of the $I_{ds} - V_{gs}$ characteristics with the drain-source voltage held constant. The mathematical statement of this definition can be expressed as [1]:

$$g_m = \left. \frac{\partial I_{ds}}{\partial V_{gs}} \right|_{V_{ds} = \text{constant}} \tag{2.3}$$

The transconductance of the device is one of the most important indicators of the device quality for microwave and millimeter wave applications. When all other characteristics are equal, a device with high transconductance will provide greater gains and superior high frequency performance. The transconductance suffers from what is called low frequency dispersion. The low frequency dispersion is the phenomenon of a parameter variation at low frequencies. The low frequency dispersion takes place as a result of the deep levels in the device structure. So, it significantly depends on the semiconductor material quality and fabrication processes.

Therefore, the transconductance varies with frequency below a frequency of about 1 MHz. Transconductance values vary directly with gate width and inversely with gate length for both MESFETs and HEMTs. In practice, the transconductance of HEMTs is slightly higher than that of MESFETs with equivalent geometries [1].

2.3.7 Transconductance Delay

The transconductance cannot respond instantaneously to changes in the gate-source voltage. The delay inherent to this process is described by the transit time (transconductance delay) τ. Physically, the transconductance delay represents the time it takes for the charge to redistribute itself after a fluctuation of the gate voltage. Typical values of τ are on the order of 1 pSec. From physical considerations, transconductance delay is expected to be shorter in HEMTs than in MESFETs and tend to decrease with decreasing gate length [1].

2.3.8 Output Conductance:

The output conductance is a measure of the incremental change in output current I_{ds} with the output voltage V_{ds}. So, it can be defined as the slope of the I_{ds}-V_{ds} characteristics with the gate-source voltage held constant. Mathematically, the output conductance and resistance can be defined by [1]:

$$g_{ds} = \frac{1}{R_{ds}} = \left.\frac{\partial I_{ds}}{\partial V_{ds}}\right|_{V_{gs} = \text{constant}} \tag{2.4}$$

The output conductance of the device is an important characteristic in analog applications. It plays a significant role in determining the maximum voltage gain attainable from a device and is extremely important for determining optimum output matching properties. In general, it is desirable to have a device with extremely high output resistance, or equivalently, low output conductance. Values of g_{ds} are on the order of 1 mS/mm gate width at typical amplifier biases. Also, as gate length is reduced, output conductance tends to increase. The low frequency dispersion is more significant in output conductance than in the transconductance. The RF output conductance can be more than 100% higher than the DC output conductance. The RF values for both transconductance and output conductance are of primary concern for small-signal modeling applications while both RF and DC values are important for accurate large-signal modeling [1].

2.4 Literature Review

The basic equivalent circuit model shown in Figure 2.6 has been the key for many researches and it is commonly used in CAD. Some researchers modified it slightly to increase its accuracy or to ease its parameter-extraction process. In this section, we will review the existing works done to extract the parameters of this model.

Two main trends for parameter extraction process were typically followed by previous researchers. The first trend is to extract the extrinsic parameters C_{pg}, C_{pd}, R_g, R_d, R_s, L_g, L_d, and L_s, then the remaining (intrinsic) parameters are extracted analytically (or by optimization) [7]-[11]. The second trend is to extract all the parameters using an optimization algorithm [12]-[15].

Minasian [7] proposed a simplified model working up to 10 GHz. In his model, he

removed all the extrinsic parameters. The relation between his model and the more complex model was presented and the characteristics of both models were compared. The elements values were calculated analytically from the measurements and his simple model showed good agreement with the measured parameters up to 10 GHz for 1 μm gate length. However, the values of the model's elements did not represent their physical values because they had to compensate for the removed elements.

Fukui [8] described a technique to determine the basic properties of the active channel of a GaAs MESFET along with the parasitic resistances R_g, R_d, and R_s. His technique was based on the forward I-V characteristics of a gate junction while source and drain are connected together, source is alone, and drain is alone. His technique was employed by some authors after him to extract the complete model's parameters where parasitic resistances are known. Nevertheless, the values of R_d and R_s are bias dependent. As a result, their values at reverse gate bias, where most of the applications are, are different from those extracted by Fukui's method. Moreover, The DC value of the gate resistance obtained from the Fukui measurements is not directly applicable to the small-signal microwave equivalent circuit model because of the skin effect [16].

Diamant et *al.* [9] exploited that MESFET at zero drain-source voltage is fairly simpler than that at normal bias voltages. For zero drain-source voltage, the region under the gate can be described by a distributed uniform RC transmission line. They derived analytical expressions for Z-parameters of the model to determine the parasitic elements. The parasitic inductances were calculated by optimizing them over the frequency range of interest to best fit the imaginary parts of Z-parameters data at any gate bias voltage. The parasitic resistances were calculated from the real parts of Z-parameters under different gate bias voltages. Gate bias voltages should be chosen such that a channel opening is higher than 20%.

Dambrine et *al.* [10] proposed a systematic and fast method to determine the small-signal equivalent circuit of a MESFET. This method consisted of a direct determination of all parasitic elements as well as the pad capacitances. The parasitic elements were calculated first from S-parameters measured at zero drain-to-source bias voltage with the gate forward biased. The pad capacitances were determined from S-parameters measured at zero drain-to-source bias with a gate bias voltage lower than the pinch-off voltage. The knowledge of these parasitic element values allowed determining the intrinsic small-signal parameters after a few simple matrix manipulations to remove the parasitics from the data. This method implied some approximations so that all parameters were extracted

from data at a low frequency band. Moreover, the additional relation of parasitic drain and source resistances were needed to be determined by conventional method [8] or by DC measurement [17].

Eric Arnold et *al.* [11] developed a method to extract the intrinsic element values and parasitic inductance values from low frequency data by comparing the resulting Z-parameters with the extrinsic measured Z-parameters provided the parasitic resistance values are known. This method is not complete because the parasitic resistance values need to be determined beforehand and it is also limited by the low frequency range.

Kondoh [12] developed, for the first time, an optimization algorithm to extract a 13-element GaAs MESFET equivalent circuit model from measured S-parameters. The MESFET model was extracted by a least-squares fitting of measured S-parameters to those calculated from the equivalent circuit. This algorithm solves the problem iteratively. Each iteration cycle was divided into eight consecutive optimization steps. In each step, only a group of selected elements in the equivalent circuit was optimized to fit a specific S-parameter over a specific frequency range. This routine involved eight error functions to be minimized. This algorithm took into account the difference in standard deviations of errors in individual measured S-parameters which resulted in more modeling accuracy. However, it suffers from a local-minimum problem that the solution may be trapped in a local minimum. The sequence of steps, in each iteration, as well as the assignment of the optimized elements to the corresponding S-parameters was concluded experimentally with no analytical evidence.

Lin and Kompa [13] introduced a new concept for an optimization procedure applied to the FET model parameter extraction. In this technique, the elements are divided into two sets of optimization variables. The objective function is minimized by a bidirectional search technique. The extrinsic elements comprise the first set of optimization parameters whereas the intrinsic elements comprise the second set. In each iteration, the extrinsic parameters are updated; then, the Y-parameters of the intrinsic plane are calculated which are employed to calculate the intrinsic elements by simple weighted polynomial curve fitting. An improved simplex method was used. Although this technique shows good results to avoid the local minima problem and to desensitize the extracted values to the measurement error, it depends on the starting values. Therefore, the starting values should be generated from the model at pinch-off bias. This ensures that the minimum is as close to the starting point as possible. The authors suggested the use of l_1-norm for the external objective function as it showed faster convergence.

Shirakawa et *al.* [14] proposed a technique to determine a HEMT equivalent circuit. Intrinsic elements are written in terms of extrinsic elements using a conventional analytical parameter transformation technique. The authors used the variance of the intrinsic elements as an optimization criterion for the first time. The extrinsic elements are the optimization parameters which are iteratively determined to minimize the variance of the intrinsic elements over a wide frequency band up to 62.5 GHz. Another optimization criterion for the discrepancy between the measured and the calculated S-parameters were considered.

Ooi et *al.* [15] applied the Shirakawa's method [14] to MESFET. The intrinsic elements and one of the extrinsic elements are described as functions of the remaining extrinsic parameters. The optimization search space was reduced from 6 parameters to 5 parameters. They presented a comparison in terms of both accuracy and speed between the proposed method and some other methods on a 400μm gate-width MESFET over 0.5-26.5 GHz frequency band. Both Shirakawa's method and Ooi's method suffer from uniqueness problem between the resistive elements of the model over limited frequency bands in the presence of the unavoidable measurement errors.

As we have seen from the above survey, no clear technique was proposed to extract MESFET or HEMT model elements accurately and consistently. Each proposed technique has some advantages and disadvantages. In the following chapters, we will deal with some techniques in details showing advantages and disadvantages of each one. Some solutions to these problems will be proposed.

Chapter 3. Noise Models

Noise is usually generated by the random motions of charges or charge carriers in devices and materials. Such motions can be caused by any of several mechanisms, leading to various source of noise [18].

- ***Thermal noise*** is the most basic type of noise, being caused by thermal vibration of bound charges. Also known as Johnson or Nyquist noise.
- ***Shot noise*** is due to random fluctuation of charge carriers in an electron tube or solid-state device.
- ***Flicker noise*** occurs in solid-state components and vacuum tubes. Flicker noise power varies inversely with frequency, and so is often called 1/f-noise.
- ***Plasma noise*** is caused by random motion of charges in an ionized gas, such as plasma, the ionosphere, or sparking electrical contacts.
- ***Quantum noise*** results from the quantized nature of charge carriers and photons; often insignificant relative to other noise sources.

In electrical systems *noise* is the internal generation of signals that causes degradation from the desired or theoretical response. Fluctuations in signal phase, amplitude, and spectral content are forms of noise. The physical properties of materials result in various classes of noise, including white, phase, etc. The *white* refers to the distribution in the spectral content. For MESFET and HEMT, particularly in amplifiers and mixers, thermal noise is a critical concern while other types of noise can be neglected [1].

Thermal noise originates because heat in the electrical device provides energy to the carriers causing random fluctuations in their movement. This noise generated only in systems or circuit elements that dissipate power (resistive); purely reactive elements (ideal capacitors, inductors, and transmission lines) do not generate noise. The RMS thermal voltage produced by a thermal source such as a resistor R is given by [1]:

$$V_N = (4kTBR)^{1/2} \tag{3.1}$$

where

k = Boltzmann's constant ($1.374 \times 10^{-23}\, J/K$)
T = temperature in kelvin, and
B = bandwidth in hertz

The noise voltage described in equation (3.1) can also be discussed in terms of power. The maximum power generated by a resistor (Figure 3.1) occurs for a matched load and is given by the simplified expression

$$p_N = \frac{V_N^2}{4R} = kTB \tag{3.2}$$

where

p_N = the maximum power delivered to the matched load

k = Boltzmann's constant ($1.374 \times 10^{-23}\, J/K$)

T = temperature in kelvin, and

B = bandwidth in hertz

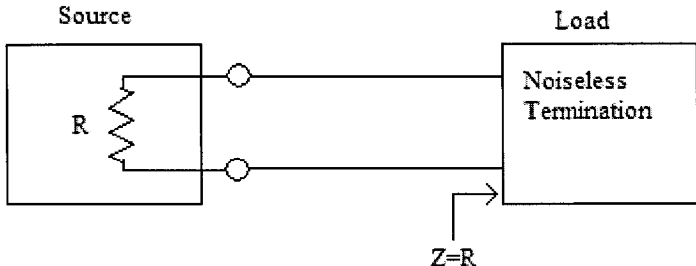

Figure 3.1 The maximum transfer of noise power generated in a resistor requires a matched load.

When the load is not matched to the resistor (Figure 3.2), the power delivered to the load is less than maximum and is given by

$$P_N = (1-|\Gamma|^2)kTB \tag{3.3}$$

Here Γ is the voltage reflection coefficient.

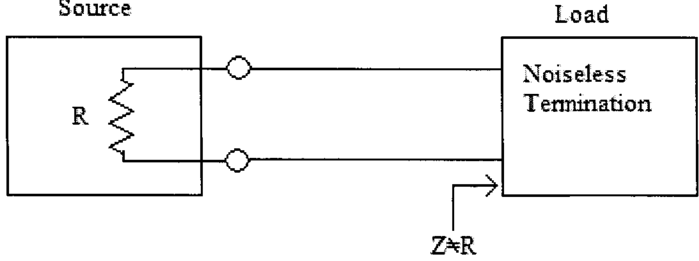

Figure 3.2 An unmatched load reflects noise power

3.1 Noise in linear Two-ports

In a linear passive two-port network, noise arises only from the losses in the two-port; thermodynamic considerations indicate that such losses result in the random changes that we call noise. When the two-port contains active devices, such as transistors, there are other noise mechanisms that are present. A very important consideration in a system is the amount of noise that it adds to the transmitted signal. This is often judged by the ratio of the output signal power to the output noise power (S/N). The ratio of signal plus noise power to noise power [(S+N)/N] is generally easier to measure, and approaches S/N when signal is large [19].

In the characterization of a two-port, it is important to know the amount of noise added to a signal passing through it. An important parameter for expressing this characteristic is noise factor. The signal energy coming from a generator or antenna is amplified or attenuated in passing from the input to the output of a two-port, as is the noise that accompanies the input signal energy. The noise factor of a system is defined as the ratio of signal-to-noise ratio available at input and output [19].

$$F = \frac{(S/N)_{input}}{(S/N)_{output}} \geq 1 \tag{3.4}$$

When this ratio of powers is converted to decibels, it is generally referred to as noise figure, which is defined as:

$$F_N = 10\log_{10} F \tag{3.5}$$

For an amplifier with the power gain G, the noise factor can be obtained as

$$F = \frac{S_i / N_i}{GS_i / G(N_i + N_a)} = 1 + N_a / N_i \tag{3.6}$$

where N_a is the additional noise power added by the amplifier referred to the input. Since the thermal noise power caused by internal system can also be expressed by the effective noise temperature, the equation above may be rewritten as

$$F = 1 + \frac{kT_e B}{kT_0 B} = 1 + \frac{T_e}{T_0} \tag{3.7}$$

where T_e is the effective noise temperature of the system or circuit and T_0 is the temperature of the generator resistor (usually the room temperature, i.e. 290 K).

In non-ideal systems (systems containing resistors that act only as thermal sources), the noise factor can be expressed by [1]

$$F = 1 + \frac{T_e}{T_0}\left(\frac{1}{G} - 1\right) \tag{3.8}$$

In systems containing only thermal sources, the input and output noise is the same ($N_i = N_0$), while the output signal S_0 is attenuated.

3.1.1 Noise Description in Two-Port Networks

Based on the convention by Rothe and Dahlke [20], any noisy linear two-port can be in the form in Figure 3.3 (a). This general case of noisy two-port can be redrawn showing noise sources at the input and at the output. Figure 3.3 (b) shows this in admittance form. (c) is in impedance form, and (d) is in ABCD form. The internal noise sources are assumed to produce very small currents and voltages, and we assume that linear two-port equations are valid. The internal noise contributions have been expressed by using external noise source where $I_{n1}, I_{n2}, V_{n1}, V_{n2}, V_n$, I_n are the external noise sources.

1) For admittance form, the expression is written by

$$\begin{bmatrix} I_1 \\ I_2 \end{bmatrix} = \begin{bmatrix} y_{11} & y_{12} \\ y_{21} & y_{22} \end{bmatrix} \begin{bmatrix} V_1 \\ V_2 \end{bmatrix} + \begin{bmatrix} I_{n1} \\ I_{n2} \end{bmatrix} \tag{3.9}$$

and the corresponding noise parameters are:

$$G_1 = \frac{\overline{|I_1|^2}}{4kT_0 B} \qquad G_2 = \frac{\overline{|I_2|^2}}{4kT_0 B}$$

$$\rho = \frac{\overline{I_1 * I_2}}{\sqrt{\overline{|I_1|^2 |I_2|^2}}} \tag{3.10}$$

Where G_1 and G_2 are the equivalent noise conductance in the port 1 and 2. ρ is the correlation coefficient between two noise source i_1 and i_2. T_0 is the standard or room temperature of 290 K, and B is the bandwidth.

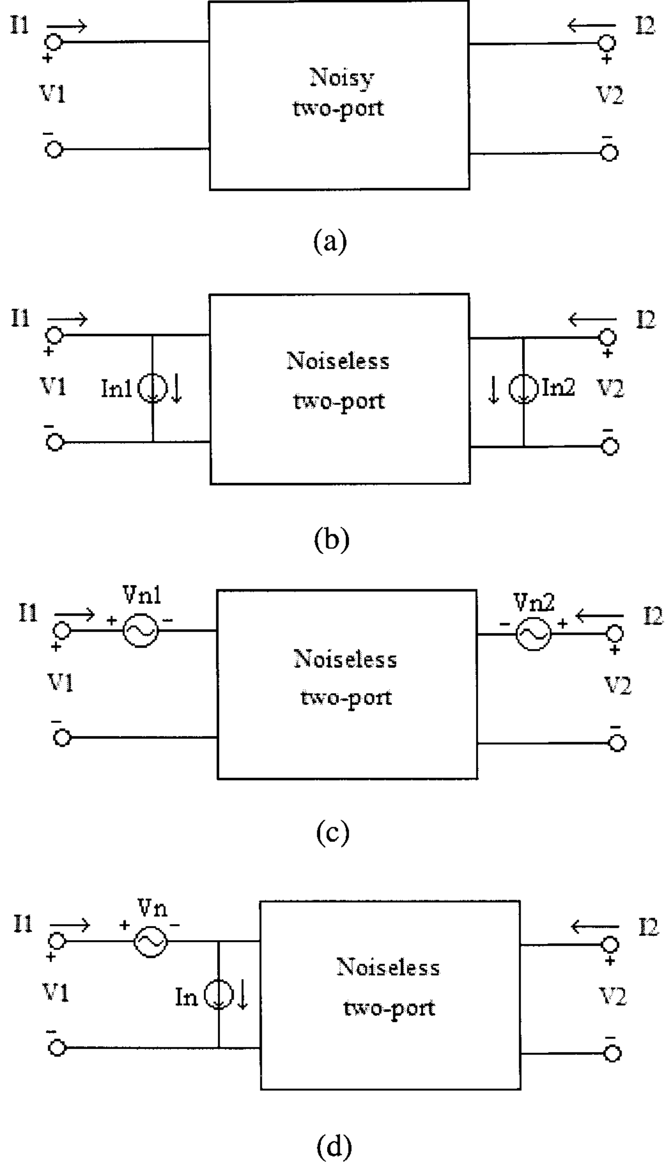

Figure 3.3: Noisy linear two-ports: (a) general form (b) admittance form (c) impedance form (d) ABCD form.

2) For impedance form, the expression is written by

$$\begin{bmatrix} V_1 \\ V_2 \end{bmatrix} = \begin{bmatrix} z_{11} & z_{12} \\ z_{21} & z_{22} \end{bmatrix} \begin{bmatrix} I_1 \\ I_2 \end{bmatrix} + \begin{bmatrix} V_{n1} \\ V_{n2} \end{bmatrix} \tag{3.11}$$

and the corresponding noise parameters are:

$$R_1 = \frac{\overline{|V_1|^2}}{4kT_0B} \qquad R_2 = \frac{\overline{|V_2|^2}}{4kT_0B}$$

$$\rho = \frac{\overline{V_1 * V_2}}{\sqrt{\overline{|V_1|^2|V_2|^2}}} \tag{3.12}$$

Where R_1 and R_2 are the equivalent noise resistance in the port 1 and 2. ρ is the correlation coefficient between two noise source V_1 and V_2. T_0 is the standard temperature of 290 K, and B is the bandwidth.

3) For ABCD form, the expression is written by

$$\begin{bmatrix} V_1 \\ I_1 \end{bmatrix} = \begin{bmatrix} A & B \\ C & D \end{bmatrix} \begin{bmatrix} V_2 \\ I_2 \end{bmatrix} + \begin{bmatrix} V_n \\ I_n \end{bmatrix} \tag{3.13}$$

and the corresponding noise parameters are:

$$R_n = \frac{\overline{|V_n|^2}}{4kT_0B} \qquad g_n = \frac{\overline{|I_n|^2}}{4kT_0B}$$

$$\rho = \frac{\overline{V_n * I_n}}{\sqrt{\overline{|V_n|^2|I_n|^2}}} \tag{3.14}$$

Where R_n is the equivalent noise resistance and g_n is the equivalent noise conductance. ρ is the correlation coefficient between two noise source $V_{n,}$ and I_n. T_0 is the standard temperature of 290 K, and B is the bandwidth.

4) In microwave applications, the noisy linear two-port can also be represented by noise wave and scattering parameters [21], which is shown in Fig 3.4

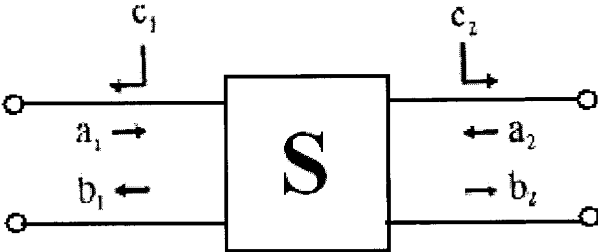

Figure 3.4: noisy linear two-ports in S-parameters form.

The expression for the S-parameters form can be written by

$$\begin{pmatrix} b_1 \\ b_2 \end{pmatrix} = \begin{pmatrix} s_{11} & s_{12} \\ s_{21} & s_{22} \end{pmatrix} \begin{pmatrix} a_1 \\ a_2 \end{pmatrix} + \begin{pmatrix} c_1 \\ c_2 \end{pmatrix} \tag{3.15}$$

where c_1 and c_2 are noise waves. The correlation matrix C_s can be expressed by

$$C_s = \begin{pmatrix} \overline{|c_1|^2} & \overline{c_1 c_2^*} \\ \overline{c_2 c_1^*} & \overline{|c_2|^2} \end{pmatrix} \tag{3.16}$$

where the overbar indicates time averaging with an implicit assumption of ergodicity and jointly wide-sense stationary processes. The vector representation can be written by

$$b = Sa + c \tag{3.17}$$

and

$$C_s = \overline{cc^{\dagger}}$$

where the dagger indicates the Hermitian conjugate.

3.1.2 Representation of Noise Parameters

When a two-port component contains active devices such as a MESFET, HEMT, or diode, noise is generated by these devices and is added to the output of the two-port device. The generation of this noise is typically modeled using an equivalent circuit for the device that contains current or voltage sources to model the noise effects. These internal noise sources contribute only to the overall noise of the two-ports and not to the gain. However, because the noise sources are internal to the device, the overall noise is affected by the matching circuitry connected to the FET [1].

Figure 3.5 is a two-port network for a device with a circuitry connected at the input and a load connected at output.

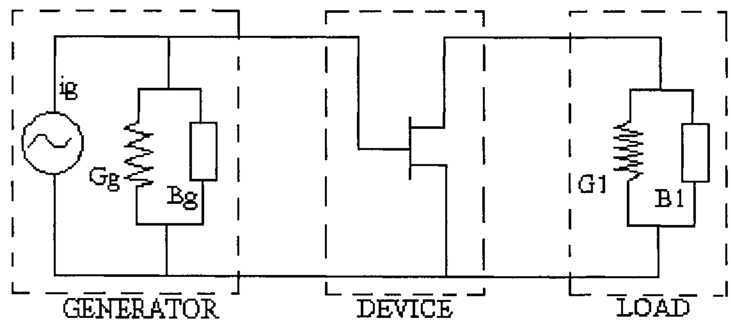

Figure 3.5: A Circuitry is connected at the input of a device

There are three noise figure expressions in the linear two-port circuit [19]:

1) Generator impedance form

$$F = F_{\min} + \frac{G_n}{R_g}[(R_g - R_{opt})^2 + (X_g - X_{opt})^2] \tag{3.18}$$

where

$F_{\min}$ = minimum value of F with respect to the generator impedance Zg

$Z_{opt} = R_{opt} + jX_{opt}$ is the optimal generator impedance value at which F=Fmin, and

G_n = equivalent noise conductance of the DUT (device under test)

2) Generator admittance form

$$F = F_{\min} + \frac{R_n}{G_g}[(G_g - G_{opt})^2 + (B_g - B_{opt})^2] \tag{3.19}$$

where

$F_{\min}$ = minimum value of F with respect to the generator admittance Yg

$Y_{opt} = G_{opt} + jB_{opt}$ is the optimal generator admittance value at which F=Fmin

R_n = equivalent noise resistance of the DUT (device under test)

and

$$R_n = G_n \mid Z_{opt} \mid^2$$

3) Source reflection coefficient form

$$F = F_{\min} + \frac{4R_n \mid \Gamma_g - \Gamma_{opt} \mid^2}{Z_0(1 - \mid \Gamma_g \mid^2) \mid 1 + \Gamma_{opt} \mid^2} \tag{3.20}$$

where

$$\Gamma_g = \frac{Y_0 - Y_g}{Y_0 + Y_g}$$

Y_0 is a reference admittance. Z_0 is a reference resistance.

$$\Gamma_{opt} = \frac{Y_0 - Y_{opt}}{Y_0 - Y_{opt}}$$

Equations (3.18) through (3.20) provide the basis for evaluating the noise figure when external circuitry is connected to the input of a device. The noise performance of any linear two-port can be determined if the values of the four noise parameters, $F_{\min}$, R_n, G_{opt} and B_{opt} are known.

The meaning of Γ_{opt} and $F_{\min}$ are obvious from their definitions. The parameter R_n is useful as an indication of the dependence of $F_{\min}$ on the source admittance Y_g. A low value of R_n is desirable for most circuit applications because this allows source

admittance considerably different from Y_{opt} to be used without seriously degrading the noise figure.

The noise parameters $F_{\min}$ R_n and Γ_{opt} are properties only of the active device and are independent of any external circuitry connected to the device. For MESFET and HEMT, they depend on temperature, frequency, drain-source current, and to a much lesser extent, drain-source voltage. They also depend on the physical properties of the device, including geometrics and material properties of the structure.

3.1.3 Noise Figure of Cascaded Networks

If a number of two-port networks are cascaded, the total noise figure of the long chain of cascaded circuits can be written by [19]

$$F = F_1 + \frac{F_2 - 1}{G_1} + \frac{F_3 - 1}{G_1 G_2} + \frac{F_4 - 1}{G_1 G_2 G_3} + \cdots \qquad (3.21)$$

where $F_1, F_2, \cdots$ are noise figures of cascaded circuits, and $G_1, G_2 \cdots$ are gain of correspond circuits. The Noise Measure M is defined as:

$$M = F - 1 \qquad (3.22)$$

3.2 Noise Models

Noise models are used to predict the noise figure for an arbitrary circuit topology, which incorporates a particular device, or to predict the ultimate noise performance of a device. Several modeling methods of the noise properties of MESFETs and HEMTs have been proposed. Some typical models will be discussed in the following sections.

3.2.1 Gupta noise model

Gupta et *al.* [22] proposed a model that simplifies the measurement requirements while improving the noise figure prediction. This model also eliminates assumptions required

of the earlier work related to circuit losses, noise correlations, and the functional form of the output noise current.

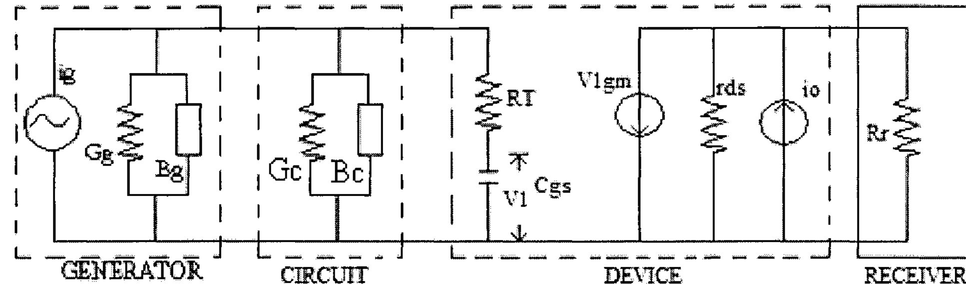

Figure 3.6 An equivalent circuit of a FET amplifier consisting of a generator, input circuit, an active device and a receiver (load).

Figure 3.6 illustrates the equivalent circuit model of an amplifier. $Y_c = G_c + jB_c$ is the admittance of the input matching circuit. The device is represented by a five-element equivalent circuit model consisting of input resistance $R_T = R_g + R_s + R_i$, gate-source capacitance C_{gs}, transconductance g_m, output resistance r_{ds}, and a white noise current source of spectral density S_{io}. The first four equivalent circuit element values can be determined using S-parameter measurements and the small-signal analysis.

Evaluation of spectral density of the white noise current source requires one noise measurement by directly using a low noise receiver, a band pass filter and a spectrum analyzer. The noise power generated by the device is dissipated in both the output resistance (r_{ds}) and the input resistance of the receiver (R_r).

From Figure 3.6, the noise power spectral density generated in the device can be calculated by [22]

$$S_{io}(f_L) = \frac{P_{out}(R_r + r_{ds})^2}{Br_{ds}^2 R_r} A^2 / Hz \tag{3.23}$$

where p_{out} is the measured noise power at receiver, B is the effective noise bandwidth, and f_L is the measurement frequency. The model can be simplified by assuming the operating frequency f_0 is significantly below the gain-bandwidth product of the device

$$\omega_0^2 C_{gs} R_T^2 << 1$$

From the circuit model shown in Figure 3.6, the input conductance and susceptance of the device can be expressed as [22]

$$G_{in} = \frac{\omega^2 C_{gs}^2 R_T}{1 + \omega^2 C_{gs}^2 R_T^2}$$

$$B_{in} = \frac{\omega C_{gs}}{1 + \omega^2 C_{gs}^2 R_T^2}$$

The four noise parameters can be calculated by following expressions [22]

$$R_n = S_{io}(f_L)\left(\frac{1 + \omega^2 C_{gs}^2 R_T^2}{4kTg_m^2}\right) \tag{3.24}$$

$$G_{opt} = \left(G_{in}^2 + \frac{G_{in}}{R_n}\right)^{1/2} \tag{3.25}$$

$$B_{opt} = -B_{in} \tag{3.26}$$

$$F_{\min} = 1 + 2R_n G_{in} + 2(R_n G_n + R_n^2 G_{in}^2)^{1/2} \tag{3.27}$$

When the measurement frequency f_L is high enough, the power spectral density S_{io} is frequency independent, particularly in the microwave frequency range. However, the power spectral density S_{io} is dependent on the bias state of the device. Thus, the noise prediction from the Gupta model is limited to the device bias conditions in which S_{io} is measured.

3.2.2 Fukui Noise Model

Another useful noise model was proposed by Fukui [23], [24]. By evaluating the FET noise properties, Fukui developed several empirical equations that describe the frequency dependence of the two-port FET noise parameters. This model is of particular advantage for low noise amplifier design applications, for which a convenient and quick method of predicting FET noise characteristics is needed.

Similar to the Gupta method, one noise figure measurement and a small-signal equivalent circuit model of the device is required, as shown in Figure 3.7. This method is also limited to the bias conditions of the device.

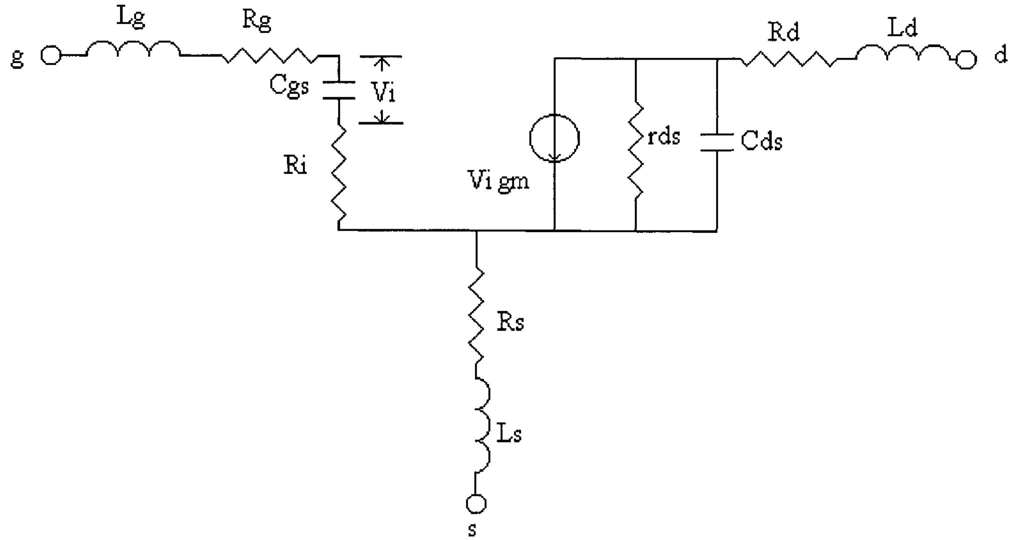

Figure 3.7: Equivalent model of a FET to predict noise performance based on the Fukui method.

The following equations are to predict the noise characteristics [23],[24]

$$F_{\min} = 1 + k_1 f C_{gs} \left(\frac{R_g + R_s}{g_m}\right)^{1/2} \tag{3.28}$$

$$R_n = k_2 / g_m \tag{3.29}$$

$$R_{opt} = \frac{k_3}{f}\left(\frac{1}{4 g_m} + R_s + R_g\right) \tag{3.30}$$

$$X_{opt} = \frac{k_4}{f C_{gs}} \tag{3.31}$$

where k_1, k_2, k_3, and k_4 are empirical fitting factors and f is the operating frequency.

From S-parameters measured at the same bias condition, small-signal element values for the noise model shown in Figure 3.7 can be extracted. Using measured noise parameters, the empirical fitting factors, k_1 through k_4, can be calculated in the frequency range.

Another important application of this model is that it allows a simple method of predicting the dependence of noise parameters by means of device geometry, such as gate width. For example, when the noise parameters are known for a given gate width Z, this model allows prediction of noise parameters for a FET scaled in width Z'. So the scaled noise parameters are given by [1]:

$$R_n^{'} = R_n / s_1 \tag{3.32}$$

$$X_{opt}^{'} = X_{opt} / s_1 \tag{3.33}$$

$$F_{\min}^{'} = 1 + \left(F_{\min} - 1\right)\left[\frac{1 + \left(R_g / R_s\right)\left(s_1 s_2\right)}{1 + \left(R_g / R_s\right)}\right]^{1/2} \tag{3.34}$$

$$R_{opt}^{'} = R_{opt}\left[\frac{1 + \left(4 g_m R_s\right) + \left(4 g_m R_g s_1 s_2\right)}{1 + 4 g_m R_s + 4 g_m G_g}\right] \tag{3.35}$$

$$s_1 = Z^{'} / Z \tag{3.36}$$

$$s_2 = \frac{Z^{'} / N^{'}}{Z / N} \tag{3.37}$$

where s_1 and s_2 are scaling factors that relate a known FET of width Z to a scaled one of width $Z^{'}$ by the equation given in [1]. N is the number of gate fingers of a given FET and N' is the number of gate fingers of a scaled FET.

The noise parameters of a device with a new gate width will be computed using equations (3.32) through (3.37) in the frequency domain. Fukui model gives good agreement over a wide bias range, but it does not provide any insight into the nature of a noise-generating mechanism in a FET as the fitting factors do not possess physical meanings.

3.2.3 Cappy Noise Model

Cappy et *al.* [25] relate the empirical fitting factor k_1 in equation (3.28) to physical parameters of the device. Additionally, $F_{\min}$ is expressed in a form given by

$$F_{\min} = 1 + k_f (f / f_T)[g_m (R_s + R_g)]^{1/2} \tag{3.38}$$

where k_f is an empirical fitting factor and f_T is the cutoff frequency given by

$$f_T = g_m /(2\pi C_{gs})$$

$$k_f = 2(\frac{\langle i_d^2 \rangle}{4kTg_m B})^{1/2}$$

where B is the bandwidth in Hz and i_d is the equivalent current generator for the drain noise and is given by

$$\langle i_d^2 \rangle = 4kTB\delta(\omega)(g_m / C_{gs})[L(\alpha Z + \beta I_{ds})] \quad (3.39)$$

with

$\delta(\omega) = (g_{ds}^2 + \omega^2 C_{gd}^2)/ g_{ds}^2$

$Z =$ FET gate width

$L =$ FET gat length

$\alpha, \beta =$ fitting factors

$g_{ds} = 1/ r_{ds}$

When $\delta(\omega)$ is close to unity, the $F_{\min}$ can be simplified to

$$F_{\min} = 1 + (8\pi)^{1/2} f[\frac{L}{f_T}(\alpha Z + \beta I_{ds})(R_s + R_g)]^{1/2} \quad (3.40)$$

Thus, the minimum noise figure is related to the FET physical parameters, FET gat length L and FET gate width. But the fitting factors do not possess physical meanings.

3.2.4 Pucel Noise Model

The noise model proposed by Pucel et *al.* [26] is a comprehensive model of the MESFET that is derived from general principles in terms of fundamental physical parameters. The noise model is shown in Figure 3.8.

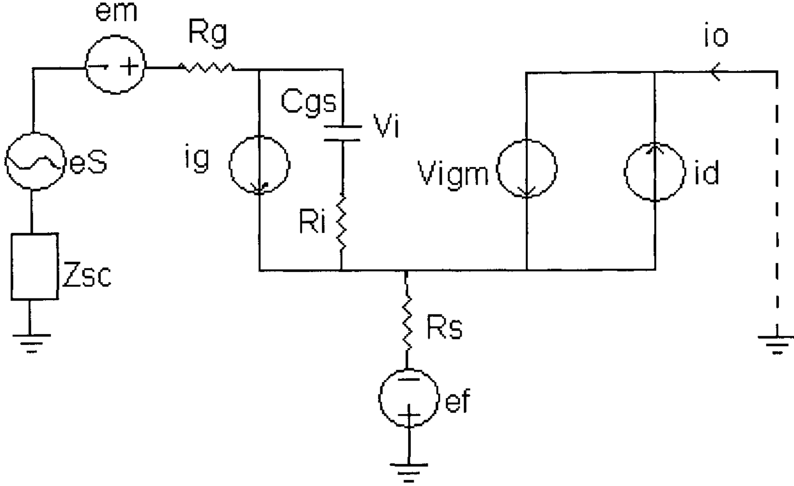

Figure 3.8: The Pucel noise model based on a simplified FET model with noise sources represented by voltage and current sources

Through the circuit analysis, the noise figure is then written by

$$F = 1 + (1/R_{sc})(r_n + g_n \,|\, Z_{sc} + Z_c \,|^2) \tag{3.41}$$

where g_n *and* r_n are referred to as the noise conductance and noise resistance, respectively. The parameter Z is called the *correlation impedance.* The parameters are defined as

$$r_n = (R_g + R_s) + Kr(\frac{1+\omega^2 C_{gs}^2 R_i^2}{g_m}) \tag{3.42}$$

$$g_n = K_g \frac{\omega^2 C_{gs}^2}{g_m} \tag{3.43}$$

$$Z_c = (R_g + R_s) + K_c / Y_{11} \tag{3.44}$$

The terms K_g, K_r, *and* K_c are functions of P, R, and C. They are defined as the fundamental noise coefficients and the expressions are:

$$K_r = \frac{R(1-C^2)}{\left[1 - C(R/P)^{1/2}\right]^2 + (1-C^2)R/P} \tag{3.45}$$

$$K_c = \frac{1 - C(R/P)^{1/2}}{\left[1 - C(R/P)^{1/2}\right]^2 + (1 - C^2)R/P} \quad (3.46)$$

$$K_g = P\left\{\left[1 - C(R/P)^{1/2}\right]^2 + (1 - C^2)R/P\right\} \quad (3.47)$$

where P and R are dimensionless noise coefficients, and C is the correlation coefficient. They are related to device geometry, material properties, and the bias conditions of the device.

The noise parameters can be obtained and given by

$$F_{\min} = 1 + 2g_n(R_c + R_{sc,opt}) \quad (3.48)$$

$$R_{sc,opt} = [R_c^2 + (r_n / g_n)]^{1/2} \quad (3.49)$$

$$X_{sc,opt} = -X_c \quad (3.50)$$

The Pucel noise model allows prediction of FET noise parameters as a function of device geometry, material properties, and the bias conditions of the device, and obtained good agreement between measured and predicted results. But it is too comprehensive and it requires detailed knowledge of the device's structure.

3.2.5 POSPIESZALSKI Noise Model

Pospieszalski [27] proposed a noise model of a microwave MESFET (HEMT) by using the equivalent noise temperatures of intrinsic gate resistance and drain conductance, T_g and T_d.

An equivalent circuit of a FET chip is shown in Figure 3.9 [27]. Parasitic resistances contribute only thermal noise and with a knowledge of the ambient temperature T_a. Their influence can be easily taken into account. The noise properties of an intrinsic chip are then treated by assigning equivalent temperature T_g and T_d to the resistive (frequency-independent) elements of the equivalent circuit r_{gs} and g_{ds}, respectively. No correlation is assumed between the noise sources represented by the equivalent temperatures T_g and

T_d. This yields a noise equivalent network for an intrinsic chip shown in Figure 3.10 [27].

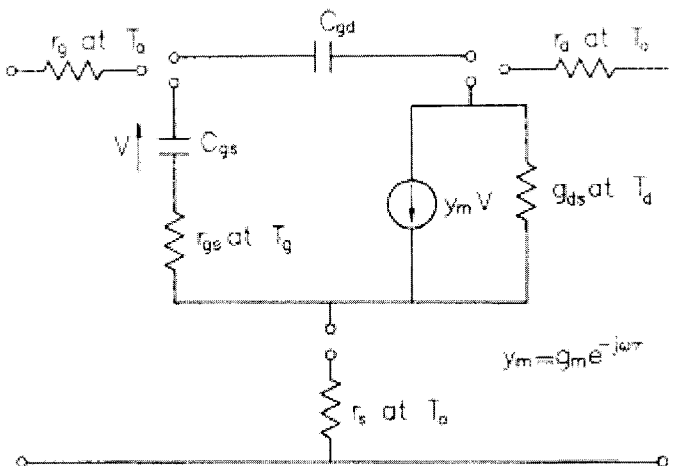

Figure 3.9: Equivalent circuit of FET (HEMT, MODFET) chip. Noise properties of an intrinsic chip are represented by equivalent temperatures: T_g *of* R_{gs}, and T_d *of* g_{ds}. Noise contribution of ohmic resistances $r_s, r_g,$ *and* r_d are determined by physical temperature T_a of a chip.

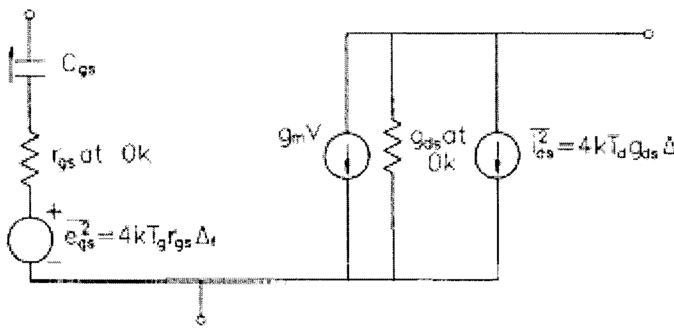

Figure 3.10: Noise equivalent circuit of an intrinsic chip

The noise temperature, T_n, of a two-port driven by generator impedance Z_g can be written by [27]

$$T_n = T_{\min} + NT_0 \frac{|Z_g - Z_{opt}|^2}{R_g R_{opt}} \tag{3.51}$$

or

$$T_n = T_{\min} + NT_0 \frac{|\Gamma_g - \Gamma_{opt}|^2}{(1-|\Gamma_{opt}|^2)(1-|\Gamma_g|^2)} \quad (3.52)$$

where

$$\Gamma_{opt} = \frac{Z_{opt} - Z_0}{Z_{opt} + Z_0} \text{ and } \Gamma_g = \frac{Z_g - Z_0}{Z_g + Z_0}$$

Based on the above noise equivalent circuit (Figure 3.19 and 3.10), the noise parameters of the FET chip can be expressed as [27]:

$$X_{opt} = \frac{1}{\omega C_{gs}} \quad (3.53)$$

$$R_{opt} = \sqrt{(\frac{f_T}{f})^2 \frac{r_{gs}}{g_{ds}} \frac{T_g}{T_d} + r_{gs}^2} \quad (3.54)$$

$$T_{\min} = 2\frac{f}{f_T}\sqrt{g_{ds} r_{gs} T_g T_d + (\frac{f}{f_T})^2 r_{gs}^2 g_{ds}^2 T_d^2} + 2\left(\frac{f}{f_T}\right)^2 r_{gs} g_{ds} T_d \quad (3.55)$$

$$g_n = (\frac{f}{f_T})^2 \frac{g_{ds} T_d}{T_0} \quad (3.56)$$

$$\frac{4NT_0}{T_{\min}} = \frac{2}{1 + \frac{r_{gs}}{R_{opt}}} \quad (3.57)$$

$$R_n = \frac{T_g}{T_0} r_{gs} + \frac{T_d}{T_0} \frac{g_{ds}}{g_m^2} (1 + \omega^2 C_{gs}^2 r_{gs}^2) \quad (3.58)$$

$$cor = \rho\sqrt{R_n g_n} = \frac{T_d}{T_0} \frac{g_{ds}}{g_m^2} (\omega^2 C_{gs}^2 r_{gs} + j\omega C_{gs}) \quad (3.59)$$

where

$$f_T = \frac{g_m}{2\pi C_{gs}}$$

$T_{\min}$, minimum noise temperature

$Z_{opt} = R_{opt} + jX_{opt}$, optimal source impedance

g_n, equivalent noise conductance

$N = R_{opt} g_n$ (as defined by Lange [28])

R_n, equivalent noise resistance

cor, correlation expression

The available gain can be written by:

$$\frac{1}{G_a} = \frac{1}{G_{a\max}} + \frac{g_g}{R_g} | Z_g - Z_{opt}^G |^2 \tag{3.60}$$

Where Z_{opt}^G is the generator impedance realizing maximum available gain. For the equivalent circuit of an intrinsic chip (Figure 3.9), $G_{a\max}, g_g, and\, Z_{opt}^G$ are given by

$$G_{a\max} = \left(\frac{f_T}{f}\right)^2 \frac{1}{4 g_{ds} r_{gs}} \tag{3.61}$$

$$g_g = \left(\frac{f}{f_T}\right)^2 g_{ds} \tag{3.62}$$

$$Z_{opt}^G = r_{gs} + j\frac{1}{\omega C_{gs}} \tag{3.63}$$

The expression of noise measure can be written by

$$M = \frac{T_n}{T_0} \frac{1}{1 - \frac{1}{G_a}} \tag{3.64}$$

Thus, for the above equivalent circuit of an intrinsic chip, the generator impedance Z_{opt}^M, which minimizes the noise measure $M_{\min}$ (note that $Z_{opt}^M \neq Z_{opt}$), can be written by

$$X_{opt}^M = X_{opt}^G = X_{opt} = j\frac{1}{\omega C_{gs}} \tag{3.65}$$

$$R_{opt}^{M} = r_{gs}\left\{\sqrt{\left(\frac{T_g}{T_d}-1\right)^2+\frac{R_{opt}^2}{r_{gs}^2}-1}-\frac{T_g}{T_d}\right\}$$
$$= r_{gs}\left\{\sqrt{\left(\frac{T_g}{T_d}-1\right)^2+4G_{a\max}\frac{T_g}{T_d}}-\frac{T_g}{T_d}\right\} \qquad (3.66)$$

The value of $M_{\min}$ may be obtained by substituting appropriate relations into (3.64).

The above expressions can be simplified to simpler forms if certain conditions are satisfied. Specifically if

$$\frac{f}{f_T} << \sqrt{\frac{Tg}{Td}\frac{1}{r_{gs}g_{ds}}} \qquad (3.67)$$

then

$$R_{opt} >> r_{gs}$$

and then

$$R_{opt} \approx \frac{f_T}{f}\sqrt{\frac{r_{gs}T_g}{g_{ds}T_d}} \qquad (3.68)$$

$$T_{\min} = 2\frac{f}{f_T}\sqrt{g_{ds}r_{gs}T_dT_g} \qquad (3.69)$$

$$\frac{4NT_0}{T_{\min}} \approx 2 \qquad (3.70)$$

Another case is for $T_g \to 0$, then only one current source in the drain exists and

$$R_{opt} = R_{opt}^{M} = R_{opt}^{G} = r_{gs} \qquad (3.71)$$

$$T_{\min} = 4(\frac{f}{f_T})^2 r_{gs}g_{ds}T_d \qquad (3.72)$$

$$\frac{4NT_0}{T_{\min}} \approx 1 \tag{3.73}$$

If the noise parameters of a FET can be described by the above model, it must satisfy

$$1 \le \frac{4NT_0}{T_{\min}} < 2 \tag{3.74}$$

From above noise models, we can see that the Pospieszalski model provides simple expressions for the noise parameters. It is also demonstrated that at both room and cryogenic temperatures the effective gate temperature is equal to the ambient temperature of the device within measurement errors, which corroborated the room temperature results of Gupta et *al.* [3]. Moreover, its validity has been experimentally confirmed throughout the years and it has been widely accepted as an easy-to-use and powerful FET noise model. Because of its simplicity and accuracy, the Pospieszalski model is chosen as the noise model in this thesis

Chapter 4 Extraction Method and Results

The process of extraction of model parameters can be divided into two steps in this thesis. First, the small-signal model parameters of MESFET or HEMT should be extracted accurately. Second, after knowledge of the small-signal equivalent circuit parameters, with measured noise parameters of packaged device and physical temperature at a single frequency, the noise model parameters T_g *and* T_d will be extracted. Consequently, the noise properties of the device at any frequency will be predicted.

Two kinds of approaches were used in modeling the intrinsic noise equivalent circuit. The first was the accurate study of the equations of transport in semiconductors. The other approach was semi-empirical using an equivalent circuit and fitting factors. Pospieszalski proposed a simple model for MESFET and HEMT devices whose validity has been experimentally confirmed throughout the years. Our approach is based on the semi-empirical modeling.

Several methods can be used to extract the MESFET or HEMT model parameters depending on the model used and the method of characterization. In this chapter, we will discuss the parameter extraction techniques that employ only S-parameter measurements in optimization algorithms. Therefore, the formulation of the problem or the parameter relationships will be derived. The use of these relationships in an optimization technique will be addressed. We will also mention the method used to solve the optimization problem.

4.1 Extraction of Small-Signal Model at Normal Bias Conditions:

Figure 4.1 shows the most common MESFET or HEMT model at normal bias conditions, i.e. when the device is biased in the saturation region. Some of those elements can be neglected in the analysis later on. The model can be divided into two sections: the extrinsic element section and the intrinsic element section. The extrinsic section includes all extrinsic elements: C_{pg} , C_{pd} , R_g , R_d , R_s , L_g , L_d , and L_s . The intrinsic section includes all the intrinsic elements: C_{gs} , R_i , C_{gd} , R_{gd} , g_m , τ, R_{ds} , and C_{ds} . The resistance R_{gd} has been added to ensure smooth transition from the symmetric cold

model (V_{ds} =0V) to operating points in the saturation region [29]. Although this element has little effect on the performance of the model and many authors neglect it, it was included here to represent full analytical expressions. Usually, R_{gd} is neglected and the Figure 2.6 is used to represent the Standard MESFET-HEMT equivalent circuit .

The main concept of the extraction process, which is employed by many researchers, is to remove the extrinsic element section from the measurements to end up with Y-parameters of the intrinsic section. The Y-parameters are the most convenient parameters since the intrinsic section exhibits a PI topology. The simple analytical expressions of the Y-parameters can be used to calculate the intrinsic elements.

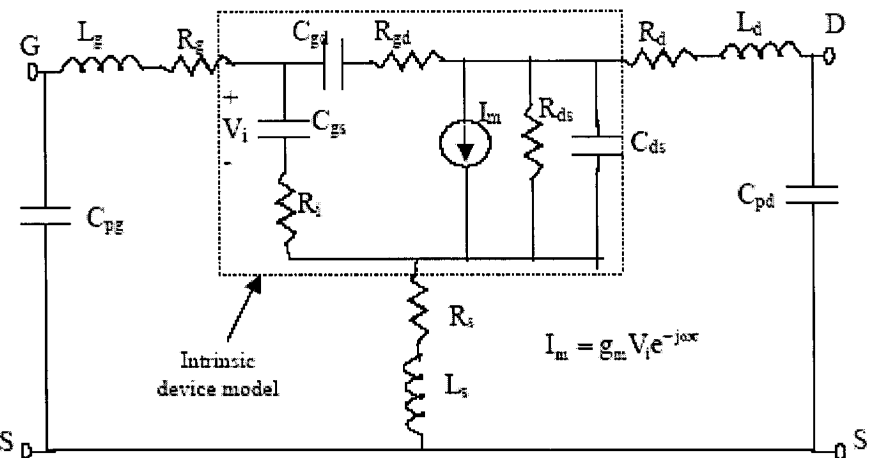

Figure 4.1 16-element small-signal FET model.

4.1.1 Determination of the Intrinsic Y-Parameters

The process of de-embedding the intrinsic Y-Parameters is depicted in Figure 4.2 [10]. We always start with the measured S- parameters of the device. S-parameters at the angular frequency (ω) are stored in the S-matrix. The S-matrix is converted to the Y-parameters matrix Y_t.

The relationship between Y-parameters and S-parameters can be written as [18]:

$$Y_{t11} = Y_0 \frac{(1-S_{11})(1+S_{22})+S_{12}S_{21}}{\Delta} \tag{4.1a}$$

$$Y_{t12} = Y_0 \frac{-2S_{12}}{\Delta} \tag{4.1b}$$

$$Y_{t21} = Y_0 \frac{-2S_{21}}{\Delta} \tag{4.1c}$$

$$Y_{t22} = Y_0 \frac{(1+S_{11})(1-S_{22})+S_{12}S_{21}}{\Delta} \tag{4.1d}$$

where

$\Delta = (1+S_{11})(1+S_{22}) - S_{12}S_{21}$

$Y_0 = \dfrac{1}{Z_0}$, Yo and Zo are characteristic admittance and characteristic impedance of the measuring system, respectively.

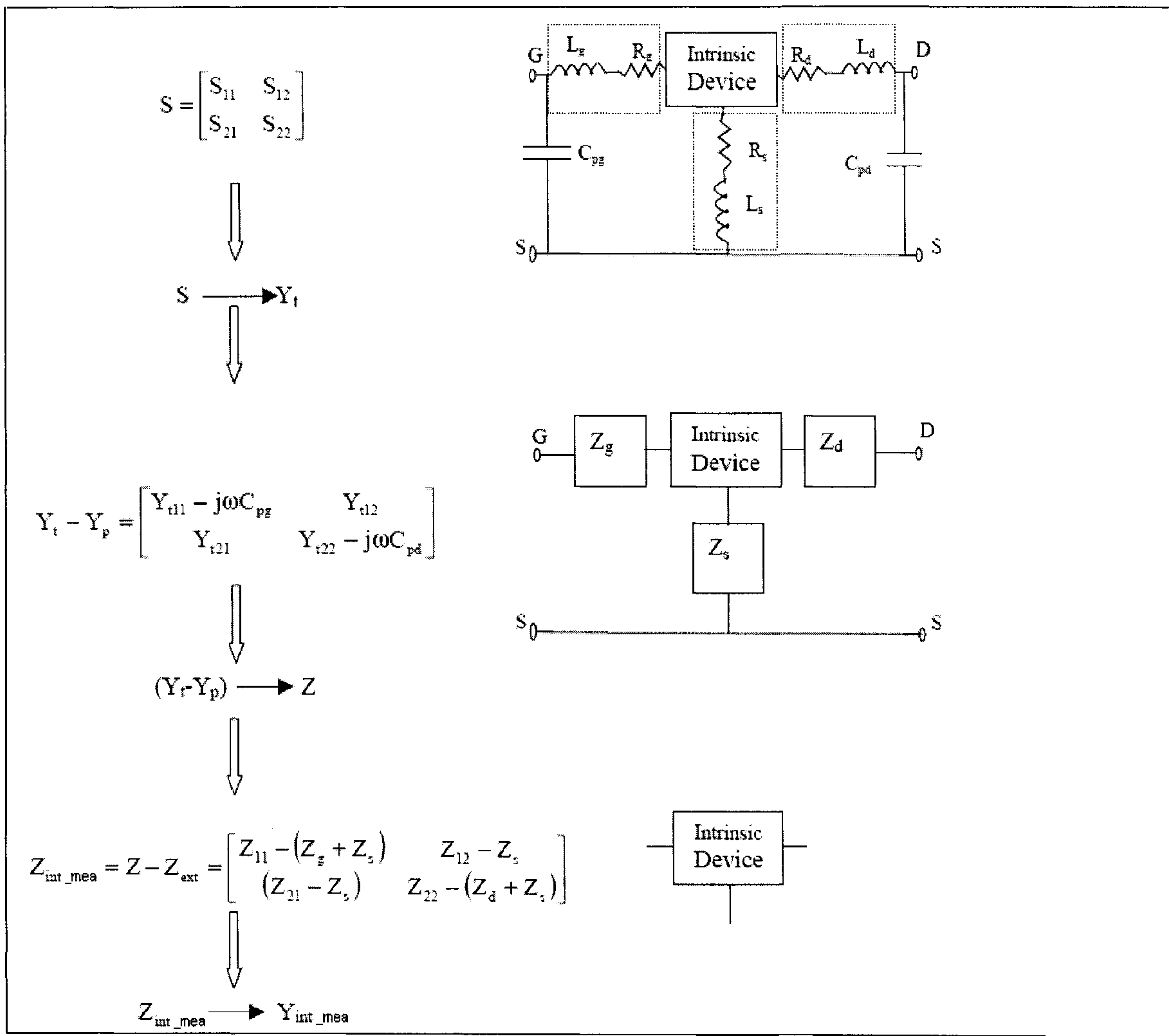

Figure 4.2 Extraction of intrinsic Y-parameters from measured S-parameters.

In the above process, the intrinsic Y-Parameters can be de-embedded from measured S-parameters. The various matrixes can be further expressed as following:

$$Y_p = \begin{bmatrix} j\omega C_{pg} & 0 \\ 0 & j\omega C_{pd} \end{bmatrix} \tag{4.2}$$

$$Z_{mea} = (Y_t - Y_p)^{-1} \tag{4.3}$$

$$Z_{ext} = \begin{bmatrix} Z_g + Z_s & Z_s \\ Z_s & Z_d + Z_s \end{bmatrix} = \begin{bmatrix} (R_g + R_s) + j\omega(L_g + L_s) & R_s + j\omega L_s \\ R_s + j\omega L_s & (R_d + R_s) + j\omega(L_d + L_s) \end{bmatrix} \tag{4.4}$$

$$Y_{\mathrm{int}_mea} = Z^{-1}_{\mathrm{int}_mea} = [Z_{mea} - Z_{ext}]^{-1} \tag{4.5}$$

$$Y_{\mathrm{int}_mea} = \begin{bmatrix} Y_{i11_mea} & Y_{i12_mea} \\ Y_{i21_mea} & Y_{i22_mea} \end{bmatrix} = \begin{bmatrix} \mathrm{Re}(Y_{i11_mea}) + j\,\mathrm{Im}(Y_{i11_mea}) & \mathrm{Re}(Y_{i12_mea}) + j\,\mathrm{Im}(Y_{i12_mea}) \\ \mathrm{Re}(Y_{i21_mea}) + j\,\mathrm{Im}(Y_{i21_mea}) & \mathrm{Re}(Y_{i22_mea}) + j\,\mathrm{Im}(Y_{i22_mea}) \end{bmatrix} \tag{4.6}$$

Equation (4.6) shows the elements of Y_{int_mea} while they are decomposed into real and imaginary parts. Real parts are denoted by "Re" whereas imaginary parts are denoted by "Im".

On the other hand, the analytical form of the Y-Parameters matrix Y_{int} can be easily derived from the intrinsic device model shown in Figure 4.1:

$$Y_{\mathrm{int}} = \begin{bmatrix} \dfrac{\omega^2 R_i C_{gs}^2}{|D_1|^2} + \dfrac{\omega^2 R_{gd} C_{gd}^2}{|D_2|^2} + j\omega\left(\dfrac{C_{gs}}{|D_1|^2} + \dfrac{C_{gd}}{|D_2|^2}\right) & -\dfrac{\omega^2 R_{gd} C_{gd}^2}{|D_2|^2} - j\omega\dfrac{C_{gd}}{|D_2|^2} \\ \dfrac{g_m e^{-j\omega\tau}}{D_1} - j\dfrac{\omega C_{gd}}{D_2} & g_{ds} + \dfrac{\omega^2 R_{gd} C_{gd}^2}{|D_2|^2} + j\omega\left(C_{ds} + \dfrac{C_{gd}}{|D_2|^2}\right) \end{bmatrix} \tag{4.7}$$

where

$$D_1 = 1 + j\omega R_i C_{gs}$$

$$D_2 = 1 + j\omega R_{gd} C_{gd}$$

Equation (4.7) can be further simplified if R_{gd} is assumed to be equal to zero. This assumption has been used by many authors and it makes sense because R_{gd} has been added for the purpose of symmetry with R_i. R_i itself has no specific physical meaning and it is added in the model to account for the real part of Y_{int11}. The simplified form of equation (4.7), while R_{gd} =0, can be written as:

$$Y_{int} = \begin{bmatrix} \frac{\omega^2 R_i C_{gs}^2}{|D_1|^2} + j\omega\left(\frac{C_{gs}}{|D_1|^2} + C_{gd}\right) & -j\omega C_{gd} \\ \frac{g_m e^{-j\omega\tau}}{D_1} - j\omega C_{gd} & g_{ds} + j\omega(C_{ds} + C_{gd}) \end{bmatrix} \tag{4.8}$$

where

$$D_1 = 1 + j\omega R_i C_{gs}$$

Equation (4.8) is more commonly used than equation (4.7). In the next section, we will derive the intrinsic elements in terms of intrinsic Y-parameters by using equations (4.8).

4.1.2 Extracting Intrinsic Elements from Intrinsic Y-Parameters

From the view point of theory, Y_{int} should be equal to Y_{int_mea}. It means that the expression (4.8) is equivalent to the expression (4.6). So, all intrinsic parameters can be extracted at each frequency point in terms of Y_{int} data in (4.8). The intrinsic parameters can be stated as:

$$C_{gs} = \frac{(1+d^2)}{\omega}(\text{Im}(Y_{i11_mea}) + \text{Im}(Y_{i12_mea})) \tag{4.9a}$$

$$R_i = \frac{d}{(1+d^2)(\text{Im}(Y_{i11_mea}) + \text{Im}(Y_{i12_mea}))} \tag{4.9b}$$

$$C_{gd} = -\frac{\text{Im}(Y_{i12_mea})}{\omega} \tag{4.9c}$$

$$g_m = |G| \quad (4.9d)$$

$$\tau = -\frac{1}{\omega}\angle(G) \quad (4.9e)$$

$$g_{ds} = \mathrm{Re}(Y_{i22_mea}) \quad (4.9f)$$

$$C_{ds} = \frac{\mathrm{Im}(Y_{i22_mea}) + \mathrm{Im}(Y_{i12_mea})}{\omega} \quad (4.9g)$$

where

$$d = \frac{\mathrm{Re}(Y_{i11_mea})}{\mathrm{Im}(Y_{i11_mea}) + \mathrm{Im}(Y_{i12_mea})}$$

$$G = g_m e^{-j\omega\tau} = (Y_{i21_mea} - Y_{i12_mea})(1 + jd)$$

$$|G| = \sqrt{((\mathrm{Re}(Y_{i21_mea}))^2 + (\mathrm{Im}(Y_{i21_mea}) - \mathrm{Im}(Y_{i12_mea}))^2)(1+d^2)}$$

$$\angle(G) = \angle\tan^{-1}\left(\frac{d\,\mathrm{Re}(Y_{i21_mea}) + (\mathrm{Im}(Y_{i21_mea}) - \mathrm{Im}(Y_{i12_mea}))}{\mathrm{Re}(Y_{i21_mea}) - d(\mathrm{Im}(Y_{i21_mea}) - \mathrm{Im}(Y_{i12_mea}))}\right)$$

Equations (4.9) will be used later on in the optimization process to extract the values of the intrinsic parameters at normal bias conditions.

4.2 New Method for Determining the FET Small-Signal Equivalent Circuit Elements

Because the small-signal model plays a crucial role in the analysis of the noise model, we should firstly determine the FET Small-Signal equivalent circuit. As we discussed in section 2.4, many techniques have been proposed on this subject [7]-[15]. These techniques can be divided into two kinds. The first is to extract the extrinsic parameters C_{pg}, C_{pd}, R_g, R_d, R_s, L_g, L_d, and L_s, then the remaining (intrinsic) parameters are extracted analytically (or by optimization) [7]-[11]. The second is to extract all the parameters using a multi-dimensional optimization algorithm [12]-[15]. But the first kind technique needs extra DC measurements to determine the parasitic resistances in addition to the S-parameter measurement [7]-[11]. The extra DC measurements require forward gate bias

which can sometimes bring about serious problem such as damage to device during or after measurement [30]. The second kind technique also has the initial value dependent problem and the local minimum problem [12].

In order to overcome all the problems mentioned above, we proposed a new method to determine the FET small-signal equivalent circuit. In this method, there is no need for additional DC measurement, and there is no initial value dependent problem and local minimum constraint. This will be demonstrated in Appendix B.4. There are two basic and important facts that our method is based on. The first is that there exist a finite difference between the parasitic resistances R_s and R_d, and this difference can be obtained from the S-parameters under the "cold measurement" [10]. The second is that the real part of the matrix element $Y_{\text{int},12}$ of the intrinsic Y-parameters is theoretically zero, e.g. $\text{Re}(Y_{\text{int},12}) = 0$. We can use this expression to find R_g as a function of the other extrinsic parameters [15]. The simple transformation between S-, Z-, Y-matrices and the two basic facts mentioned above will produce the unique solution for modeling the FET small-signal equivalent circuit.

4.2.1 Determination of the Pad Capacitances

The value of pad capacitance C_{pg} *and* C_{pd} can be calculated from the measurement at zero drain bias and the gate voltage lower than the pinch-off voltage V_p ($V_{ds} = 0, and\ V_{gs} < -|V_p|$). Under these bias conditions, the FET equivalent circuit is shown in Fig. 4.3 [10].

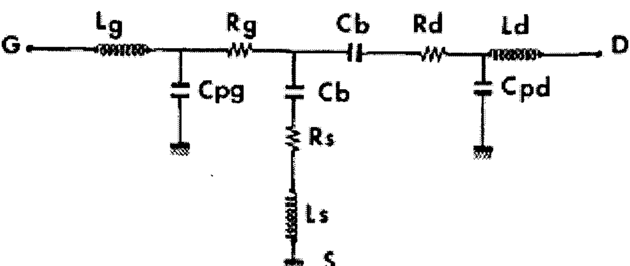

Figure 4.3. Small-signal equivalent circuit of a FET with zero drain bias voltage and gate voltage lower than the pinchoff voltage.

In this figure, C_b represents the fringing capacitance due to the depleted layer extension at each side of the gate. For frequencies up to a few gigahertz, the resistances

and inductances have no influence on the imaginary part of the Y parameters, which can be written as [10]

$$\mathrm{Im}(Y_{11}) = j\omega(C_{pg} + 2C_b) \tag{4.10}$$

$$\mathrm{Im}(Y_{12}) = \mathrm{Im}(Y_{21}) = -j\omega C_b \tag{4.11}$$

$$\mathrm{Im}(Y_{11}) = j\omega(C_{pd} + C_b) \tag{4.12}$$

Thus,

$$C_b = -\frac{1}{2\omega}(\mathrm{Im}(Y_{12}) + \mathrm{Im}(Y_{21})) \tag{4.13}$$

$$C_{pg} = \frac{1}{\omega}\mathrm{Im}(Y_{11}) - 2C_b \tag{4.14}$$

$$C_{pd} = \frac{1}{\omega}\mathrm{Im}(Y_{22}) - C_b \tag{4.15}$$

where the Y-parameters can be derived from measured S-parameters. C_b can be calculated from either $\mathrm{Im}(Y_{12})$ or $\mathrm{Im}(Y_{21})$, however, we will assume its value as the average of both of them so that all parts are taken into consideration for reasonable balance between the different parameters.

4.2.2 Determination of the parasitic inductances and ΔR_{ds}

The parasitic inductance values can be extracted from what we called S-parameter cold-modeling method ($V_{ds} = 0$ and $V_{gs} > -|V_p|$) [9]. Under this bias condition, the FET can be considered as a symmetric device shown in Figure 4.4 [10].

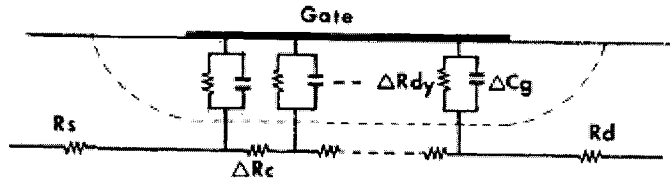

Figure 4.4 Sketch of the distributed RC network under V_{ds}=0 and V_{gs} fairly above pinchoff voltage.

The intrinsic section of the FET can be expressed by sum of channel resistance and

equivalent impedance of Schottky barrier. The following Z-parameter expressions, given in [10], are valid.

$$Z_{11} = R_s + R_g + \frac{R_c}{3} + \frac{nkT}{qI_g} + j\omega(L_s + L_g) \tag{4.16}$$

$$Z_{12} = Z_{21} = R_s + \frac{R_c}{2} + j\omega L_s \tag{4.17}$$

$$Z_{22} = R_s + R_d + R_c + j\omega(L_s + L_d) \tag{4.18}$$

where R_c is the channel resistance under given gate bias, nkT / qI_g is the equivalent resistance of Schottky barrier. n is the ideality factor, k is the Boltzmann constant, T is the temperature, q is the electron charge, I_g is the dc gate current. Therefore, the inductances can be calculated.

$$L_s = \frac{1}{2\omega}(\text{Im}(Z_{12}) + \text{Im}(Z_{21})) \tag{4.19}$$

$$L_g = \frac{\text{Im}(Z_{11})}{\omega} - L_s \tag{4.20}$$

$$L_d = \frac{\text{Im}(Z_{22})}{\omega} - L_s \tag{4.21}$$

L_s can be calculated from either $\text{Im}(Z_{12})$ or $\text{Im}(Z_{21})$, however, we will assume its value as the average of both of them so that all parts are taken into consideration for reasonable balance between the different parameters.

Additionally, the relation between the parasitic resistances R_s and R_d can be obtained from (4.17)-(4.18) by eliminating R_c.

$$\text{Re}(Z_{22}) - 2\,\text{Re}(Z_{12}) = R_d - R_s = \Delta R_{ds} \tag{4.22}$$

This means that either R_d or R_s can be expressed by the other one provided ΔR_{ds} is obtained.

On the other hand, from the fact that the real part of the matrix element $Y_{\text{int},12}$ of the intrinsic Y-parameters is theoretically zero, e.g. $\text{Re}(Y_{\text{int},12}) = 0$. The relation between R_g,

R_d and R_s can be obtained.

$$Z_{ext} = \begin{bmatrix} Z_g + Z_s & Z_s \\ Z_s & Z_g + Z_s \end{bmatrix} = \begin{bmatrix} R_g + R_s + j\omega(L_g + L_s) & R_s + j\omega L_s \\ R_s + j\omega L_s & R_d + R_s + j\omega(L_d + L_s) \end{bmatrix} \tag{4.23}$$

$$Z_{\text{int}} = Z - Z_{ext} \tag{4.24}$$

$$Y_{\text{int}} = Z_{\text{int}}^{-1} = [Z - Z_{ext}]^{-1} = \begin{bmatrix} Z_{11} - (R_g + R_s + j\omega(L_g + L_s)) & Z_{12} - (R_s + j\omega L_s) \\ Z_{21} - (R_s + j\omega L_s) & Z_{22} - (R_d + R_s + j\omega(L_d + L_s)) \end{bmatrix}^{-1} \tag{4.25}$$

$$Y_{\text{int},12} = -\frac{Z_{\text{int},12}}{\Delta Z} \tag{4.26}$$

From $\text{Re}(Y_{\text{int},12}) = 0$, we can obtain following expressions [15].

$$\begin{aligned} R_g = {} & [(R_s - Z_{12r})(\omega L_g\{Z_{22i} - \omega L_d - \omega L_s\} + R_d(R_s - Z_{11r}) \\ & - R_s(Z_{11r} - Z_{12r} - Z_{21r} + Z_{22r}) - \omega L_d(\omega L_s - Z_{11i}) \\ & + \omega L_s(Z_{11i} - Z_{12i} - Z_{21i} + Z_{22i}) - Z_{11i}Z_{22i} + Z_{12i}Z_{21i} \\ & - Z_{12r}Z_{21r} + Z_{22r}Z_{11r}) + (\omega L_S - z_{12i}) \\ & \cdot (\omega L_g(R_d + R_s - Z_{22r}) + R_d(\omega L_s - Z_{11i}) \\ & + R_s(\omega L_d - Z_{11i} + Z_{12i} + Z_{21i} - Z_{22i}) - \omega L_d Z_{11r} \\ & - \omega L_s(Z_{11r} - Z_{12r} - Z_{21r} + Z_{22r}) + Z_{11r}Z_{22i} \\ & - Z_{21i}Z_{12r} - Z_{12i}Z_{21r} + Z_{22r}Z_{11i})] \\ & \cdot [(R_s - Z_{12r})(R_d + R_s + Z_{22r}) + (\omega L_s - Z_{12i}) \\ & \cdot (\omega L_d + \omega L_s - Z_{22i})]^{-1} \end{aligned} \tag{4.27}$$

By substituting $R_d = R_s + \Delta R_{ds}$ into (4.27), R_g can be expressed as a function of R_s.

Now, Knowing C_{pg}, C_{pd}, L_g, L_d, L_s, and ΔR_{ds}, all the intrinsic parameters C_{gs}, R_i, C_{gd}, g_m, τ, g_{ds}, C_{ds} can be calculated from S-parameter measurements at normal bias condition using equations (4.9) in section 4.1.2. Therefore, the intrinsic elements and the parasitic resistances R_g can be expressed as a function of R_s in addition to $R_d = R_s + \Delta R_{ds}$.

$$C_{gs} = f_{1i}(\omega_i, R_s) \tag{4.28a}$$

$$C_{ds} = f_{2i}(\omega_i, R_s) \tag{4.28b}$$

$$C_{gd} = f_{3i}(\omega_i, R_s) \tag{4.28c}$$

$$R_i = f_{4i}(\omega_i, R_s) \tag{4.28d}$$

$$g_m = f_{5i}(\omega_i, R_s) \tag{4.28e}$$

$$\tau = f_{6i}(\omega_i, R_s) \tag{4.28f}$$

$$g_{ds} = f_{7i}(\omega_i, R_s) \tag{4.28g}$$

$$R_g = f_{8i}(\omega_i, R_s) \tag{4.28h}$$

The first objective is to find the value of R_s so that the other parameter values are independent of frequency. In other words, they have the same values at all frequency points. Thus, criteria should be formulated to describe this objective. The variances are chosen as criteria so that variances should be as minimum as possible:

$$\varepsilon_1^k(\omega_i, R_s) = \frac{1}{N}\sum_{i=1}^{N} |\rho_k(f_{ki} - \overline{f_k})|^2 \tag{4.29}$$

where

$$\overline{f_k} = \frac{1}{N}\sum_{i=1}^{N} f_{ki}$$

$\overline{f_k}$ is the mean value of f_k where k varies from 1 to 8. The normalizing factor ρ_k is formulated in such a way so that all errors for different k's are confined within the same order of magnitudes. ρ_k can be written in the following mathematical form:

Assuming: max $f_k = \max\limits_i(f_{ki})$ where i varies from 1 to N

$$\rho_k = \frac{1}{\max f_k}$$

Another criterion is added for stable calculations. This criterion is intended to minimize the error between the measured and calculated S-parameters. The mean values of the intrinsic parameters are used to calculate S-parameters.

The criterion is:

$$\varepsilon_2(\omega_{i,}R_s)=\sum_{p=1}^{2}\sum_{q=1}^{2}\sum_{i=1}^{N}W_{pq}\,|\frac{S_{pq}(\omega_i)-S_{cpq}(\omega_{i,}R_s)}{G_{pq}}|^2 \tag{4.30}$$

where

$$G_{11}=G_{22}=\max_i(|S_{11}(\omega_i)|)$$

$$G_{12}=G_{21}=\max_i(|S_{21}(\omega_i)|)$$

The weighting factor W_{pq} is set to 0.5. The normalization factor of S_{22} is equated to the normalization factor of S_{11} since the measurements show that S_{22} is noisier than S_{11} at most bias points. In addition, the magnitude of S_{22} is usually smaller than the magnitude of S_{11}. For these reasons, G_{22} is set to be equal to G_{11} to inhibit the effect of the noise of S_{22} on the optimization process. Similarly, G_{12} is set to be equal to G_{21}. The total error function can be determined as:

$$\varepsilon(\omega_{i,}R_s)=\sum_k \varepsilon_1^k+\varepsilon_2 \tag{4.31}$$

Equation (4.31) is called the error function (or the objective function) of our technique. The minimum of the objective function should be calculated using an optimization algorithm. In our model, we use the Gauss-Newton and Levenberg-Marquart methods. The optimization variable is R_s. There is only one optimization variable in our problem. So our technique has neither initial value-dependence problem nor the local minimum problem.

4.2.3 The Procedure of the New Method for the extraction of the FET Small-Signal Equivalent-Circuit Elements

Our new technique exploits the advantages of all previous techniques to end up with a robust and reliable method. It can work over any frequency bandwidth for the measured S-parameters, which may have certain unavoidable measurement errors. The procedure can be explained over the following steps:

1) Evaluate the FET pad capacitances C_{pg} *and* C_{pd} from (4.10)-(4.15) at pinch-off bias condition.

2) Calculate the FET parasitic inductance values of $L_g, L_d\ and\ L_s$, and ΔR_{ds} (the difference between R_d and R_s) from (4.16)-(4.22) using the Cold-Measurement.

3) Calculate all other parameters from S-parameter measurements at normal bias condition.

3.1) Set the initial value for the extrinsic parameters R_s. The initial values have little effect on the final results. Consequently, zero initial values can be assumed.

3.2) Employ the optimization technique to minimize the objective function in (4.31) to best fit the measured S-parameters and to best describe the frequency independence of the intrinsic elements.

4.2.4 The Iterative Scheme for Extracting FET Small-Signal Model Parameters at Normal Bias Condition

The flow chart of this iterative scheme is shown in Figure 4.5.

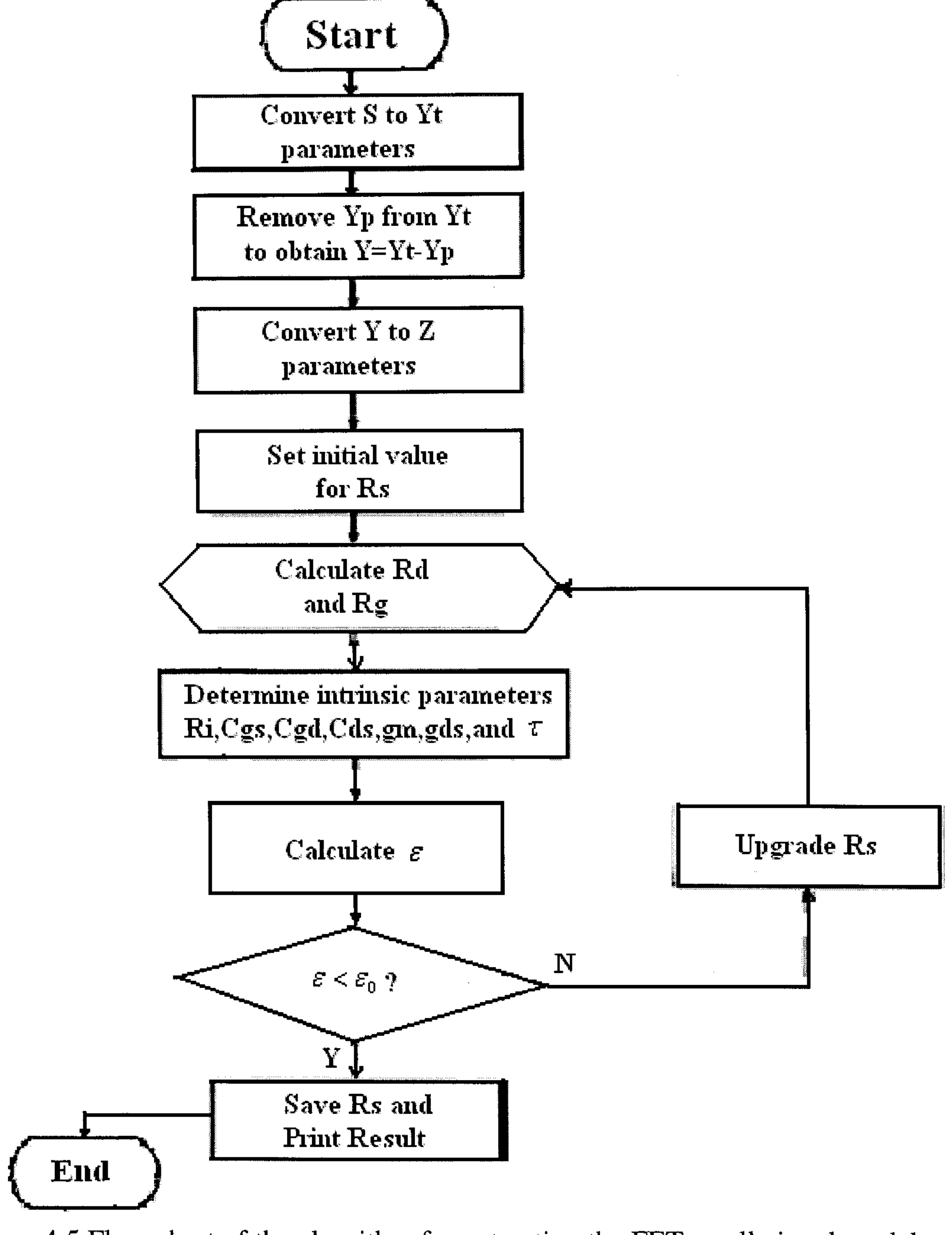

Figure 4.5 Flow chart of the algorithm for extracting the FET small-signal model parameters

The value of R_s is updated to reduce the error ε using the Gauss-Newton or Levenberg-Marquart method. If ε is not small enough, the loop is repeated. The program is written in MATLAB, and is easy to modify for a particular equivalent circuit structure.

4.3 Method of Extracting Noise Parameters

In order to describe the RF noise of a MESFET or HEMT, one has to determine the parameters of the noise model in addition to the small-signal equivalent-circuit elements. Although, in principle, a set of N linearly independent equations is sufficient to determine N unknowns, in practice, a much larger number of measurements is required to extract the two to four unknowns of the noise models. Thereby, measurement inaccuracies cancel out and the accuracy of the model parameters and stability of the extraction algorithm are enhanced.

The noise performance of field-effect transistors (FETs) has been a subject of study for many years. Several noise models have been developed. Such as the Van der Ziel noise model [31], the Gupta noise model [22], the Fukui noise model [23], [24], the Cappy noise model [25], the *PRC* model [26] and the Pospieszalski model [27] *etc.*

Among those studies of noise properties of the FET, two kinds of approaches were used in modeling the intrinsic equivalent circuit. The first was the accurate study of the equations of transport in semiconductors. The typical examples are the *PRC* noise model [26] and the Pospieszalski model [27].

The other approach was semi-empirical using an equivalent circuit and fitting factors. The typical example is the Fukui noise model [23], [24]. Although it is widely used by device technology, it does not provide any insight into the nature of a noise-generating mechanism in a FET as the fitting factors do not possess physical meanings.

The two most commonly used FET noise models are the *PRC* noise model [26], and the Pospieszalski model [27]. But the *PRC* noise model is the most comprehensive model of the FET that is derived from general principles in terms of fundamental physical parameters and it requires detailed knowledge of the device's structure. Comparatively, the Pospieszalski model [27] provides simple expressions for the noise parameters. It is also demonstrated that at both room and cryogenic temperatures the effective gate temperature is equal to the ambient temperature of the device within measurement errors, which corroborated the room temperature results of Gupta et *al.* [22]. Moreover, Its validity has been experimentally confirmed throughout the years and it has been widely accepted as an easy-to-use and powerful FET noise model. Because of its simplicity and accuracy, the Pospieszalski model is chosen as the noise model in this work.

4.3.1 New Method for Extracting the FET Two Noise Temperatures

In our thesis, we use the Pospieszalski's temperature noise model [27], which has been widely accepted as an easy-to-use and powerful FET noise model. The high-frequency noise from FET chips can be modeled as thermal noise in a small-signal equivalent circuit. It was already described in detail in section 3.2.5.

If the small-signal equivalent circuit has been extracted, the noise parameters for the intrinsic chip can be found by [27]:

$$X_{opt} = \frac{1}{\omega C_{gs}} \tag{4.32}$$

$$R_{opt} = \sqrt{(\frac{f_T}{f})^2 \frac{r_{gs}}{g_{ds}} \frac{T_g}{T_d} + r_{gs}^2} \tag{4.33}$$

$$T_{\min} = 2\frac{f}{f_T}\sqrt{g_{ds} r_{gs} T_g T_d + (\frac{f}{f_T})^2 r_{gs}^2 g_{ds}^2 T_d^2} + 2\left(\frac{f}{f_T}\right)^2 r_{gs} g_{ds} T_d \tag{4.34}$$

$$g_n = (\frac{f}{f_T})^2 \frac{g_{ds} T_d}{T_0} \tag{4.35}$$

$$\frac{4NT_0}{T_{\min}} = \frac{2}{1 + \frac{r_{gs}}{R_{opt}}} \tag{4.36}$$

$$R_n = \frac{T_g}{T_0} r_{gs} + \frac{T_d}{T_0} \frac{g_{ds}}{g_m^2} (1 + \omega^2 C_{gs}^2 r_{gs}^2) \tag{4.37}$$

$$cor = \rho\sqrt{R_n g_n} = \frac{T_d}{T_0} \frac{g_{ds}}{g_m^2} (\omega^2 C_{gs}^2 r_{gs} + j\omega C_{gs}) \tag{4.38}$$

where

$$f_T = \frac{g_m}{2\pi C_{gs}}$$

In the above representations, if the equivalent circuit element values have been extracted, noise parameters $T_{\min}$, R_{opt} and g_n of the model will be determined by T_g and T_d. So the noise parameters can be looked as functions as T_g and T_d as well as frequency except that X_{opt} is the only function of ω.

They can be written by

$$T_{\min} = f_{1i}(\omega_i, T_g, T_d) \tag{4.39a}$$

$$R_{opt} = f_{2i}(\omega_i, T_g, T_d) \tag{4.39b}$$

$$g_n = f_{3i}(\omega_i, T_g, T_d) \tag{4.39c}$$

The objective is to find the values of T_g and T_d so that the calculated noise parameters are best fit in the mean square sense to the de-embedded measured noise parameters. So the error or objective function is expressed as:

$$\varepsilon(T_g, T_d) = \frac{1}{N}\sum_{k=1}^{3}\sum_{i=1}^{N} W_k \left| (f_{ki}^{m}(\omega_i) - f_{ki}^{c}(\omega_i, T_g, T_d)) \right|^2 \tag{4.40}$$

where the subscripts c and m denote calculated and measured values respectively. The weighting factor W_k is set to 0.5 and N is the total number of frequency points. The optimization method will be used to solve this nonlinear least-square problem.

4.3.2 The Procedure for Extraction of FET Noise Parameters

Any noisy two-port can be replaced by a noise equivalent circuit which consists of a noiseless two-port and two additional noise sources. There are three common representations which are admittance, impedance, and chain representations respectively. Their correlation matrix and electrical matrix are summarized in Table 4.1 [32]

Table 4.1 Correlation matrices and electrical matrices of various representations

	admittance representation	impedance representation	chain representation
equivalent noise circuit	i_1, i_2 current sources with noiseless two-port	u_1, u_2 voltage sources with noiseless two-port	u, i sources with noiseless two-port
correlation matrix	$\underline{C}_Y = \begin{bmatrix} C_{i_1 i_1^*} & C_{i_1 i_2^*} \\ C_{i_2 i_1^*} & C_{i_2 i_2^*} \end{bmatrix}$	$\underline{C}_Z = \begin{bmatrix} C_{u_1 u_1^*} & C_{u_1 u_2^*} \\ C_{u_2 u_1^*} & C_{u_2 u_2^*} \end{bmatrix}$	$\underline{C}_A = \begin{bmatrix} C_{uu^*} & C_{ui^*} \\ C_{iu^*} & C_{ii^*} \end{bmatrix}$
electrical matrix	$\underline{Y} = \begin{bmatrix} y_{11} & y_{12} \\ y_{21} & y_{22} \end{bmatrix}$	$\underline{Z} = \begin{bmatrix} z_{11} & z_{12} \\ z_{21} & z_{22} \end{bmatrix}$	$\underline{A} = \begin{bmatrix} a_{11} & a_{12} \\ a_{21} & a_{22} \end{bmatrix}$

The elements of matrices are denoted by $C_{s_1 s_2^*}$ where the subscript indicates that the spectral density refers to the noise sources s_1, and s_2. The matrices themselves are denoted by C and by a subscript which specifies the representation. The noiseless part of the noise equivalent two-port is described by electrical matrices.

If two or more representations exist (and they generally do), these representations can be transformed into each other by simple transformation operations. As the system is linear, the auto- and cross-correlation functions can be calculated from one representation to another by the transformation formula [32]

$$C' = TCT^+ \qquad (4.41)$$

where C and C' denote the correlation matrix of the original and resulting representation, respectively. T is the transformation matrix. A set of matrices covering all possible transformations between impedance, admittance, and chain representation are resented in Table 4.2 [32].

Table 4.2: Transformation Matrices T

resulting representation	original representation: admittance	original representation: impedance	original representation: chain
admittance	$\begin{bmatrix} 1 & 0 \\ 0 & 1 \end{bmatrix}$	$\begin{bmatrix} y_{11} & y_{12} \\ y_{21} & y_{22} \end{bmatrix}$	$\begin{bmatrix} -y_{11} & 1 \\ -y_{21} & 0 \end{bmatrix}$
impedance	$\begin{bmatrix} z_{11} & z_{12} \\ z_{21} & z_{22} \end{bmatrix}$	$\begin{bmatrix} 1 & 0 \\ 0 & 1 \end{bmatrix}$	$\begin{bmatrix} 1 & -z_{11} \\ 0 & -z_{21} \end{bmatrix}$
chain	$\begin{bmatrix} 0 & a_{12} \\ 1 & a_{22} \end{bmatrix}$	$\begin{bmatrix} 1 & -a_{11} \\ 0 & -a_{21} \end{bmatrix}$	$\begin{bmatrix} 1 & 0 \\ 0 & 1 \end{bmatrix}$

In noise analysis, interconnections of two two-ports either in parallel, in series or in cascade are often encountered. For these interconnections, the resulting correlation matrix is related to the correlation matrices of the original two-ports by [32]

$$C_Y = C_{Y1} + C_{Y2} \qquad \text{(Parallel)} \qquad (4.42)$$

$$C_Z = C_{Z1} + C_{Z2} \qquad \text{(Serial)} \qquad (4.43)$$

$$C_A = A_1 C_{A2} A_1^{+} + C_{A1} \qquad \text{(Cascade)} \qquad (4.44)$$

where the subscripts 1 and 2 refer to the two-ports to be connected. As shown by these equations interconnection in parallel and in series corresponds to addition of the correlation matrices in admittance and impedance representation, respectively.

For cascading (in an order indicated by the subscripts) a more complicated relation is obtained which additionally contains the electrical matrix A_1 of the first two-port.

If the noise two-ports consists only of passive elements, and based on thermodynamic grounds, the correlation matrices in impedance and admittance representation of such a two-port are [32]

$$C_Z = 2KT\,\mathrm{Re}\{Z\} \tag{4.45}$$

$$C_Y = 2KT\,\mathrm{Re}\{Y\} \tag{4.46}$$

If knowing the equivalent noise resistance R_n, the optimal source admittance Y_{opt} and the minimum noise figure $F_{\min}$, the chain representation of the correlation matrix can be written by [32]

$$C_A = 2KT\begin{bmatrix} R_n & \frac{F_{\min}-1}{2} - R_nY_{opt} \\ \frac{F_{\min}-1}{2} - R_nY_{opt}^* & R_n\,|Y_{opt}|^2 \end{bmatrix} \tag{4.47}$$

where T is the absolute temperature. Similarly, once the correlation matrix C_A has been determined in chain representation, the noise parameters can be calculated [32].

$$Y_{opt} = \sqrt{\frac{C_{22}}{C_{11}} - (\mathrm{Im}\{C_{12}/C_{11}\})^2} - j\,\mathrm{Im}\{C_{12}/C_{11}\} \tag{4.48}$$

$$F_{\min} = 1 + (C_{12} + C_{11}Y_{opt})/kT \tag{4.49}$$

$$R_n = C_{11} \tag{4.50}$$

where

$$C_A = \begin{bmatrix} C_{11} & C_{12} \\ C_{21} & C_{22} \end{bmatrix}$$

So if knowing the equivalent circuit and the noise parameters of a packaged device, the noise performance of the intrinsic chip for the device can be obtained by the application of the interconnection rules and the relations between noise parameters and correlation matrix, vise versa. Then, the two noise temperatures T_g and T_d can be extracted using the optimization method in section 4.3.1

For the equivalent circuit shown in Figure 4.1, the Procedure for Extraction of FET Noise Parameters will be described as following steps:

1) Extract the FET small-signal equivalent circuit element values (described in detail in section 4.2)
2) Calculate the whole packaged FET correlation matrix (chain representation) from (4.47) using measured noise parameters $F_{\min}$, Y_{opt}, and R_n at some frequencies.
3) De-embed the intrinsic chip noise correlation matrix C_{A_in} from the packaged device using formula (4.42)-(4.46)
4) Calculate the intrinsic chip noise parameters $F_{\min_in}$, Y_{opt_in}, and R_{n_in} using formula (4.48)-(4.50)
5) Calculate the values of the two noise temperatures T_g and T_d using the optimization method in section 4.31
6) Compute the noise parameters of the device at any frequency using (4.32)-(4.35)

4.3.3 The Iterative Scheme for Extraction of FET Noise Parameters

The flow chart of the iterative scheme for extraction of FET noise parameters is shown in Figure 4.6. The values of T_g and T_d are updated to reduce ε using least-square optimization method.

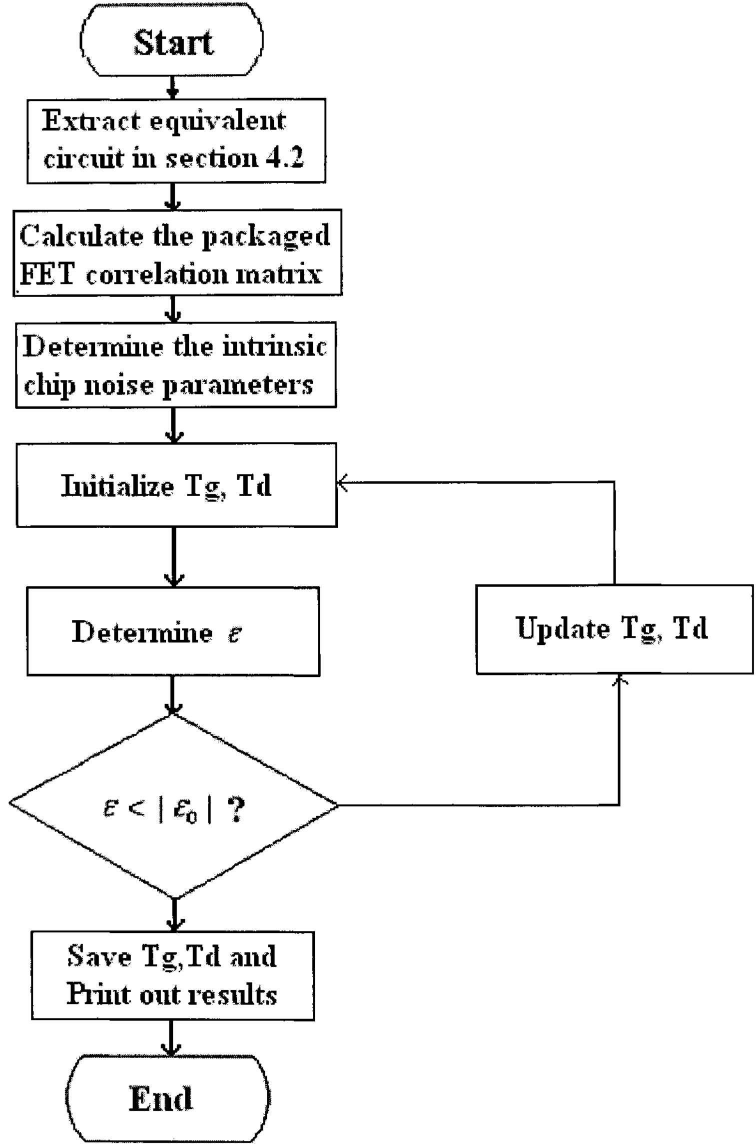

Figure 4.6: The flow chart of the iterative scheme for extraction of FET noise parameters

4.4 Results and Analyses

In the previous sections, we addressed our techniques for extracting small-signal model parameters for microwave FET devices. In this section, we will discuss the results of our techniques and argue their significance and accuracy. We will also show how accurate this technique is. The argument will be supported by hypothetical measurement data analysis.

4.4.1 S-Parameter Data

To verify the modeling techniques discussed in the previous chapter, a hypothetical MESFET or HEMT model is assumed. In this hypothetical model a set of small-signal model parameters, which resemble typical values of a MESFET or a HEMT device, are assumed. In addition to verification, using known model parameters allows us to evaluate the reliability and robustness of the modeling technique and estimate the accuracy of each extracted parameter in the model. In addition, the hypothetical model can be used to investigate the technique and its convergence properties.

We will investigate our technique and its associated programming code using a hypothetical set of data first. If it shows good results, then we will apply it to the actual device measurements. The MESFET small-signal model parameters of the hypothetical device are tabulated in Table 4.3. These data is obtained from the *Excelics Semiconductor Inc. website* [33]. The low distortion GaAs power FET EFA018A is thought as the hypothetical device. The pad capacitances C_{pg} and C_{pd} are excluded for simplicity during evaluation of each extraction technique because the study of each technique does not require the presence of these elements.

Table 4.3 Equivalent circuit element values for a hypothetical device.

R_g (Ω)	R_d (Ω)	R_s (Ω)	L_g (nH)	L_d (nH)	L_s (nH)	C_{gs} (pF)	R_i (Ω)	C_{gd} (pF)	g_m (mS)	τ (ps)	g_{ds} (mS)	C_{ds} (pF)
0.5	1	0.23	0.23	0.22	0.063	0.17	0.53	0.016	32	2.4	1.786	0.006

A set of S-parameters can be obtained from these equivalent circuit element values over a range of frequencies (1-40GHz). This set of S-parameters is called "Ideal (noiseless) S-parameters Data" because it has no measurement errors. They are shown in table 4.4.

Table 4.4 IDEAL S-PARAMETERS of EF018A

FREQ	S11		S21		S12		S22	
(GHz)	MAG	ANG	MAG	ANG	MAG	ANG	MAG	ANG
1.0000	0.9984	-7.5147	2.9102	173.9241	0.0093	86.1979	0.8367	-1.5650
2.0000	0.9937	-15.0549	2.9045	167.8459	0.0184	82.3939	0.8342	-3.1228
3.0000	0.9860	-22.6454	2.8947	161.7637	0.0275	78.5864	0.8301	-4.6658
4.0000	0.9753	-30.3101	2.8808	155.6767	0.0365	74.7751	0.8244	-6.1859
5.0000	0.9618	-38.0713	2.8624	149.5857	0.0452	70.9611	0.8170	-7.6741
6.0000	0.9458	-45.9492	2.8393	143.4932	0.0536	67.1472	0.8082	-9.1202
7.0000	0.9275	-53.9610	2.8112	137.4038	0.0617	63.3385	0.7979	-10.5133
8.0000	0.9073	-62.1203	2.7780	131.3244	0.0694	59.5425	0.7863	-11.8415
9.0000	0.8856	-70.4361	2.7393	125.2640	0.0766	55.7686	0.7734	-13.0924
10.0000	0.8630	-78.9117	2.6952	119.2339	0.0833	52.0287	0.7595	-14.2537
11.0000	0.8400	-87.5437	2.6458	113.2467	0.0894	48.3363	0.7448	-15.3137
12.0000	0.8173	-96.3202	2.5912	107.3168	0.0949	44.7064	0.7294	-16.2620
13.0000	0.7955	-105.2201	2.5319	101.4588	0.0998	41.1546	0.7137	-17.0905
14.0000	0.7752	-114.2116	2.4683	95.6876	0.1040	37.6967	0.6978	-17.7940
15.0000	0.7568	-123.2524	2.4010	90.0176	0.1076	34.3482	0.6821	-18.3706
16.0000	0.7410	-132.2904	2.3308	84.4618	0.1105	31.1233	0.6667	-18.8225
17.0000	0.7280	-141.2656	2.2584	79.0317	0.1128	28.0348	0.6518	-19.1553
18.0000	0.7180	-150.1137	2.1845	73.7370	0.1145	25.0937	0.6377	-19.3785
19.0000	0.7111	-158.7703	2.1100	68.5850	0.1156	22.3090	0.6244	-19.5043
20.0000	0.7071	-167.1755	2.0354	63.5811	0.1163	19.6874	0.6120	-19.5472
21.0000	0.7059	-175.2778	1.9613	58.7284	0.1165	17.2338	0.6006	-19.5230
22.0000	0.7071	176.9633	1.8885	54.0279	0.1164	14.9512	0.5901	-19.4481
23.0000	0.7105	169.5758	1.8172	49.4790	0.1159	12.8407	0.5806	-19.3383
24.0000	0.7157	162.5756	1.7478	45.0797	0.1151	10.9022	0.5718	-19.2086
25.0000	0.7224	155.9676	1.6806	40.8266	0.1141	9.1344	0.5639	-19.0724
26.0000	0.7302	149.7480	1.6159	36.7153	0.1129	7.5349	0.5567	-18.9415
27.0000	0.7389	143.9057	1.5537	32.7407	0.1116	6.1008	0.5500	-18.8256
28.0000	0.7482	138.4250	1.4942	28.8972	0.1101	4.8283	0.5438	-18.7328
29.0000	0.7579	133.2869	1.4373	25.1788	0.1086	3.7135	0.5381	-18.6691
30.0000	0.7678	128.4709	1.3830	21.5792	0.1071	2.7522	0.5326	-18.6392
31.0000	0.7777	123.9558	1.3313	18.0922	0.1055	1.9397	0.5274	-18.6466
32.0000	0.7877	119.7203	1.2822	14.7115	0.1039	1.2713	0.5223	-18.6933
33.0000	0.7975	115.7441	1.2355	11.4308	0.1024	0.7422	0.5173	-18.7808
34.0000	0.8071	112.0077	1.1911	8.2441	0.1009	0.3472	0.5123	-18.9097
35.0000	0.8164	108.4928	1.1490	5.1453	0.0994	0.0812	0.5072	-19.0800
36.0000	0.8255	105.1823	1.1091	2.1289	0.0980	-0.0616	0.5020	-19.2915

37.0000	0.8343	102.0606	1.0711	-0.8109	0.0968	-0.0871	0.4967	-19.5438
38.0000	0.8428	99.1130	1.0351	-3.6792	0.0956	-0.0014	0.4911	-19.8360
39.0000	0.8510	96.3263	1.0009	-6.4812	0.0945	0.1884	0.4852	-20.1674
40.0000	0.8589	93.6883	0.9683	-9.2219	0.0936	0.4752	0.4791	-20.5372

But noise typically presents in actual measurement data. To make our verification realistic, noise (errors) should be introduced to the hypothetical model. But first, we need to examine type of errors and noise present in actual measured S-parameters of the devices. Network-analyzer measurements experience three types of errors [36]: systematic errors, random errors, and drift errors. For this reason, noise (errors) should be introduced to the simulated S-parameters of the hypothetical device to emulate the unavoidable measurement errors; and it is assumed for simplicity that the noise has uniform real and imaginary distribution whose limits are (+/-0.2%). They are shown in table 4.5.

Table 4.5 NOISY S-PARAMETERS of EF018A

FREQ	S11		S21		S12		S22	
(GHz)	MAG	ANG	MAG	ANG	MAG	ANG	MAG	ANG
1.0000	0.9990	-7.5147	2.9118	173.9241	0.0093	86.1979	0.8374	-1.5650
2.0000	0.9946	-15.0549	2.9063	167.8459	0.0184	82.3939	0.8350	-3.1228
3.0000	0.9863	-22.6454	2.8967	161.7637	0.0275	78.5864	0.8304	-4.6658
4.0000	0.9762	-30.3101	2.8828	155.6767	0.0365	74.7751	0.8248	-6.1859
5.0000	0.9619	-38.0713	2.8649	149.5857	0.0452	70.9611	0.8174	-7.6741
6.0000	0.9459	-45.9492	2.8393	143.4932	0.0536	67.1472	0.8083	-9.1202
7.0000	0.9277	-53.9610	2.8121	137.4038	0.0617	63.3385	0.7980	-10.5133
8.0000	0.9081	-62.1203	2.7802	131.3244	0.0694	59.5425	0.7867	-11.8415
9.0000	0.8857	-70.4361	2.7401	125.2640	0.0767	55.7686	0.7740	-13.0924
10.0000	0.8632	-78.9117	2.6977	119.2339	0.0833	52.0287	0.7598	-14.2537
11.0000	0.8408	-87.5437	2.6476	113.2467	0.0894	48.3363	0.7451	-15.3137
12.0000	0.8175	-96.3202	2.5914	107.3168	0.0950	44.7064	0.7296	-16.2620
13.0000	0.7959	-105.2201	2.5321	101.4588	0.0998	41.1546	0.7143	-17.0905
14.0000	0.7754	-114.2116	2.4683	95.6876	0.1041	37.6967	0.6982	-17.7940
15.0000	0.7573	-123.2524	2.4015	90.0176	0.1077	34.3482	0.6674	-18.3706
16.0000	0.7417	-132.2904	2.3320	84.4618	0.1106	31.1233	0.6823	-18.8225
17.0000	0.7286	-141.2656	2.2594	79.0317	0.1129	28.0348	0.6522	-19.1553
18.0000	0.7185	-150.1137	2.1860	73.7370	0.1146	25.0937	0.6378	-19.3785

19.0000	0.7112	-158.7703	2.1112	68.5850	0.1156	22.3090	0.6248	-19.5043
20.0000	0.7072	-167.1755	2.0364	63.5811	0.1164	19.6874	0.6124	-19.5472
21.0000	0.7059	-175.2778	1.9614	58.7284	0.1165	17.2338	0.6007	-19.5230
22.0000	0.7073	176.9633	1.8889	54.0279	0.1165	14.9512	0.5901	-19.4481
23.0000	0.7111	169.5758	1.8179	49.4790	0.1159	12.8407	0.5808	-19.3383
24.0000	0.7164	162.5756	1.7483	45.0797	0.1152	10.9022	0.5719	-19.2086
25.0000	0.7224	155.9676	1.6819	40.8266	0.1142	9.1344	0.5639	-19.0724
26.0000	0.7308	149.7480	1.6164	36.7153	0.1130	7.5349	0.5572	-18.9415
27.0000	0.7394	143.9057	1.5547	32.7407	0.1116	6.1008	0.5501	-18.8256
28.0000	0.7486	138.4250	1.4957	28.8972	0.1101	4.8283	0.5438	-18.7328
29.0000	0.7581	133.2869	1.4380	25.1788	0.1087	3.7135	0.5385	-18.6691
30.0000	0.7684	128.4709	1.3843	21.5792	0.1072	2.7522	0.5329	-18.6392
31.0000	0.7779	123.9558	1.3324	18.0922	0.1055	1.9397	0.5275	-18.6466
32.0000	0.7883	119.7203	1.2834	14.7115	0.1040	1.2713	0.5225	-18.6933
33.0000	0.7980	115.7441	1.2356	11.4308	0.1024	0.7422	0.5173	-18.7808
34.0000	0.8073	112.0077	1.1921	8.2441	0.1010	0.3472	0.5128	-18.9097
35.0000	0.8169	108.4928	1.1500	5.1453	0.0994	0.0812	0.5076	-19.0800
36.0000	0.8260	105.1823	1.1093	2.1289	0.0981	-0.0616	0.5021	-19.2915
37.0000	0.8349	102.0606	1.0712	-0.8109	0.0968	-0.0871	0.4970	-19.5438
38.0000	0.8430	99.1130	1.0359	-3.6792	0.0957	-0.0014	0.4912	-19.8360
39.0000	0.8515	96.3263	1.0016	-6.4812	0.0945	0.1884	0.4855	-20.1674
40.0000	0.8590	93.6883	0.9689	-9.2219	0.0936	0.4752	0.4793	-20.5372

Therefore, the correspond "Ideal Data" and "Noisy Data" of S-parameters obtained from the hypothetical model are shown in Figure 4.7

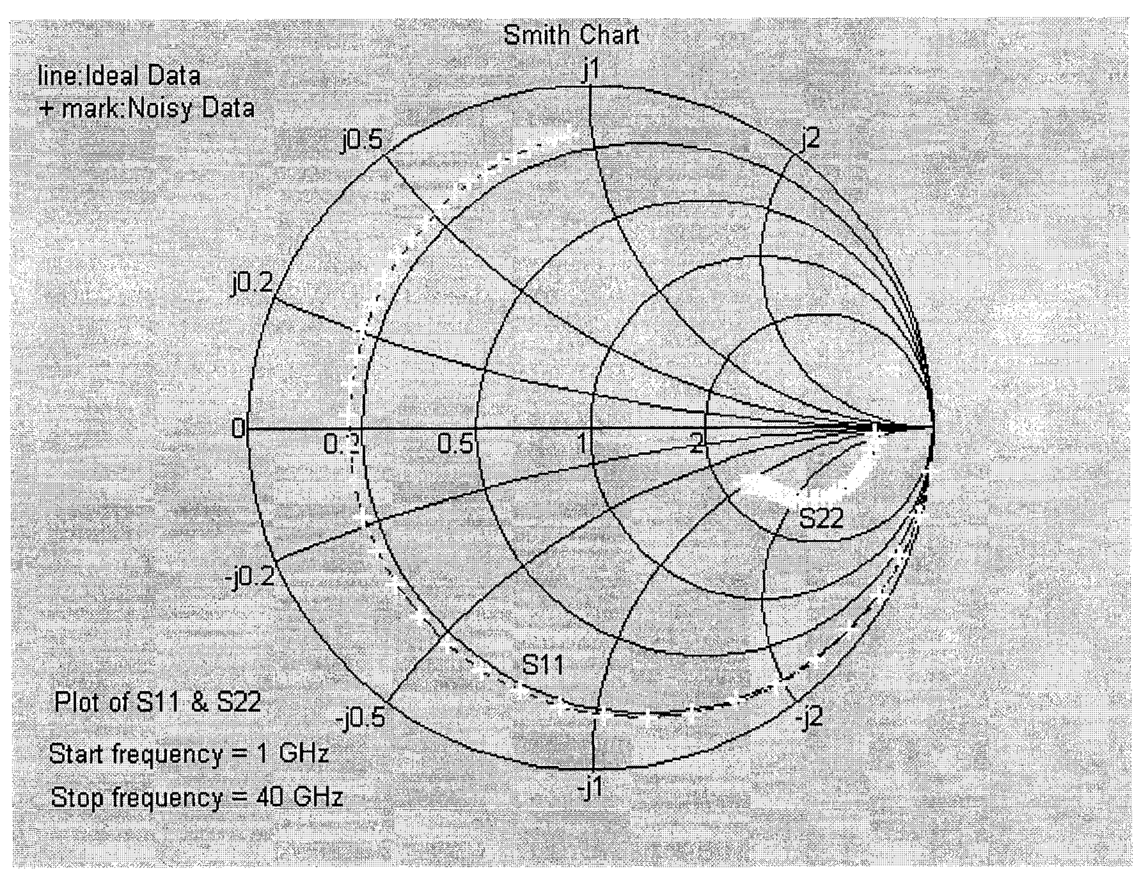

(a) Plot of S11 and S22

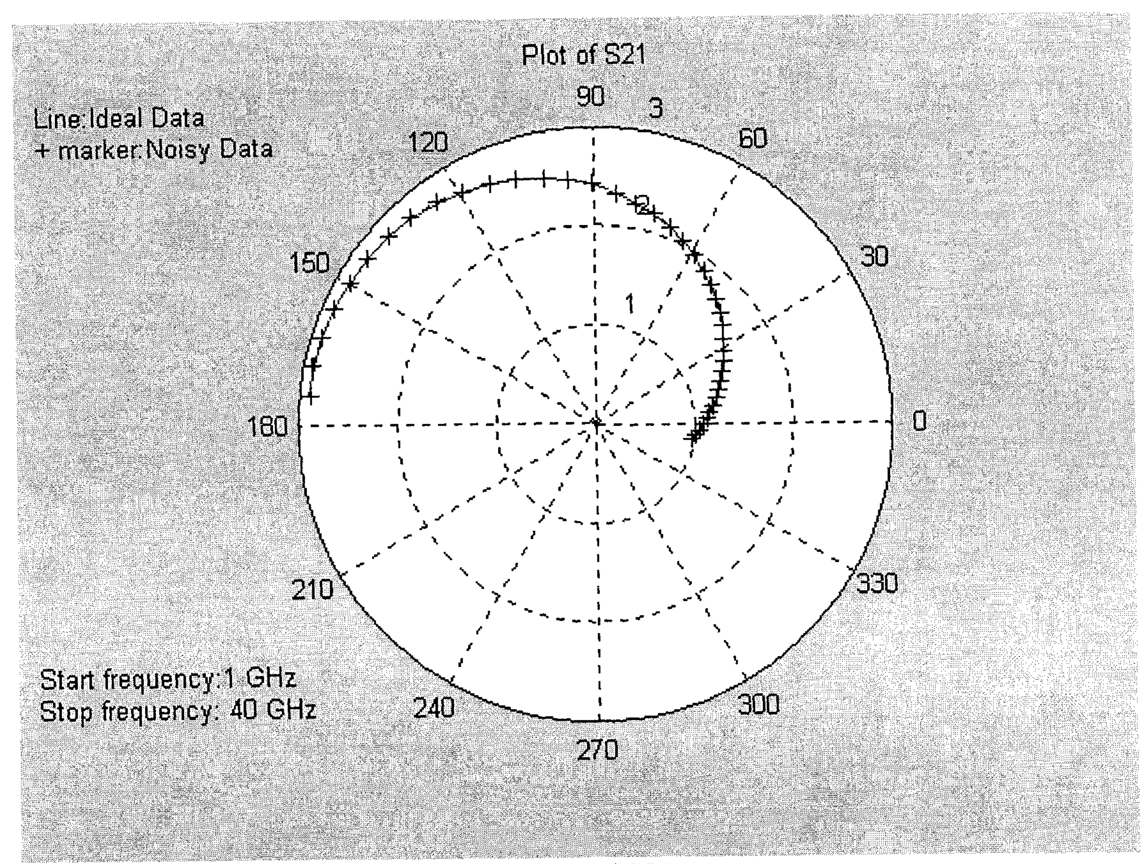

(b) Plot of S21

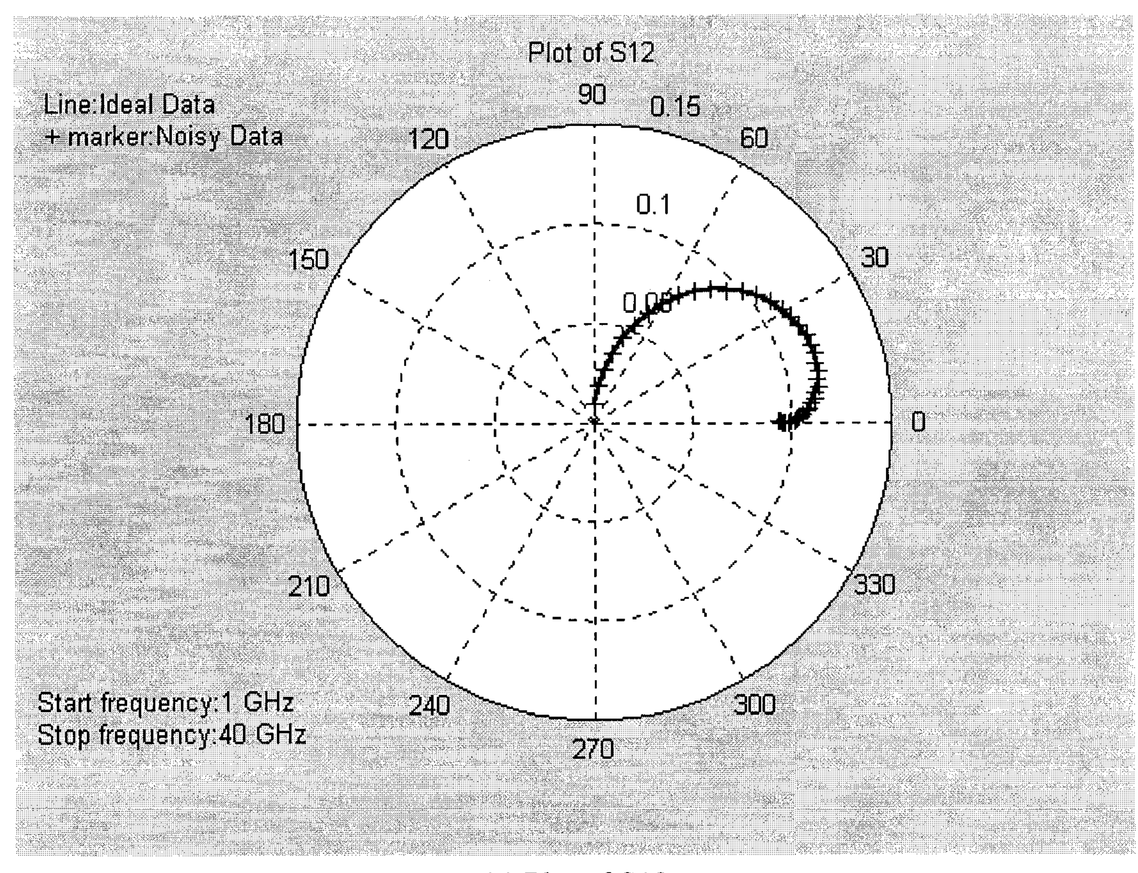

(c) Plot of S12

Figure 4.7 "Ideal Data" and "Noisy Data" of S-parameters for the hypothetical model

4.4.2 Results of Extracting Small-Signal Equivalent Circuit on "Ideal Data"

Knowing the hypothetical model's S-parameters, we use our method explained in detail in section 4.2 to extract its equivalent circuit element values, and then to calculate its model's S-parameters. The solutions for the "Ideal Data" are shown in table 4.6. With zero initial values and as expected, the calculated results are exactly the same as the original equivalent circuit values, since we mostly used analytical derivations. These results were obtained on the assumption that the elements C_{pg} *and* C_{pd}, L_g, L_d *and* L_s, and ΔR_{ds} are extracted correctly and their values equal to the hypothetical model values.

Table 4.6 The extracted equivalent circuit element values for a hypothetical device based on "Ideal Data" with initial value x=0.

Parameter	Calculated Value	Hypothetical Value	Err%	Parameter	Calculated Value	Hypothetical Value	Err%
Rg (Ω)	0.499988	0.5	2.4e-5	Ri (Ω)	0.530048	0.53	-9.1e-5
Rd (Ω)	0.999945	1.0	5.5e-6	Cgs (pF)	0.170000	0.17	
Rs (Ω)	0.229945	0.23	2.4e-4	Cds (pF)	0.00599998	0.006	3.3e-6
Lg (nH)	0.23	0.23		Cgd (pF)	0.016000	0.016	
Ld (nH)	0.22	0.22		gm (mS)	31.99990	32	3.1e-6
Ls (nH)	0.063	0.063		gds (mS)	1.785710	1.786	1.6e-4
ΔR_{ds}	0.77	0.77		τ (ps)	2.400000	2.4	

The error (Err%) of a variable is defined as:

$$Err\% = \frac{Hypothetical - Calculated}{Hypothetical} \times 100$$

The calculated S-parameters versus the hypothetical device's S-parameters using the "Ideal Data" are shown in Figure 4.8

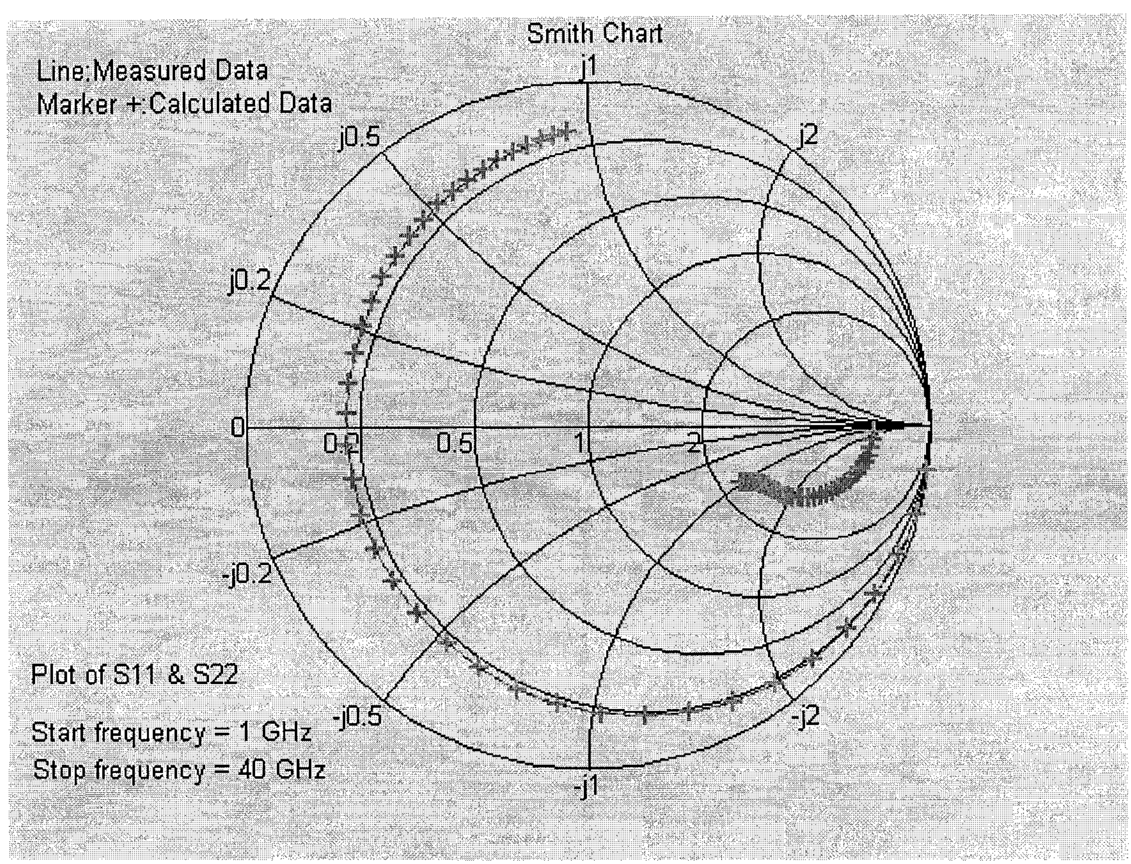

(a) Plot of S11 and S22

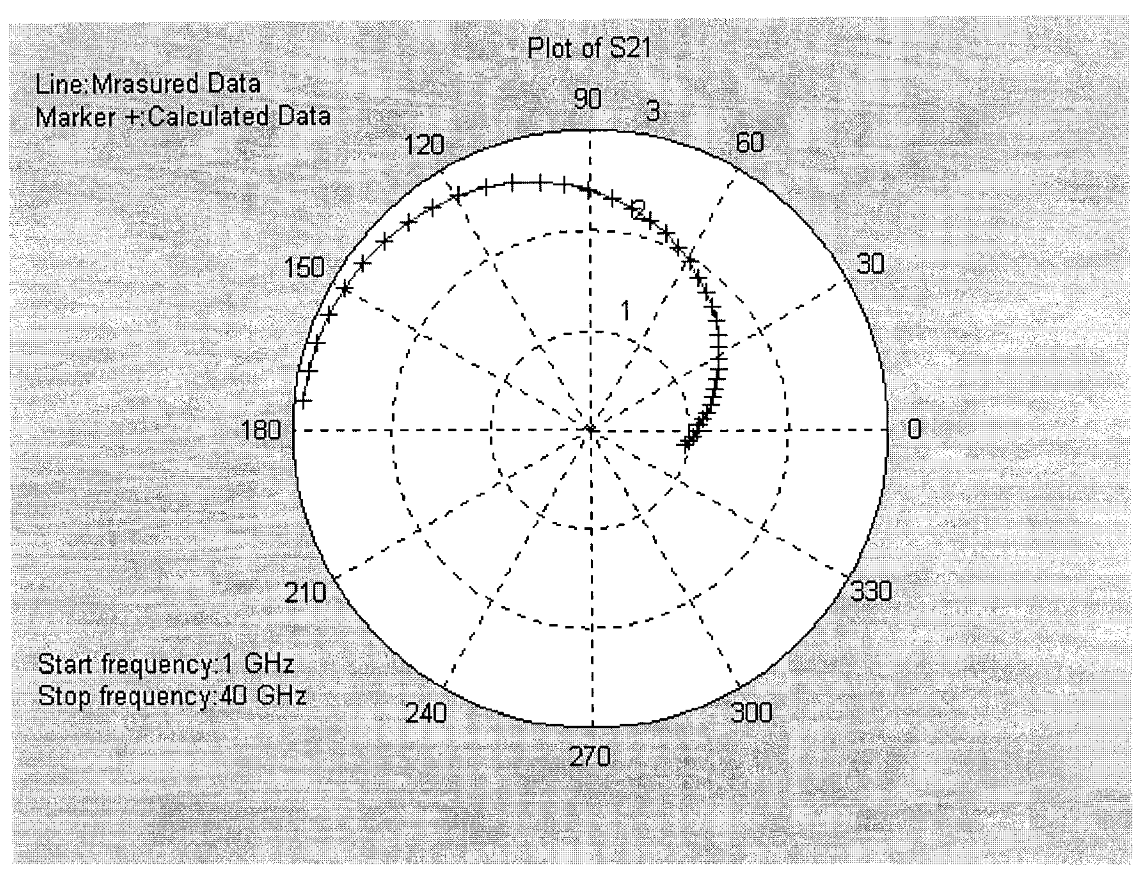

(b) Plot of S21

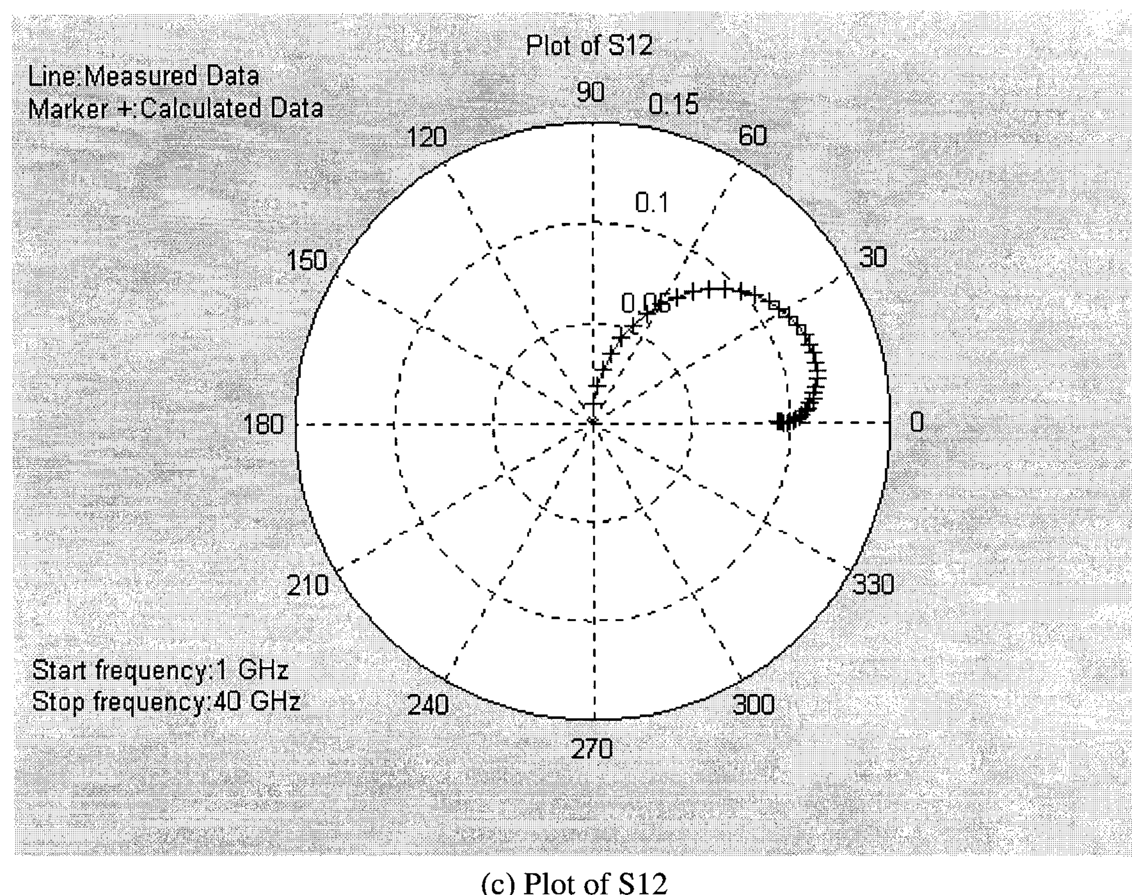

(c) Plot of S12

Figure 4.8 S-parameters of the hypothetical device versus calculated model using the "Ideal Data"

4.4.3 Results of Extracting Small-Signal Equivalent Circuit on "Noisy Data"

The equivalent circuit extraction results based on the "Noisy Data" are shown in table 4.7. It is also assumed that the element values of C_{pg} *and* C_{pd} , L_g, L_d *and* L_s , and ΔR_{ds} are already extracted correctly and their values equal to the hypothetical model values.

Table 4.7 The extracted equivalent circuit element values for a hypothetical device using new method based on "Noisy Data".

Parameter	Calculated Value	Hypothetical Value	Err%	Parameter	Calculated Value	Hypothetical Value	Err%
Rg (Ω)	0.51	0.5	-2	Ri (Ω)	0.22	0.53	58
Rd (Ω)	1.14	1.0	-14	Cgs (pF)	0.171	0.17	-0.59
Rs (Ω)	0.37	0.23	-61	Cds (pF)	0.006	0.006	
Lg (nH)	0.230	0.23		Cgd (pF)	0.016	0.016	
Ld (nH)	0.22	0.22		gm (mS)	32.2	32	-0.62
Ls (nH)	0.063	0.063		gds (mS)	1.789	1.786	-0.17
ΔR_{ds}	0.77	0.77		τ (ps)	2.43	2.4	-1.3

The calculated S-parameters versus the hypothetical device's S-parameters using the "Noisy Data" are shown in Figure 4.9.

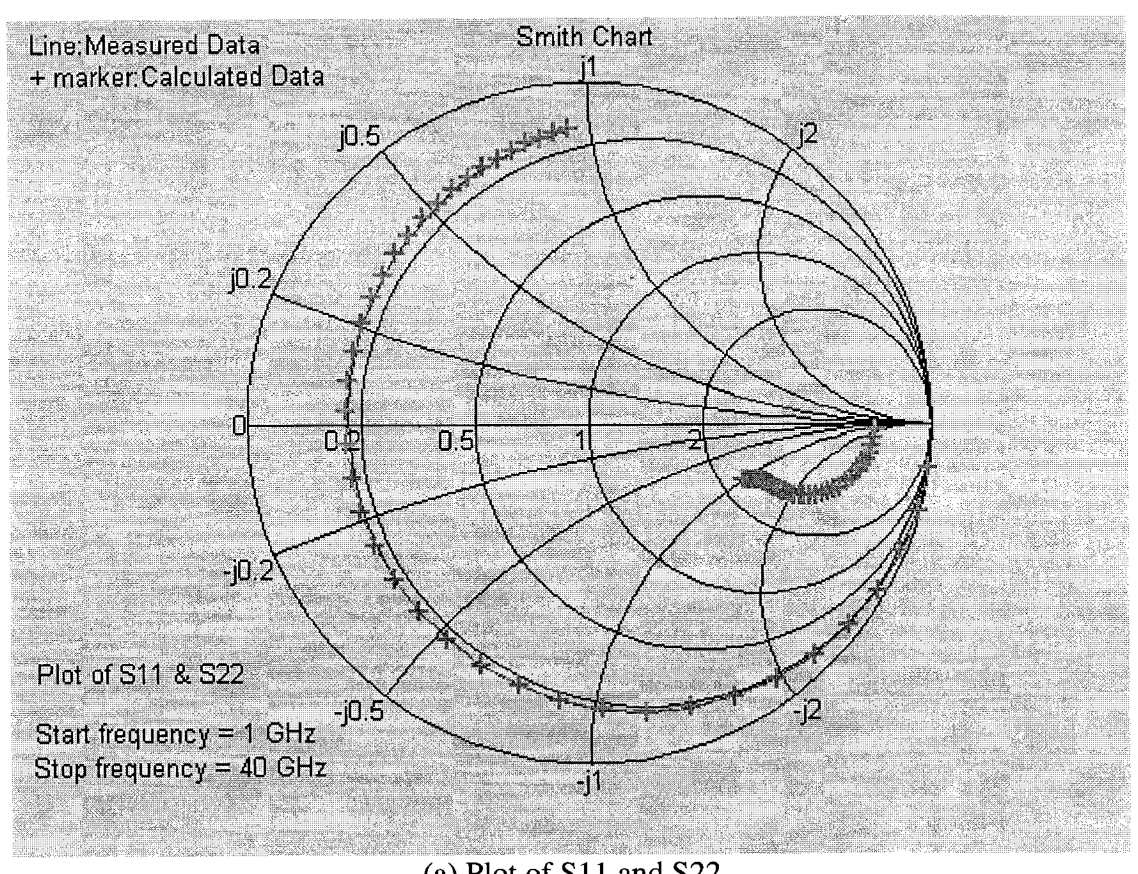

(a) Plot of S11 and S22

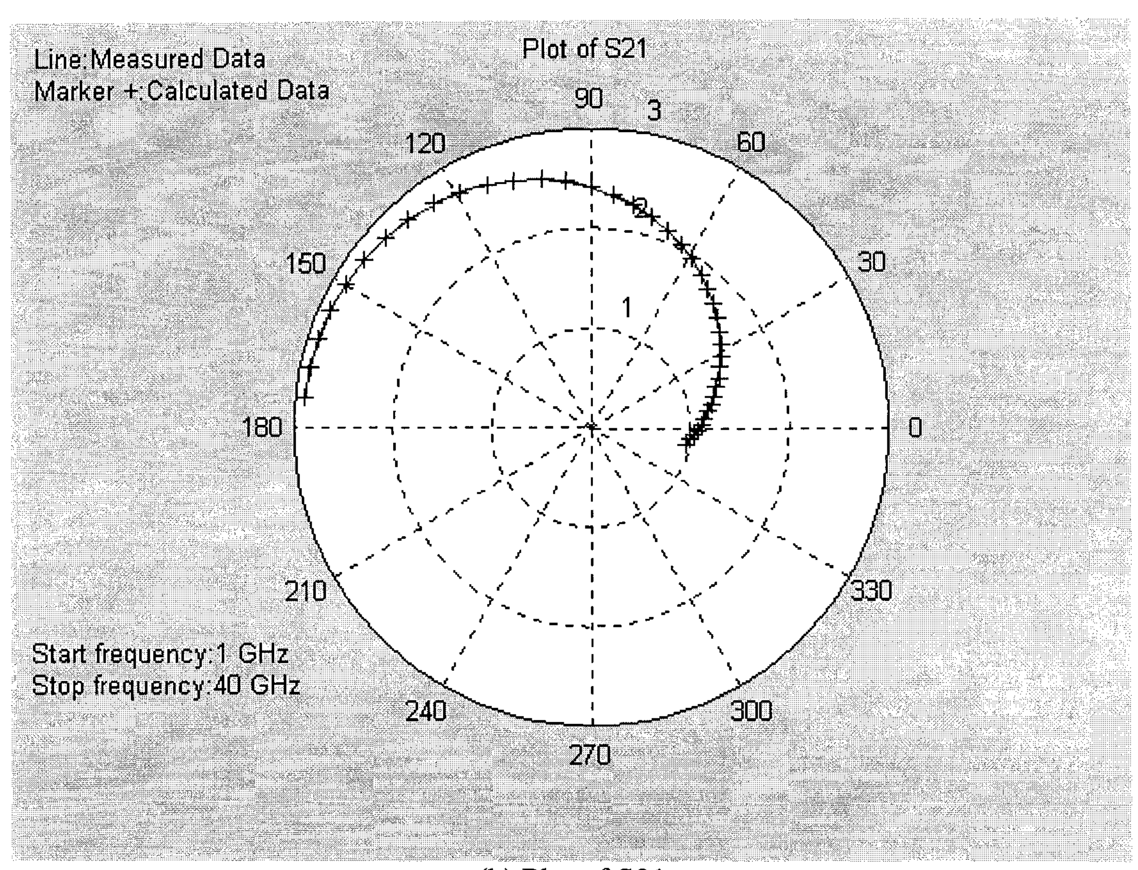

(b) Plot of S21

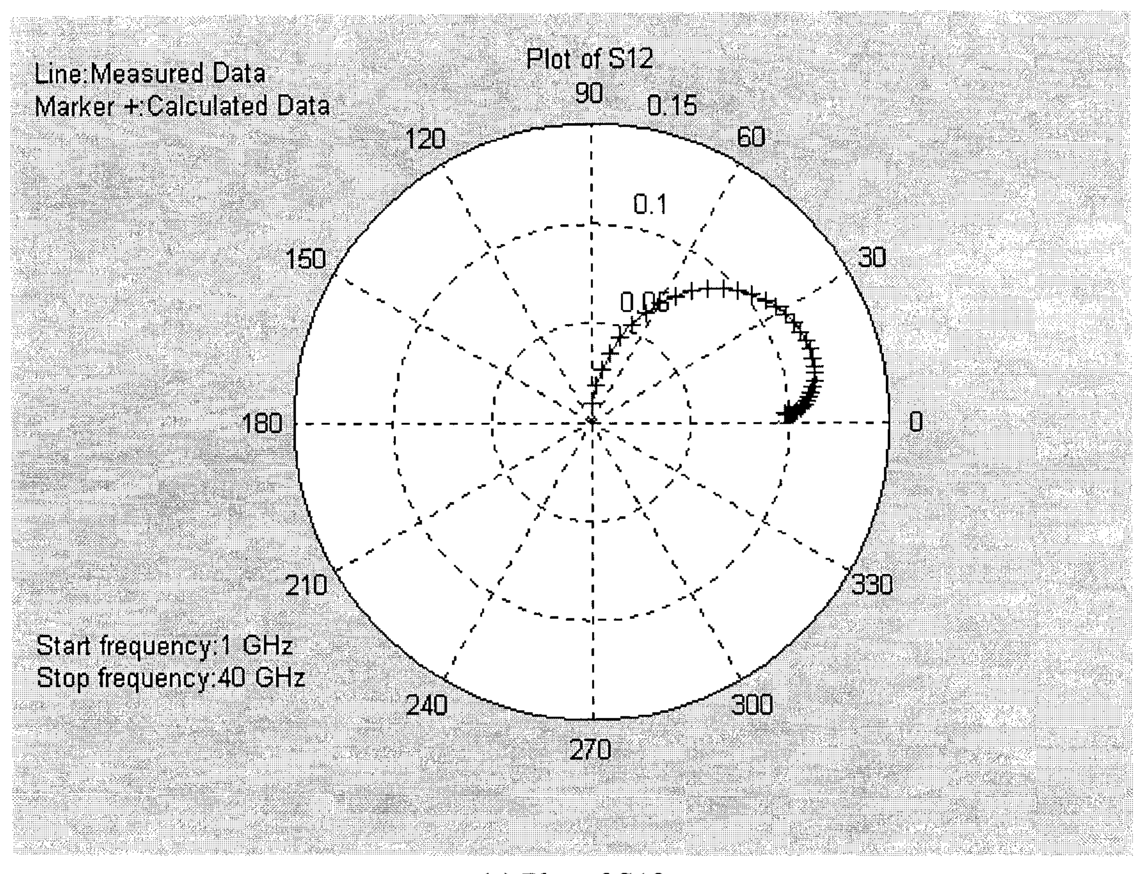

(c) Plot of S12

Figure 4.9 S-parameters of the hypothetical device versus calculated model using the "Noisy Data"

It is noticed from the results that the element values obtained from "Noisy Data" are different from the hypothetical values. This is because the minimum of the optimal solution is deviated for the noisy file. This can be proved by comparing the objective function values by substituting the "Noisy Data" solution and the hypothetical values into the objective function for the noisy file. We can find that the objective function value at the hypothetical values is larger than that at the "Noisy Data" solution. This interprets that adding noise to the measured data moves the global minimum from the hypothetical point to another solution point.

Another interesting point can be observed from Table 4.7. The error percentage of all resistive elements is relatively large. This is because the real parts of Y_{int11}, Y_{int12}, Y_{int21} and Y_{int22} have significant amount of noise compared with their imagine parts. Those components are the most sensitive parts to noise. In addition, these noisy components are used to calculate the resistive elements of the intrinsic model.

Therefore, if there is a large error level in the intrinsic Y-parameters, it might be difficult to extract the resistive elements of the model in the presence of the dominating capacitance impedances. The reason is that the resistive values might become comparable to the noise level. So if the measured S-parameters contain large errors, the extracted resistive elements by optimizer results might have relatively large errors. However, Figure 4.9 shows an acceptable agreement between the input S-parameters and the calculated ones.

4.4.4 Comparison with other methods

For the verification of the proposed method, we also use the previous typical multi-dimensional optimization method proposed by *Ooi et al* [15] and *Shirakawa et al* [14] to extract the small-signal model circuit elements.

Ooi's method is very similar to Shirakawa's method except that R_g is not an optimization parameter. It is calculated in terms of the other optimization parameters. Thus, the number of the optimization parameters decreases to five instead of six, and in contrast the number of objective error function elements increases to eight instead of seven.

Both methods have the initial value-dependence problem and the local minimum problem. The equivalent circuit element values based on the "Ideal Data" using Ooi's and Shirakawa's method with initial value **x=0** and **x** close to optimal solutions are calculated respectively. The results are shown in Table 4.8, 4.9, 4.10, and 4.11. Also, the equivalent circuit element values based on the "Noisy Data" using Ooi's and Shirakawa's method with initial value **x=0** are calculated. Both results are shown in Table 4.12 and 4.13 respectively. The convergence condition used in each extracting iteration is the same as the new proposed method.

Table 4.8 The extracted equivalent circuit element values for a hypothetical device using Ooi's method based on "Ideal Data" with initial value: Lg=0, Ld=0, Ls=0, Rd=0, Rs=0.

Parameter	Calculated Value	Hypothetical Value	Parameter	Calculated Value	Hypothetical Value
Rg (Ω)	15.92	0.5	Ri (Ω)	-11.710	0.53
Rd (Ω)	91.95	1.0	Cgs (pF)	0.426	0.17
Rs (Ω)	9.817	0.23	Cds (pF)	0.029	0.006
Lg (nH)	0.004	0.23	Cgd (pF)	0.036	0.016
Ld (nH)	-0.193	0.22	gm (mS)	445.8	32
Ls (nH)	-0.011	0.063	gds (mS)	0.4644	1.786
			τ (ps)	-3.05	2.4

Table 4.9 The extracted equivalent circuit element values for a hypothetical device using Ooi's method based on "Ideal Data" with initial value: Lg = 2.2e-010; Ld = 2.2e-010; Ls = 6.2e-011; Rd = 0.98; Rs = 0.22

Parameter	Calculated Value	Hypothetical Value	Parameter	Calculated Value	Hypothetical Value
Rg (Ω)	0.50	0.5	Ri (Ω)	0.529	0.53
Rd (Ω)	1.00	1.0	Cgs (pF)	0.170	0.17
Rs (Ω)	0.231	0.23	Cds (pF)	0.0060	0.006
Lg (nH)	0.23	0.23	Cgd (pF)	0.0160	0.016
Ld (nH)	0.22	0.22	gm (mS)	32.0	32
Ls (nH)	0.063	0.063	gds (mS)	1.786	1.786
			τ (ps)	2.40	2.4

Table 4.10 The extracted equivalent circuit element values for a hypothetical device using Shirakawa's method based on "Ideal Data" with initial value: Lg=0, Ld=0, Ls=0, Rg=0,Rd=0, Rs=0.

Parameter	Calculated Value	Hypothetical Value	Parameter	Calculated Value	Hypothetical Value
Rg (Ω)	-1.89	0.5	Ri (Ω)	1.054	0.53
Rd (Ω)	59.20	1.0	Cgs (pF)	0.689	0.17
Rs (Ω)	5.75	0.23	Cds (pF)	0.045	0.006
Lg (nH)	-0.002	0.23	Cgd (pF)	0.013	0.016
Ld (nH)	-0.035	0.22	gm (mS)	285.9	32
Ls (nH)	0.026	0.063	gds (mS)	6.573	1.786
			τ (ps)	-3.8	2.4

Table 4.11 the extracted equivalent circuit element values for a hypothetical device using Shirakawa's method based on "Ideal Data" with initial value: Lg =2.22e-010; Ld =2.2e-010; Ls =6.29e-011; Rd =0.98; Rs =0.22; Rg =0.49

Parameter	Calculated Value	Hypothetical Value	Parameter	Calculated Value	Hypothetical Value
Rg (Ω)	0.5	0.5	Ri (Ω)	0.529	0.53
Rd (Ω)	1.0	1.0	Cgs (pF)	0.17	0.17
Rs (Ω)	0.231	0.23	Cds (pF)	0.006	0.006
Lg (nH)	0.23	0.23	Cgd (pF)	0.016	0.016
Ld (nH)	0.22	0.22	gm (mS)	32	32
Ls (nH)	0.063	0.063	gds (mS)	1.786	1.786
			τ (ps)	2.4	2.4

Table 4.12 The extracted equivalent circuit element values for a hypothetical device using Ooi's method based on "Noisy Data" with initial value: Lg=0, Ld=0, Ls=0, Rd=0, Rs=0.

Parameter	Calculated Value	Hypothetical Value	Parameter	Calculated Value	Hypothetical Value
Rg (Ω)	28.0	0.5	Ri (Ω)	-17.52	0.53
Rd (Ω)	33.2	1.0	Cgs (pF)	-8.57	0.17
Rs (Ω)	3.30	0.23	Cds (pF)	0.13	0.006
Lg (nH)	0.0018	0.23	Cgd (pF)	-0.61	0.016
Ld (nH)	0.014	0.22	gm (mS)	2167	32
Ls (nH)	-0.024	0.063	gds (mS)	131	1.786
			τ (ps)	-4.29	2.4

Table 4.13 the extracted equivalent circuit element values for a hypothetical device using Shirakawa's method based on "Noisy Data" with initial value: Lg =0; Ld =0; Ls =0; Rd =0; Rs =0; Rg =0

Parameter	Calculated Value	Hypothetical Value	Parameter	Calculated Value	Hypothetical Value
Rg (Ω)	-22.8	0.5	Ri (Ω)	30.0	0.53
Rd (Ω)	87.8	1.0	Cgs (pF)	-0.62	0.17
Rs (Ω)	7.23	0.23	Cds (pF)	0.037	0.006
Lg (nH)	0.012	0.23	Cgd (pF)	0.017	0.016
Ld (nH)	-0.23	0.22	gm (mS)	463	32
Ls (nH)	-0.03	0.063	gds (mS)	13.4	1.786
			τ (ps)	-1.8	2.4

Table 4.8, 4.9, 4.10 and 4.11 demonstrated that both Ooi's and Shirakawa's methods have the initial value-dependence problem and the local minimum problem. When the initial values are zero, some unrealistic values could be obtained in both methods. For example, it doesn't make any sense that Cgs and Ls are negative. So, in both methods, initial values are usually generated by [13] in order to find correct solution.

Comparing Table 4.7, 4.12 and 4.13, it can be seen that under the same convergence condition and zero initial values, the equivalent circuit element values extracted by the new method are more accurate and reliable than both Ooi's and Shirakawa's methods.

Finally, the comparison of the new proposed method with the Ooi's and Shirakawa's method is summarized in the Table 4.14.

Table 4.14 the comparison of the new proposed method with the Ooi's and Shirakawa's method for extraction of small-signal equivalent circuit

Item	Shirakawa's method	Ooi's method	The proposed method
Number of optimization variable	6	5	1
Convergence rate	Slow	Slow	Fast
Initial value-dependence	Yes	Yes	No
Need other measurement	No	No	Yes (pinch-off and cold measurement)

4.4.5 Results of Extraction of FET Noise Parameters

A knowledge of the small-signal equivalent circuit and the noise parameters of a packaged device and its physical temperature at a single frequency, one can predict the noise performance of the device at any frequency by using Pospieszalski's noise model.

To investigate our method for extraction of FET noise parameters, the device is used the same as [27]. Its equivalent circuit is show in Fig. 4.10. The equivalent circuit elements values are shown in Table 4.15. The measured noise parameters of FHR01FH as a packaged device at room temperature are given in Table 4.16.

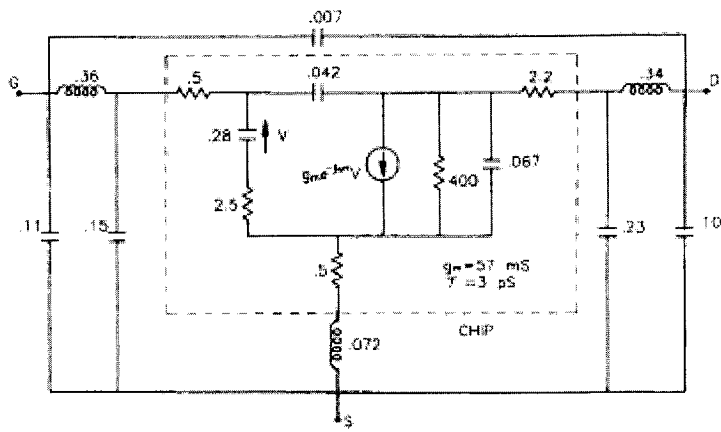

Figure 4.10 Equivalent circuit of FHR01F HEMT at $T_a = 297$ K, $V_{ds} = 2V$, $I_{ds} = 10mA$.

Values of resistance, capacitance, and inductance are given in Ω, pF, and nH .

Table 4.15 Equivalent circuit of FHR01F HEMT at $T_a = 297$ K, $V_{ds} = 2V$, $I_{ds} = 10mA$.

R_g (Ω)	R_d (Ω)	R_s (Ω)	L_g (nH)	L_d (nH)	L_s (nH)	C_{gs} (pF)	R_i (Ω)	C_{gd} (pF)	g_m (mS)	τ (ps)	g_{ds} (mS)	C_{ds} (pF)
0.5	2.2	0.5	0.36	0.34	0.072	0.28	2.5	0.042	57	3	2.5	0.067

C_{pg} (pF)	C_{pd} (pF)	C_{GS} (pF)	C_{GD} (pF)	C_{DS} (pF)
0.15	0.23	0.11	0.007	0.10

Table 4.16 Noise parameters of FHR01FH as a packaged FET at $f = 8.5$ GHz, $V_{ds} = 2V$

	$T_a = 297K$, $I_{ds} = 10mA$			
Noise parameters	$T_{\min}(K)$	$R_{opt}(\Omega)$	$X_{opt}(\Omega)$	$g_n(mS)$
Packaged FET	78.0	10.5	17.5	9.4

From these small-signal equivalent circuit element values and the noise parameters of a packaged device and its physical temperature at a single frequency, we are going to predict the noise performance of the device at any frequency using our proposed method described in section 4.3. First we use the method [32] to determine the noise parameters of the intrinsic chip without C_{gd}. The results are shown in Table 4.17. Then, we use the new proposed method to extract the two equivalent temperature T_g and T_d, which shown in Table 4.18. Finally, the noise parameters can be obtained at any frequency within our

interesting frequency range (here it is assumed that the frequency range is 2GHz-22GHz). They are shown in Figure 4.11.

Table 4.17 De-embedding the noise parameters of FHR01FH at different stages ($f = 8.5\ GHz$, $V_{ds} = 2V$)

	$T_a = 297\ K$, $I_{ds} = 10mA$			
Noise parameters	$T_{\min}(K)$	$R_{opt}(\Omega)$	$X_{opt}(\Omega)$	$g_n(mS)$
Packaged FET	78.0	10.5	17.5	9.4
Intrinsic chip without C_{gd}	65.6	26.3	59.5	3.0

Table 4.18 Computation of T_g ,T_d, and noise parameters of modeled FHR01FH intrinsic chip ($f = 8.5\ GHz$, $V_{ds} = 2V$)

$T_a = 297\ K$, $I_{ds} = 10mA$						
Comments	$T_{\min}$ K	R_{opt} Ω	X_{opt} Ω	g_n mS	T_g K	T_d K
Noise parameters of Intrinsic chip without C_{gd} from Table 5.9	65.6	26.3	59.5	3.0		
Computed values	65.6	26.3	66.9	3.8	312	6619
Computed values from [27]	58.7	28.4	66.9	3.27	304	5514

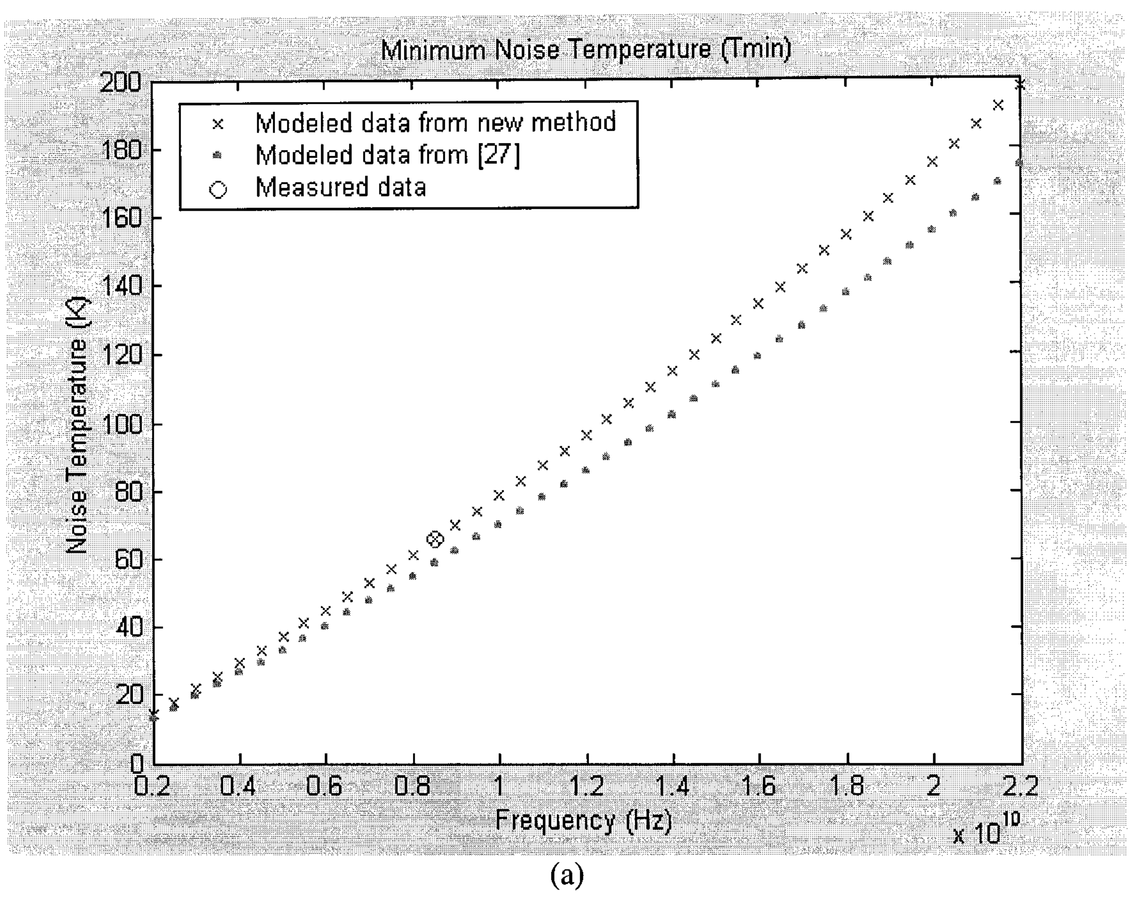

(a)

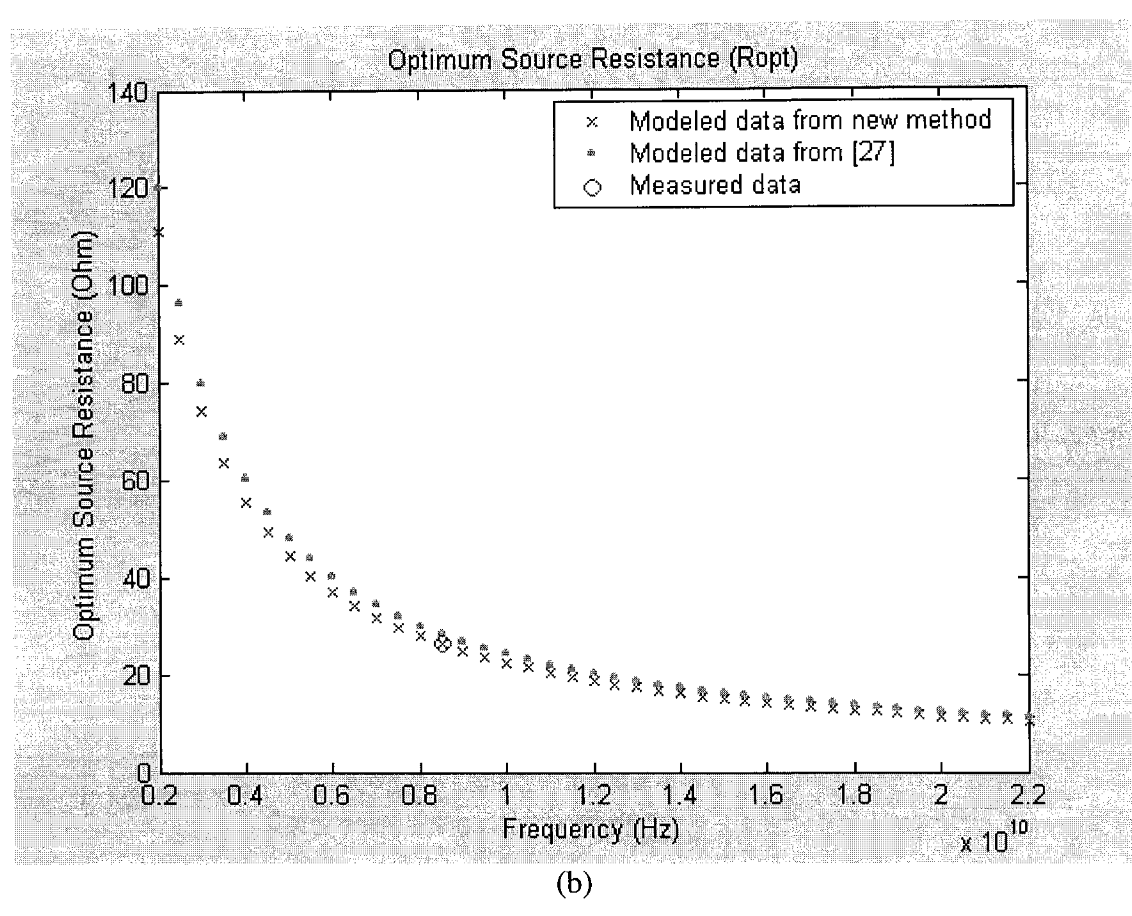

(b)

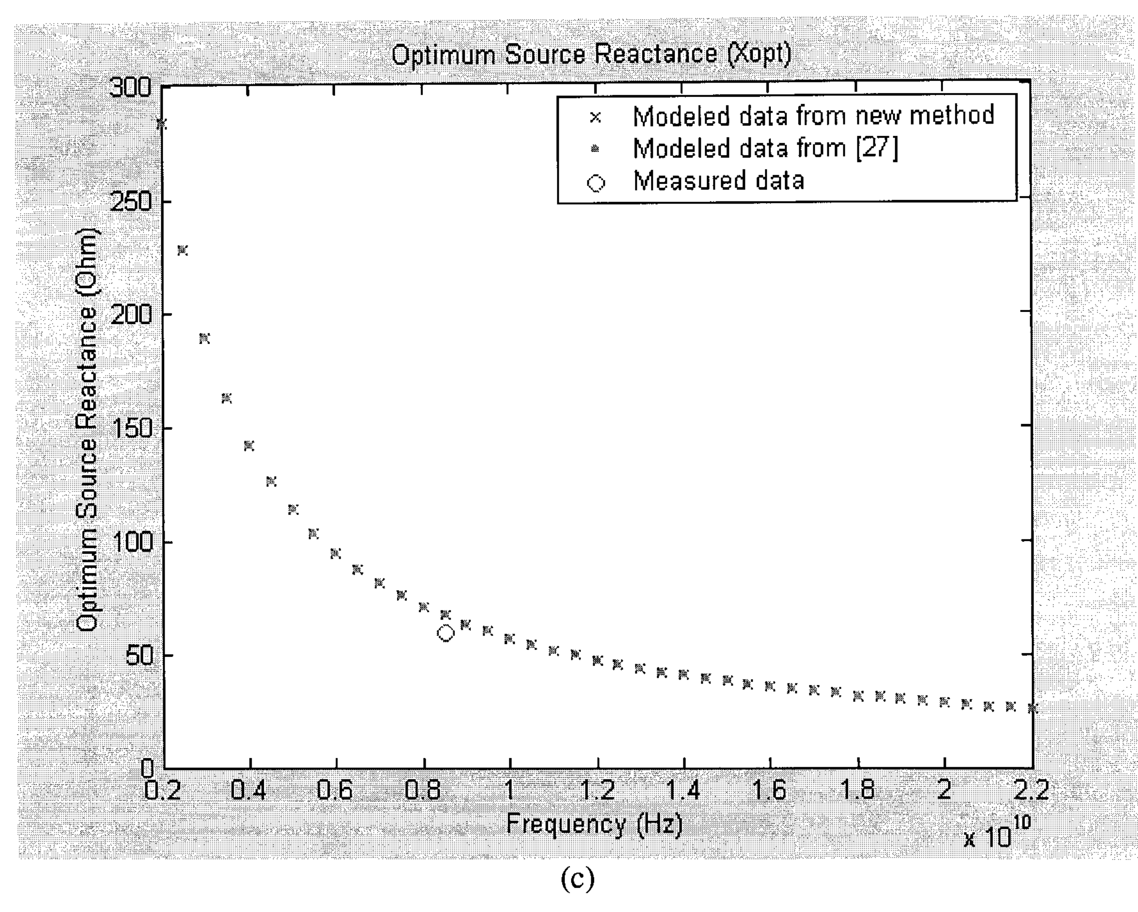

(c)

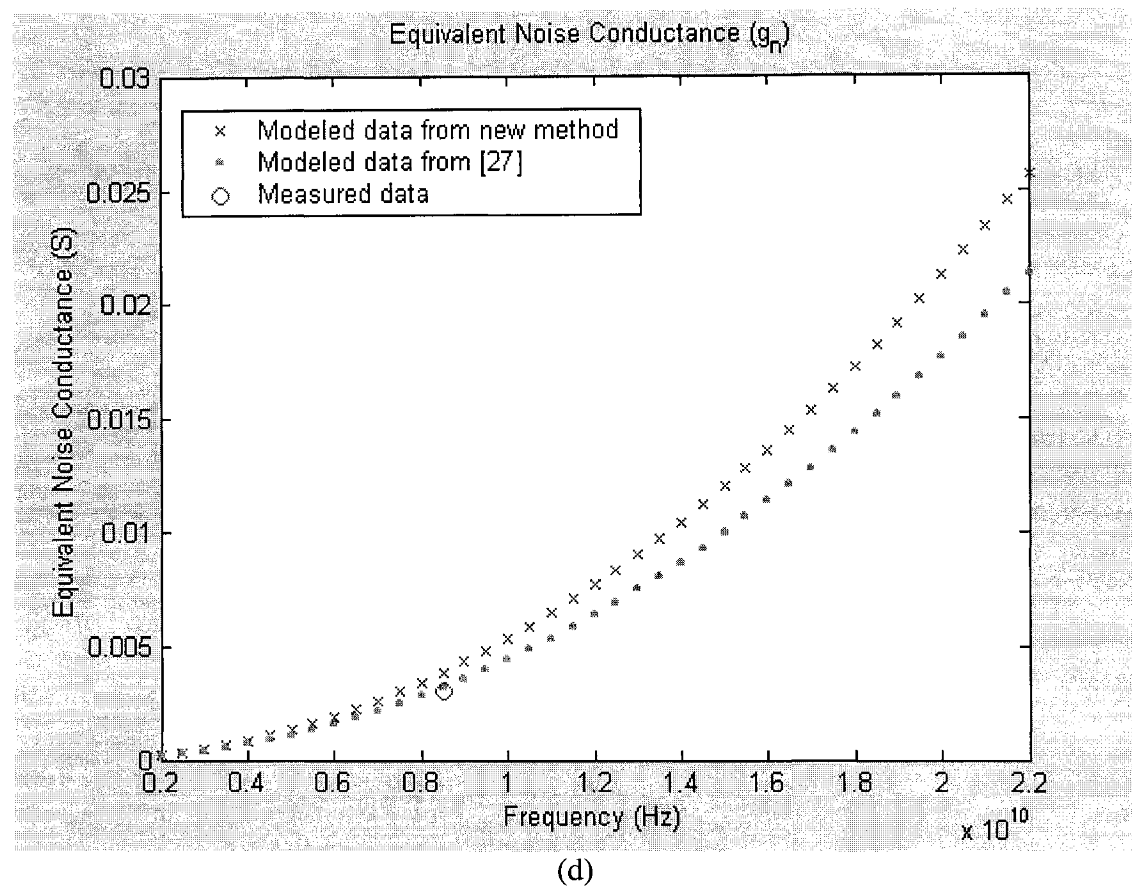

(d)

Figure 4.11 Noise parameters of FHR01FH (chip) HEMT at $T_a = 297K$, $V_{ds} = 2V$ $I_{ds} = 10mA$. (a) Minimum noise temperature ($T_{\min}$) vs. frequency. (b) Optimum source resistance (R_{opt}) vs. frequency. (c) Optimum source reactance (X_{opt}) vs. frequency. (d) Equivalent noise conductance (g_n) vs. frequency.

It is noted that the results of Table 4.17 is the same as [27]. This is because the same de-embedding method [32] was used to compute the noise parameters of the intrinsic chip without C_{gd}. From the Table 4.18, it is obvious that the computed values of noise parameters using our proposed method are much more close to the measured noise parameters of intrinsic chip than those computed from [27] except the equivalent conductance (g_n). This can also be demonstrated from Figure 4.11(a)-(d).

Figure 4.11 gives four noise parameters computed from our new proposed method and from [27]. The blue x-marks indicate the data computed from the model using the new proposed method. The green points indicate the data computed from [27] with

$T_g = 304K$ and $T_d = 5514K$. And the circles indicate the data measured at $f = 8.5\ GHz$, $V_{ds} = 2V$, $T_a = 297\ K$, $I_{ds} = 10mA$.

The minimum noise temperature curves as a function of frequency is shown in Fig. 4.11.a. Both curves have almost the same noise temperature at 2 GHz and divert as the frequency increases. But the blue curve is more close to the circle measured data.

The optimum source resistance curve as a function of frequency is shown in Fig. 4.11.b. The maximum resistance of 110 Ω occurs at a 2 GHz and decreases rapidly to 10 Ω level at 22 GHz. The two curves have maximum difference at 2 GHz and go together as the frequency increases. But the blue curve is still more close to the circle measured data.

The optimum source reactance curve as a function of frequency is shown in Fig. 4.11.c. Both curves are the same and overlap each other because the optimum source reactance is independent of T_g and T_d.

The equivalent noise conductance curve as a function of frequency is shown in Fig. 4.11.d. Both curves have almost the same values at 2 GHz and divert as the frequency increases. But the green curve is more close to the circle measured data although both curves have a very similar trend.

The results of above tables and figures demonstrated that the new proposed method is more accurate than other fitting method.

Recently, some other method for direct extraction of two-parameter noise models has been proposed, such as [34]. But it is more complicated than our proposed method because it is necessary to calculate the two noise temperature parameters $T_g\ and\ T_d$ from noise figures measured at two different source admittances by using nodal analysis of circuits. More recently, another method of direct extraction of FET noise models from noise figure measurements was proposed by Matthias Rudolph *et al* [35]. This method allows for extraction of the parameters for both the Pospieszalski and Pucel *et al.* noise models directly from NF measurements. Although it is not necessary to calculate the four two-port noise parameters, it still needs to do measurements at different frequencies or at different source admittances. The computation complexity of this method is not lesser than our method.

4.4.6 Influence of gate width on device noise performance

As discussed early in section 3.2.2, an important application of Fukui noise model is that it allows a simple method of predicting the dependence of noise parameters by means of device geometry, such as gate width. That means the device noise performance can be influenced by its geometry. Equations (3.22) through (3.37) have been obtained [1] for the noise parameters as a function of gate width in Fukui noise model.

$$R_n^{'} = R_n / s_1 \tag{3.32}$$

$$X_{opt}^{'} = X_{opt} / s_1 \tag{3.33}$$

$$F_{\min}^{'} = 1 + \left(F_{\min} - 1\right)\left[\frac{1 + \left(R_g / R_s\right)\left(s_1 s_2\right)}{1 + \left(R_g / R_s\right)}\right]^{1/2} \tag{3.34}$$

$$R_{opt}^{'} = R_{opt}\left[\frac{1 + \left(4 g_m R_s\right) + \left(4 g_m R_g s_1 s_2\right)}{1 + 4 g_m R_s + 4 g_m G_g}\right] \tag{3.35}$$

$$s_1 = Z^{'} / Z \tag{3.36}$$

$$s_2 = \frac{Z^{'} / N^{'}}{Z / N} \tag{3.37}$$

where s_1 and s_2 are scaling factors that relate a known FET of width Z to a scaled one of width $Z^{'}$ by the equation given in [1]. N is the number of finger gate of a given FET and N' is the number of finger gate of a scaled FET.

Furthermore, the minimum noise figure as a function of the device physical parameters and bias current was obtained by Cappy *et al* [25] expressed by (3.40)

$$F_{\min} = 1 + (8\pi)^{1/2} f\left[\frac{L}{f_T}(\alpha Z + \beta I_{ds})(R_s + R_g)\right]^{1/2} \tag{3.40}$$

where

$f_T = g_m / (2\pi C_{gs})$

$Z =$ FET gate width

$L =$ FET gat length

$\alpha, \beta =$ fitting factors

$g_{ds} = 1 / r_{ds}$

f = Operating frequency

I_{ds} = Drain source current

R_s, R_g = parasitic resistance

From analyzing the above equations, it can be concluded that if the gate width increases, the minimum noise figure $F_{\min}$ and the optimal resistance R_{opt} will increase; the equivalent noise resistance R_n and the optimal reactance X_{opt} will decrease. This can also be verified by Figure 4.12 [37] which shows comparisons of measured and predicted noise parameters versus frequency for two MESFET's of different dimensions biased at $I_{ds} = 0.6I_{dss}$ and $I_{ds} = 0.45I_{dss}$ with $V_{ds} = 5V$.

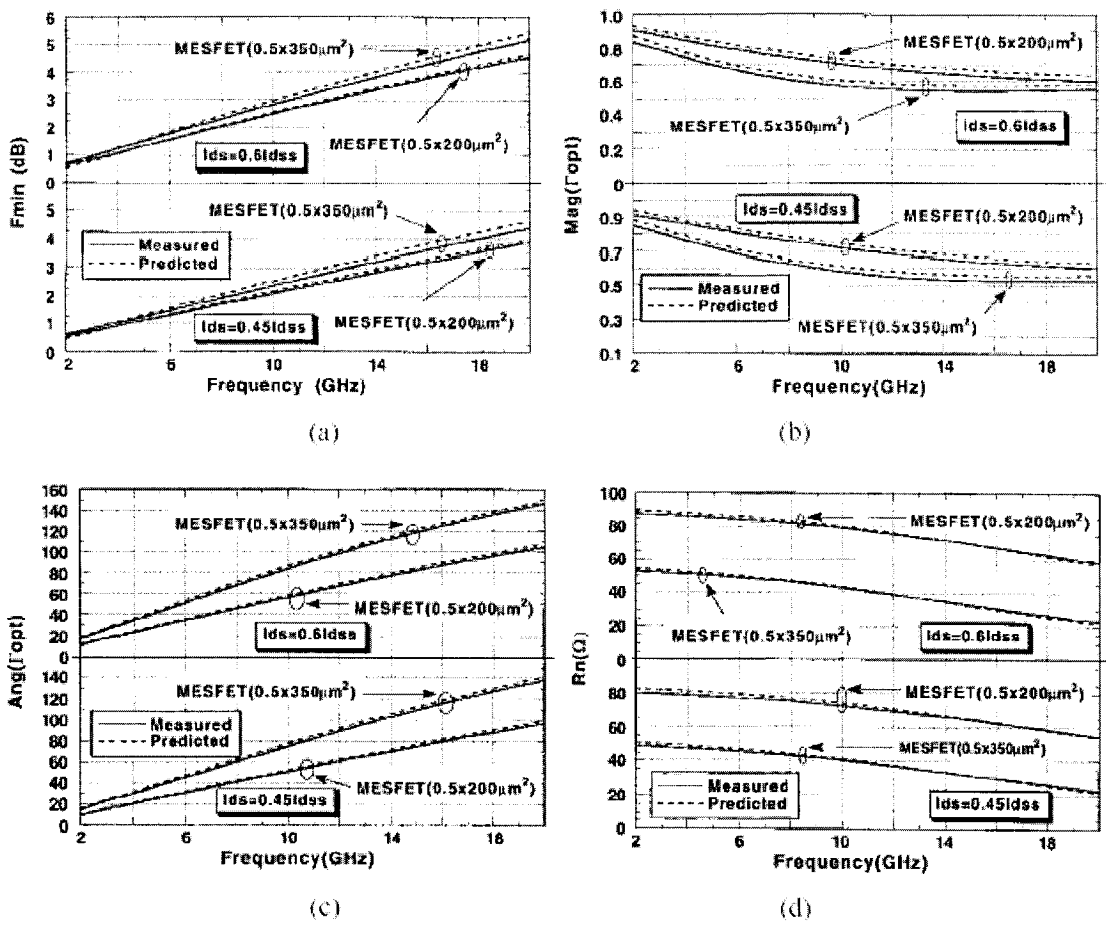

Figure 4.12 Comparisons of measured and predicted noise parameters versus frequency for two MESFET's of different dimensions biased at $I_{ds} = 0.6I_{dss}$ and $I_{ds} = 0.45I_{dss}$ with $V_{ds} = 5V$.

In Fig. 4.12, the transistors have two kind of gate dimensions $0.5\times200\mu m^2$ and $0.5\times350\mu m^2$. Under one bias condition, although the noise parameters obtained by measurement and prediction are very good agreement, they could present a large difference if the transistors' gate widths are different. The results of the Fig. 4.12 demonstrated that the qualitative analysis of the influence of gate width on device noise performance is correct.

Chapter 5. Conclusion

In this dissertation, first, a new method has been proposed to extract the FET 15-element equivalent small-signal model from a set of S-parameter measurements at different bias conditions. Then we use the extracted equivalent circuit and another new optimization method to predict the FET noise properties at any frequencies based on Pospieszalski's noise model.

The small-signal modeling technique has three major steps. The first step is aimed to estimate the pad capacitances (C_{pg} *and* C_{pd}) with the help of the measurements at pinch-off bias condition. The second step is aimed to estimate the parasitic inductance values of L_g, L_d *and* L_s , and ΔR_{ds} (the difference of R_d and R_s) with the help of Cold-measurements. The last step uses our proposed optimization technique to extract all other elements at normal bias conditions. The objective function assures good accuracy and less sensitivity to the frequency range of measurements.

The method of extraction of noise parameters from noise models goes through two major steps. The first step is to de-embed the FET intrinsic four parameters by employing the correlation method [27] under the knowledge of the equivalent circuit and the noise parameters of the packaged device and its physical temperature. The second step is aimed to extract the two equivalent noise temperatures T_g *and* T_d from Pospieszalski's noise model by employing our proposed optimization method and predict the device noise performance at any frequency.

The small-signal equivalent circuit modeling technique was investigated to reveal that it could almost work over any frequency range with the presence of the unavoidable measurement errors. We explained its accuracy, preciseness, robustness and reliability using S-parameters of hypothetical models at normal bias voltage conditions. The hypothetical S-parameters were contaminated with noise to emulate the measurement errors. We discussed other optimization-based extraction methods and investigated their ability to extract the model parameters over relatively small frequency range (1-40 GHz). We investigated how these methods are sensitive to any measurement errors. Our technique shows accurate results over this limited frequency range in the presence of noise.

The noise parameters extracting method was investigated to reveal that it is simpler but more accurate than other fitting method except its comparative complex de-embedding process.

The two optimization methods were just verified to work well on the hypothetical device. They need to be applied to the real MESFETs or HEMTs devices to verify their performance. The extraction of equivalent circuit elements and noise performance for the large-signal model of MESFET or HEMT device, their relationship to the small-signal elements, and the influence of gate various widths on device noise performance will be further studied.

All the programming and procedures in the dissertation were implemented in MATLAB. The graphs were also generated with MATLAB.

Appendix A. Intrinsic Small-Signal Model

The Intrinsic small-signal model of MESFET or HEMT devices is shown in Figure 4.1, which consists of 8 elements: C_{gs}, R_i, C_{gd}, R_{gd}, g_m, τ, R_{ds}, and C_{ds}. This appendix demonstrates the derivation of the Y-parameters of this model described by equations (4.8). It also explains how the intrinsic parameters can be derived in equations (4.9).

A.1 Derivation of Intrinsic Y-Parameters

Figure A.1 shows the intrinsic model separately out of Figure 4.1. The figure shows the intrinsic circuit as a 2-port network. The terminal voltage relations of this 2-port network can be expressed in terms of the Y-parameters as:

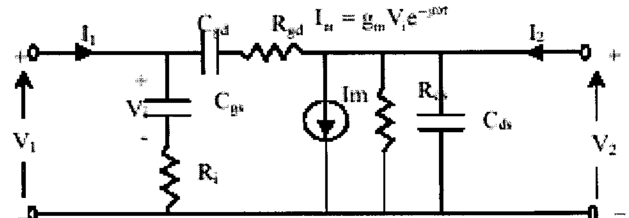

Figure A.1 Intrinsic model for MESFET or HEMT devices.

$$I_1 = y_{11}V_1 + y_{12}V_2 \tag{A.1a}$$

$$I_1 = y_{21}V_1 + y_{22}V_2 \tag{A.1b}$$

The Y-parameters of equations (A.1a) and (A.1b) can be calculated for the circuit of Figure A.1 as:

$$y_{11} = \frac{I_1}{V_1}\bigg|_{V_2=0} = \frac{1}{R_i + \frac{1}{j\omega C_{gs}}} + \frac{1}{R_{gd} + \frac{1}{j\omega C_{gd}}} = \frac{j\omega C_{gs}}{1 + j\omega R_i C_{gs}} + \frac{j\omega C_{gd}}{1 + j\omega R_{gd} C_{gd}} \tag{A.2a}$$

$$y_{21}=\frac{I_2}{V_1}\bigg|_{V_2=0}=\frac{I_m-\dfrac{V_1}{R_{gd}+\dfrac{1}{j\omega C_{gd}}}}{V_1}=\frac{g_m e^{-j\omega\tau}}{1+j\omega R_i C_{gs}}-\frac{j\omega C_{gd}}{1+j\omega C_{gd}R_{gd}} \quad \text{(A.2b)}$$

$$y_{12}=\frac{I_1}{V_2}\bigg|_{V_1=0}=-\frac{-I_1}{V_2}=-\frac{1}{R_{gd}+\dfrac{1}{j\omega C_{gd}}}=-\frac{j\omega C_{gd}}{1+j\omega R_{gd}C_{gd}} \quad \text{(A.2c)}$$

$$y_{22}=\frac{I_2}{V_2}\bigg|_{V_1=0}=g_{ds}+j\omega C_{ds}+\frac{j\omega C_{gd}}{1+j\omega R_{gd}C_{gd}} \quad \text{(A.2d)}$$

Applying simple mathematical manipulations, all Y-parameters can be rewritten in the form of equation (4.8) where the subscript 'int' is omitted for simplicity.

A.2 Derivation of Intrinsic Parameters

Equations (A.2a) through (A.2d) form eight equations with eight unknowns variables; each equation can be split into real and imaginary equations. Therefore, these equations can be solved for the intrinsic parameters. The real and imaginary parts of all Y-parameters are known after de-embedding them from the measured S-parameters. Since the real and imaginary parts of y_{11}, y_{12}, and y_{22} are needed in the following derivation, we can write them separately as:

$$\mathrm{Re}(y_{11})=\frac{\omega^2 R_i C_{gs}^2}{|D_1|^2}+\frac{\omega^2 R_{gd} C_{gd}^2}{|D_2|^2} \quad \text{(A.3a)}$$

$$\mathrm{Im}(y_{11})=\omega\left(\frac{C_{gs}}{|D_1|^2}+\frac{C_{gd}}{|D_2|^2}\right) \quad \text{(A.3b)}$$

$$\mathrm{Re}(y_{12})=-\frac{\omega^2 R_{gd} C_{gd}^2}{|D_2|^2} \quad \text{(A.3c)}$$

$$\mathrm{Im}(y_{12})=-\omega\frac{C_{gd}}{|D_2|^2} \quad \text{(A.3d)}$$

$$\mathrm{Re}(y_{22}) = g_{ds} + \frac{\omega^2 R_{gd} C_{gd}^2}{|D_2|^2} \tag{A.3e}$$

$$\mathrm{Im}(y_{22}) = \omega\left(C_{ds} + \frac{C_{gd}}{|D_2|^2} \right) \tag{A.3f}$$

Where

$$D_1 = 1 + j\omega R_i C_{gs}$$

$$D_2 = 1 + j\omega R_{gd} C_{gd}$$

Adding equation (A.3b) to equation (A.3d) reveals the following:

$$\mathrm{Im}(y_{11}) + \mathrm{Im}(y_{12}) = \frac{\omega C_{gs}}{|D_1|^2} \tag{A.4}$$

On the other hand, adding equation (A.3a) to equation (A.3c) leads to the following:

$$\mathrm{Re}(y_{11}) + \mathrm{Re}(y_{12}) = \frac{\omega^2 R_i C_{gs}^2}{|D_1|^2} \tag{A.5}$$

Dividing equation (A.5) by equation (A.4) eliminates D_1:

$$\omega R_i C_{gs} = \frac{\mathrm{Re}(y_{11}) + \mathrm{Re}(y_{12})}{\mathrm{Im}(y_{11}) + \mathrm{Im}(y_{12})} \tag{A.6}$$

The right hand side of equation (A.6) can be assumed to be equal to a variable d_1; thus equation (A.6) can be rewritten as:

$$\omega R_i C_{gs} = d_1 \tag{A.7}$$

Where

$$d_1 = \frac{\mathrm{Re}(y_{11}) + \mathrm{Re}(y_{12})}{\mathrm{Im}(y_{11}) + \mathrm{Im}(y_{12})} \tag{A.8}$$

Also, D_1 can be written in terms of d_1:

$$D_1 = 1 + jd_1 \tag{A.9}$$

Substituting D_1 from equation (A.9) into equation (A.4), C_{gs} can be evaluated:

$$C_{gs} = \frac{(1+d_1^2)}{\omega}(\mathrm{Im}(y_{11}) + \mathrm{Im}(y_{12})) \tag{A.10}$$

C_{gs} can be substituted in equation (A.7) to get R_i:

$$R_i = \frac{d_1}{(1+d_1^2)(\mathrm{Im}(y_{11}) + \mathrm{Im}(y_{12}))} \tag{A.11}$$

C_{gd} and R_{gd} can be calculated in a similar manner. Divide equation (A.3c) by equation (A.3d) to remove D_2:

$$\omega R_{gd} C_{gd} = d_2 \tag{A.12}$$

Where

$$d_2 = \frac{\mathrm{Re}(y_{12})}{\mathrm{Im}(y_{12})} \tag{A.13}$$

D_2 can be expressed in terms of d_2 as:

$$D_2 = 1 + jd_2 \tag{A.14}$$

Substitute D_2 into equation (A.3d) to estimate C_{gd}:

$$C_{gd} = -\frac{\mathrm{Im}(y_{12})}{\omega}(1+d_2^2) \tag{A.15}$$

Substitute C_{gd} into equation (A.12) and rearrange to get R_{gd}:

$$R_{gd} = -\frac{d_2}{(1+d_2^2)\,\mathrm{Im}(y_{12})} \tag{A.16}$$

The complex transconductance $G = g_m e^{-j\omega\tau}$ can be evaluated from the complex parameters y_{21} and y_{12}. The second term of y_{21} in equation (A.2b) can be removed by subtracting equation (A.2c) from (A.2b):

$$y_{21} - y_{12} = \frac{G}{1 + jd_1} \tag{A.17}$$

G can be extracted from equation (A.17):

$$G = (y_{21} - y_{12})(1 + jd_1) \tag{A.18}$$

The magnitude and phase of G represent gm and (-ωτ), respectively:

$$g_m = |G| = |(y_{21} - y_{12})| \sqrt{(1 + d_1^2)} \tag{A.19}$$

$$\tau = -\frac{1}{\omega} \angle(G) \tag{A.20}$$

The last two parameters g_{ds} and C_{ds} can be calculated using equations (A.3c) through (A.3f). Adding equation (A.3c) to equation (A.3e) results in g_{ds}, while adding equation (A3.d) to equation (A.3f) and rearranging results in C_{ds}:

$$g_{ds} = \mathrm{Re}(y_{22}) + \mathrm{Re}(y_{12}) \tag{A.21}$$

$$C_{ds} = \frac{\mathrm{Im}(y_{22}) + \mathrm{Im}(y_{12})}{\omega} \tag{A.22}$$

In summary, equations (A.10), (A.11), (A.15), (A.16), (A.19), (A.20), (A.21), and (A.22) constitute the solution set of the intrinsic parameters at single-frequency measurements. If $R_{gd} = 0$, the equations (4.8) and (4.9) can be derived.

Appendix B. Nonlinear Optimization

Nonlinear optimization can be defined as the process of finding the minimum or maximum of a nonlinear function. The nonlinear function for which the minimum or maximum should be determined is called the objective function. In our case, the objective function may be the error function stated in equation (4.31) and (4.40). The optimization subject is not that easy and has many aspects associated with it. Therefore, we will concern ourselves with the fundamentals of this subject so that we can fully understand the techniques used in this thesis. Since equations (4.41) and (4.40) are written in the form of the sum of squares, we will discuss two techniques for solving nonlinear least-squares optimization. These techniques are: Gauss-Newton and Levenberg-Marquardt methods. Both of them lie under the gradient optimization techniques.

Assume we have n independent variables, optimization parameters, x1, and x2.... xn which can be written in the vector form [38]:

$$X = \begin{bmatrix} x_1 \\ x_2 \\ \vdots \\ x_n \end{bmatrix} \qquad \text{(B.1)}$$

The objective function can be written as a sum of squares of nonlinear function:

$$R(x) = \sum_{i=1}^{m} r_i^2(x) \qquad \text{(B.2)}$$

Where m is the total number of the nonlinear functions r_i constituting the objective function. Finding the minimum of a function like (B.2) is called nonlinear least squares. The functions r_i can be written in a vector form as:

$$r(x) = \begin{bmatrix} r_1 \\ r_2 \\ \vdots \\ r_m \end{bmatrix} \qquad \text{(B.3)}$$

Then, equation (B.2) can be written in a vector notation:

$$R(x) = r^T(x) r(x) \qquad \text{(B.4)}$$

The gradient vector of R can be expressed as:

$$g(x) = \nabla f(x) = \begin{bmatrix} \partial R / \partial x_1 \\ \partial R / \partial x_2 \\ \vdots \\ \partial R / \partial x_n \end{bmatrix} \tag{B.5}$$

First partial derivatives in equation (B.5) can be calculated from equation (B.2) as:

$$g(x) = 2 \begin{bmatrix} \sum_{i=1}^{m} r_i \frac{\partial r_i}{\partial x_1} \\ \sum_{i=1}^{m} r_i \frac{\partial r_i}{\partial x_2} \\ \vdots \\ \sum_{i=1}^{m} r_i \frac{\partial r_i}{\partial x_n} \end{bmatrix} \tag{B.6}$$

If the Jacobian matrix $\boldsymbol{J}$ for the vector $\boldsymbol{r}$ is defined by

$$J(x) = \begin{bmatrix} \partial r_1 / \partial x_1 \cdots \partial r_1 / \partial x_n \\ \vdots \quad \cdots \quad \vdots \\ \partial r_m / \partial x_1 \cdots \partial r_m / \partial x_n \end{bmatrix} \tag{B.7}$$

Then, the gradient vector in equation (B.6) can be written as:

$$g(x) = 2J^T r \tag{B.8}$$

Taking the first derivatives for each element of $g(x)$ in equation (B.6), we obtain what is called the Hessian matrix of the function R . This matrix contains the second derivatives:

$$G(x) = \nabla^2 R(x) = \begin{bmatrix} \partial g_1 / \partial x_1 \cdots \partial g_1 / \partial x_n \\ \vdots \quad \cdots \quad \vdots \\ \partial g_n / \partial x_1 \cdots \partial g_n / \partial x_n \end{bmatrix} = \begin{bmatrix} \partial^2 R / \partial x_1 \partial x_1 \cdots \partial^2 R / \partial x_1 \partial x_n \\ \vdots \quad \cdots \quad \vdots \\ \partial^2 R / \partial x_n \partial x_1 \cdots \partial^2 R / \partial x_n \partial x_n \end{bmatrix} \tag{B.9}$$

The kj -element of the Hessian matrix can be calculated by differentiating the k-element of $g(x)$ in equation (B.6) with respect to x_j:

$$G_{kj} = \frac{\partial g_k}{\partial x_j} = 2 \sum_{i=1}^{m} \left(\frac{\partial r_i}{\partial x_j} \frac{\partial r_i}{\partial x_k} + r_i \frac{\partial^2 r_i}{\partial x_k \partial x_j} \right) \tag{B.10}$$

If the Hessian matrix of r_i is defined as T_i:

$$T_i(x) = \nabla^2 r_i(x) \tag{B.11}$$

then, the Hessian matrix G(x) can be written as:

$$G(x) = 2J^T J + 2\sum_{i=1}^{m} r_i T_i \tag{B.12}$$

We may notice that r_i is an error quantity or residue which should be too small at the optimization point (minimum). Thus, the second term can be neglected in equation (B.12). As a result, the Hessian matrix can be reduced to:

$$G(x) = 2J^T J \tag{B.13}$$

The equation (B.13) determines the Hessian matrix in terms of the first derivatives of the functions r_i's only. This is one of the attractive features of the least squares algorithms with small residuals that the computation of the Hessian matrix is easy.

Our optimization problem can be categorized as unconstrained optimization since we do not impose any constraints on the independent variables $\boldsymbol{x}$. This means that x_i can take any value in the real space. The necessary condition for a minimum [38] reads:

$$g(x^*) = 0 \tag{B.14}$$

where x^* is the solution at this minimum. The above condition is not a sufficient condition because this condition is also satisfied for other points such as maxima. The sufficient condition can be expressed as:

$$\Delta x^T G(x^*) \Delta x > 0 \tag{B.15}$$

where Δx is any arbitrary vector which is not equal to zero. The condition (B.15) is valid if $G(x^*)$ is positive definite. Fortunately, the Hessian matrix in equation (B.13) is at least positive semi-definite matrix. This can easily be proven by assuming $J\Delta x = Z$, then:

$$\Delta x^T J^T J \Delta x = Z^T Z \geq 0 \tag{B.16}$$

If the Hessian matrix is positive semi-definite, the solution x^* is probably not a minimum. However, the physical significance of our problem implies that this solution must be a minimum. To find the solution x^*, equation (B.14) should be solved. Many algorithms are suggested to solve this equation to find the minimum. We will explain two algorithms. The next two algorithms can be considered as modified Newton's method. The Newton's method exhibits quadratic convergence if the Hessian matrix is positive

definite. Quadratic convergence is normally the fastest convergence rate in nonlinear optimization. For this reason, Newton's method has special significance in nonlinear optimization. The Newton's method is an iterative scheme.

B.1 Gauss-Newton Method

If x_k is an arbitrary point at iteration k and S_k is an arbitrary vector, the gradient vector $g(x)$ can be expanded in Taylor's series at the new point $x_{k+1} = x_k + S_k$:

$$g_{k+1} = g(x_{k+1}) = g_k + G_k S_k \tag{B.17}$$

The higher order terms are neglected. If x_{k+1} is assumed to be the minimum of the function, then g_{k+1} must be equal to zero according to equation (B.14), and in turn equation (B.17) can be reduced to:

$$G_k S_k = -g_k \tag{B.18}$$

Substituting for g_k and G_k from equations (B.8) and (B.13), respectively, equation (B.18) can be expressed as:

$$J_k^T J_k S_k = -J_k^T r_k \tag{B.19}$$

Equation (B.19) is a set of linear equations which should be solved for S_k. S_k represents the difference between the new point and the old point in the iteration process, so, it is called the Search Vector. The new point can then be written as:

$$x_{k+1} = x_k + S_k \tag{B.20}$$

Then, equation (B.19) should be solved at the new point and the process has to be repeated iteratively until proper termination criteria are met. The flow chart in Figure A.1 shows the Gauss-Newton algorithm.

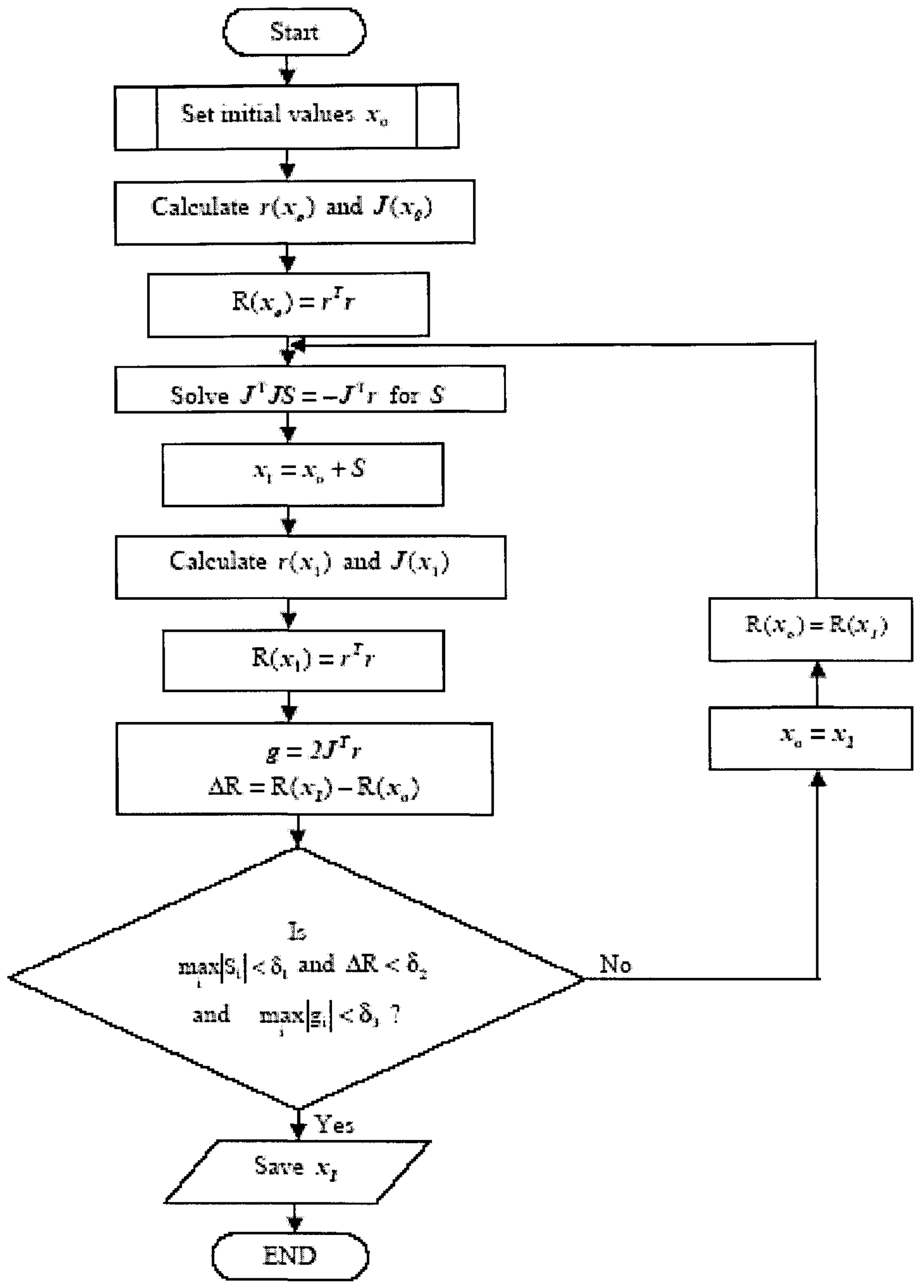

Figure B.1: Flow Chart for Gauss-Newton optimization method

The termination criteria consist of three conditions which must be satisfied simultaneously in order that the process terminates. The first criterion implies that the maximum component of the search vector should be less than certain tolerance δ_1 . δ_1 determines the number of accurate digits for $\boldsymbol{x}$. The second criterion is imposed to assure that the function reaches constant value at the minimum. In other words, the

difference in function values for two successive iterations is less than certain tolerance δ_2. The last error criterion represents the original condition of the minimum imposed by equation (B.14) that the maximum component of the gradient vector should be less than certain tolerance δ_3 . Typical values for δ_1 and δ_2 can be 10-4 and 10-8, respectively. Our experience also shows that δ_3 may be set as a combination between δ_1 and δ_2:

$$\delta_3 = 0.1(\delta_1 + \delta_2) \quad \text{(B.21)}$$

The Gauss-Newton's method shows good convergence if the function at the minimum is small. It encounters convergence problems if the function value at the minimum is relatively large because the second order term in the equation (B.12) may become significant. Other methods modify Gauss-Newton's method to overcome this problem.

B.2 Levenberg-Marquardt Method

This method is basically a modified Gauss-Newton's method. It solves the convergence problem associated with Gauss-Newton's method in case of relatively large function value at the minimum. Equation (B.19) can be simply modified to:

$$(J_k^T J_k + \mu_k I) S_k = -J_k^T r_k \quad \text{(B.22)}$$

where μ_k is a positive scalar variable and $\boldsymbol{I}$ is the unit matrix of order n. Equation (B.12) is solved to calculate the search direction at iteration k. μ_k is modified for each iteration. It can be controlled so that the matrix $(J_k^T J_k + \mu_k I)$ is positive definite. As μ_k increases, it becomes more difficult for the process to diverge. However, the convergence rate decreases. Therefore, it is important to decrease μ_k as minimum as possible to approach the quadratic convergence rate of Gauss-Newton's method. A strategy for selecting μ_k was proposed by Marquardt [38]. It compares the function value of the new iteration with that of the current value, and if it is large, μ_k should increases. Otherwise, it accepts the value of μ_k and moves to the next iteration. The change of μ_k is determined by another positive factor ν. ν is usually equal to 10 and the initial value of μ is equal to 0.01. The algorithm of Levenberg-Marquardt's method can be explained as follows:

1) Set initial values for x_0, μ =0.01, and ν=10
2) Set $\mu = \mu / \nu$
3) Repeat

4) Solve $(J_0^T J_0 + \mu I)S_0 = -J_0^T r_0$ for S_0

5) $x_1 = x_0 + S_0$

6) if $R(x_1) > R(x_0)$

7) $\mu = \mu v$

8) end

9) Until $R(x_1) < R(x_0)$

10) If all termination error criteria mentioned in the flow chart of Figure 4.5 are met, then stop the process.

11) Else, $x_0 = x_1, R(x_0) = R(x_1), r(x_0) = r(x_1), and\ J(x_0) = J(x_1)$, go to step number 2.

B.3 The First Derivative Calculation

The reader might have noticed that we need to calculate the first order derivative of all functions for the determination of the Jacobian matrix. The functions in our case are complicated and therefore it is not wise to look for analytical formula for such derivatives. In this case, we resort to a numerical technique to calculate derivatives. Finite difference approximation is a good candidate for derivatives. The derivative of the functions with respect to a variable x_j can be written in terms of the forward difference equation as:

$$J_j = \frac{\partial r}{\partial x_j} = \frac{r(x_j + \Delta_j) - r(x_j)}{\Delta_j} \quad \text{(B.23)}$$

where J_j is the jth column of the Jacobian matrix and j varies from 1 to n. Δ_j is an infinitesimal quantity which can be computed as [35]:

$$\Delta_j = \max\left(\min(|R(x)|, \Delta_j^{'}), \xi^{\frac{1}{2}} \right) \quad \text{(B.24)}$$

where

$$\Delta_j^{'} = \begin{cases} \xi^{\frac{1}{2}} & if\ |x_j| < 10^3 \xi^{\frac{1}{2}} \\ 10^{-3} & if\ |x_j| \geq 10^3 \xi^{\frac{1}{2}} \end{cases}$$

ξ is the machine relative precision which is approximately equal to 10^{-24} in our model. The above rule for choosing Δ_j was reported that its performance in our iterative

techniques is closely similar to that of the corresponding analytical derivative algorithms. It attempts to balance truncation and cancellation error to some extent when working with a digital computer precision.

B.4 Properties of the New Optimization Method

As described in section B.1, for the nonlinear least square function:

$$R(x) = \sum_{i=1}^{m} r_i^2(x) \tag{B.25}$$

The functions r_i can be written in a vector form as:

$$r(x) = \begin{bmatrix} r_1 \\ r_2 \\ \vdots \\ r_m \end{bmatrix} \tag{B.26}$$

For our case, x is only single optimization parameter. The Jacobian matrix $\boldsymbol{J}$ for the vector $\boldsymbol{r}$ is defined by

$$J(x) = \begin{bmatrix} \partial r_1 / \partial x \\ \vdots \\ \partial r_m / \partial x \end{bmatrix} \tag{B.27}$$

Then, the gradient vector can be written as:

$$g(x) = \nabla R(x) = 2J^T r = 2\sum_{i=1}^{m} r_i \frac{\partial r_i}{\partial x} \tag{B.28}$$

The Hessian matrix of the function R can be written as:

$$G(x) = \nabla^2 R(x) = 2J^T J + 2\sum_{i=1}^{m} r_i \frac{\partial^2 r_i}{\partial x^2} \tag{B.29}$$

It is noticed that r_i is an error quantity or residue which should be too small at the optimization point (minimum). Thus, the second term can be neglected in equation (B.29). As a result, the Hessian matrix can be reduced to:

$$G(x) = 2J^T J \tag{B.30}$$

Then

$$\Delta x^T G(x) \Delta x = \left[\sum_{i=1}^{m} \left(\frac{\partial r_i}{\partial x} \right)^2 \right] (\Delta x)^2 \tag{B.31}$$

For our cases, m is a large number. Δx is not equal to zero and at least one of $\frac{\partial r_i}{\partial x}$ is not equal to zero. So, expression (B.31) is greater than zero. $G(x^*)$ is positive definite. If x^* is an optimization point, it must be a global minimum point. Therefore, there is almost no initial value dependent problem and local minimum constraint in our new optimization method.

REFERENCES

[1] J. M. Golio, *Microwave MESFETs & HEMTs*, Norwood, MA: Artech House, 1991.

[2] S.M. Sze, *Semiconductor Devices Physics and Technology*, New York: John Wiley & Sons, 1985.

[3] R. Soares, *GaAs MESFET Circuit Design*, Norword, MA: Artech House, 1988.

[4] J.V. Dilorenzo and D.D. Khandelwal, *GaAs FET Principles and Technology*, Dedham, Massachusetts: Artech House, Inc., 1982.

[5] http://www.three-fives.com/latest_features/webzine_features/iainthainestory.html

[6] S.A. Mass, *Nonlinear Microwave Circuits*, Norword, MA: Artech House, 1988.

[7] R.A. Minasian, "Simplified GaAs M.E.S.F.E.T. Model to 10 GHz," *Electronics Letters*, Vol. 13, No. 18, pp. 549-551, 1st September 1977.

[8] H. Fukui, "Determination of the Basic Device Parameters of a GaAs MESFET," *The Bell System Technical Journal*, Vol. 58, No. 3, pp. 771-795, March 1979.

[9] F. Diamond and M. Laviron, "Measurements of the Extrinsic Series Elements of Microwave MESFET under Zero Current Conditions," *12th European Microwave Conference Proceedings*, pp. 451-456, September 1982.

[10] G. Dambrine, A. Cappy, F. Heliodore, and E. Playez, "A New Method for Determining the FET Small-Signal Equivalent Circuit," *IEEE Trans. Microwave Theory Tech.*, Vol. 36, No. 7, pp. 1151-1159, July 1988.

[11] E. Arnold, M. Golio, M. Miller, and B. Beckwith, "Direct Extraction of GaAs MESFET Intrinsic Element and Parasitic Inductance Values", *IEEE MTT-S Digest*, 1990

[12] H. Kondoh, "An Accurate FET Modelling from Measured S-Parameters," *IEEE MTT-S International Microwave Symposium Digest*, pp. 377-380, June 1986.

[13] F. Lin and G. Kompa, "FET Model Parameter Extarction Based on Optimization With Multiplane Data-Fitting and Bidirectional Search-A new concept," *IEEE Trans. Microwave Theory Tech.*, Vol. 42, No. 7, pp. 1114-1121, July 1994.

[14] K. Shirakawa et *al.*, "An Approach to Determining an Equivalent Circuit for HEMT's," *IEEE Trans. Microwave Theory Tech.*, Vol. 43, No. 3, pp. 499-503, March 1995.

[15] B. Ooi et *al.*, "A Novel Approach for Determining the GaAs MESFET Small-Signal Equivalent-Circuit Elements," *IEEE Trans. Microwave Theory Tech.*, Vol. 45, No. 12, pp. 2084-2088, Dec. 1997.

[16] T. Chen and M. Kumar, "Novel GaAs FET Modeling Technique for MMICs," *IEEE GaAs IC Symposium Digest*, pp. 49-52, 1988.

[17] L. Yang and S.I. Long, "New Method to Measure the Source and Drain Resistance of the GaAs MESFET," *IEEE Electron Device Letters*, Vol. EDL-7, No. 2, pp. 75-77, February 1986.

[18] D.M. Pozar, *Microwave Engineering*, USA: Wiley Publishing Company, 1998. Second Edition

[19] G.D. Vendelin, *Microwave Circuit Design Using Linear and Nonlinear Techniques.* John Wiley & Sons, Inc. 1990

[20] H. Rothe and W. Dahlke, " Theory of Noisy Four poles," proceedings of *IRE,* Vol. 44, June 1956, pp. 811-818.

[21] S.W. Wedge and D.B. Rutledge, "Wave techniques for Noise Modeling and Measurement," *IEEE Trans. Microwave Theory Tech.*, Vol. 40, No. 11, Nov. 1992

[22] M.S. Gupta, O. Pitzalis, Jr., S.E. Rosenbaum, and P.T. Geiling, "Microwave Noise Characterization of GaAs MESFET'S: Evaluation by On-Wafer Low-Frequency Output Noise Current Measurement," *IEEE Trans. Microwave Theory Tech.*, Vol. MTT-35, No. 12, Dec. 1987, pp. 1208-1218.

[23] H. Fukui, "Design of Microwave GaAs MESFET'S for Broad-Band Low-Noise Amplifiers," *IEEE Trans. Microwave Theory Tech.*, Vol. MTT-27, July 1979, pp. 643-650.

[24] H. Fukui, "Optimal Noise Figure of Microwave GaAs MESFET's" *IEEE Trans. Electron Devices,* Vol. ED-26, July 1979, pp. 1032-1037.

[25] A. Cappy, A. Vanoverschelde, M. schortgen, C. Versnaeyen, and G. Salmer, "Noise Modeling in Submicroometer-Gate Two-Dimensional Electron-Gas Field-Effect Transistors," *IEEE Trans. Electron Devices,* Vol. ED-32, December 1985, pp. 2787-2795.

[26] R.A. Pucel, H.A. Haus, and H. Statz, "Signal and Noise Properties of Gallium Arsenide Microwave Field-Effect Transistors," *Advances in Electronics and Electron Physics*, Vol. 38, New York: Academic Press, pp. 195-265.

[27] M. W. Pospieszalski, "Modeling of noise parameters of MESFET's and MODFET's and their frequency and temperature dependence," *IEEE Trans. Microwave Theory Tech.*, vol. MTT-37, pp. 1340–1350, Sept. 1989.

[28] J. Lange, "Noise characterization of linear two-ports in terms of invariant parameters," *IEEE J. Solid-State Circuits*, Vol. SC-2, pp. 37-40, June 1967.

[29] M. Berroth and R. Bosch, "High-Frequency Equivalent Circuit of GaAs FET's for Large-Signal Applications," *IEEE Trans. Microwave Theory Tech.*, Vol. 39, No. 2, pp. 224-229, Feb. 1991.

[30] V. Sommer, "A new method to determine the source resistance of FET from measured S-parameters under active-bias conditions," *IEEE Trans. Microwave Theory Tech.*, vol. 43, no.3, pp. 504–510, March 1995.

[31] A. van der Ziel, "Thermal noise in field-effect transistor," *Proc. IRE,* vol. 50, pp. 1808-1812, 1962

[32] Herbert Hillbrand and Peter H. Russer, "An Efficient Method for Computer Aided Noise Analysis of Linear Amplifier Networks," *IEEE Trans. On Circuits and Systems,* Vol. CAS-23, NO. 4, April 1976

[33] http://www.excelics.com/

[34] M. Garcia, J. Stenarson, K. Yhland, H. Zirath, and I. Angelov, "A new extraction method for the two-parameter FET temperature noise model," *IEEE Trans. Microwave Theory Tech.*, vol. 46, pp. 1679–1685, Nov. 1998.

[35] Matthias Rudolph, Ralf Doerner, Peter Heymann, Lars Klapproth, and Georg Bock, "Direct Extraction of FET Noise Models From Noise Figure Measurements", *IEEE Trans. Microwave Theory Tech.*, vol. 50, NO. 2, Feb. 2002.

[36] HP8510C Network Analyzer, *On-Site Service Manual*, Santa Rosa, CA: Hewlett-Packard Company, 1991.

[37] Ahmed Gasmi, Bernard Huyart, Eric Bergeault, and Louis P. Jallet, "A New Calculation Approach of Transistor Noise Parameters as a Function of Gate width and Bias Current", *IEEE Trans. Microwave Theory Tech.*, vol. 45, NO. 3, MARCH 1997.

[38] L.E. Scales, Introduction to Non-Linear Optimization, New York: Springer-Verlag New York Inc., 1985.